An Investigation on the Chemical and Microwave-assisted Approaches for the Reclamation of Metallic values from Computer Printed Circuit Boards (PCB) Wastes

Kwabena Offeh Gyimah

School of Chemical and Process Engineering.

The University of Leeds

Submitted in accordance with the requirements for the degree of
Doctor of Philosophy

October, 2018

Declaration

The candidate confirms that the work submitted is his own, except where work which has formed part of jointly-authored publications has been included. The contribution of the candidate and the other authors to this work has been explicitly indicated below. The candidate confirms that appropriate credit has been given within the thesis where reference has been made to the work of others.

Publication

Some results of this thesis have been submitted for publication in the following journal:

1. Offeh Gyimah, K., Sandhu, M., Sanchez-Segado, S., Hunter, I and Jha, A. (under review) *Temperature-dependent spectroscopic properties of imidazolium-based Ionic Liquids in the 100MHz to 10GHz microwave region,* Scientific reports.

This copy has been supplied on the understanding that it is copyright material and that no quotation from the thesis may be published without proper acknowledgement.

Acknowledgements

Abstract

E-waste comprises a multitude of components, some containing toxic substances that can have adverse impact on human health and the environment if not handled properly. Ghana, like many other developing countries, the management of e-waste management assumes greater significance not only due to the generation of its own e-waste but also because of the dumping of e-waste from the developed countries. This is coupled with the country's lack of appropriate infrastructure, advanced technology, safety measures and recycling procedures. As a results, the country suffers all the negative impacts that comes along with waste electronic appliances.

This research aims to develop an energy efficient and environmentally friendly processing technique for the recycling and recovery of precious and non-ferrous metals, particularly gold, nickel and copper from waste PCBs connectors, also termed as the PCB fingers. The techniques investigated will be optimized in future for developing technology for countries like Ghana, where the resources, e.g. energy, chemicals, and heavy mechanical equipment are limited. An energy efficient chemical extraction technique, when fully developed as a technology, will not only pave ways for safe treatment of e-wastes by stopping the current environmentally polluting practices of e-waste treatment in emerging and developing economies. The reclamation of purer forms of valuable metals will be a resource for creating an environment of economic regeneration in the region.

A novel route for the separation of plated gold, nickel and copper from the surface of PCB finger composites is explained in this thesis. More specifically, the role of microwave interaction with the selected leachate media (ionic liquid and mineral acid) for reducing the reaction time is discussed by characterising the chemical reaction kinetics and the reaction products thereof. The microwave absorption properties of imidazolium ionic liquids were characterized at different microwaves frequencies (from 10 MHz to 10 GHz), together with the structural properties of PCB substrate. After the dissolution of metals into a leachate medium, the metallic values are subsequently reclaimed via electrowinning technique. Finally, the recycling of ionic liquid and spent acid is also discussed in order to minimise the waste generation.

Bmim[HSO_4] was successfully used to delaminate the PCB chip samples after 2 hours in 200 W, 2.45 GHz microwave environment, at an activation energy of 17.6 kJ/mol. A regeneration process for the bmim[HSO_4] leachate after delamination process was developed. FTIR spectroscopy analysis revealed

the appearance of a peak at 2048 cm^{-1} in the regenerated bmimHSO$_4$ liquid which was attributed to a CN bond stretching and vibration ripped from the crosslinking elbows of the TEPR substrate. Irrespective of the presence of the CN bond in the regenerated ionic liquid, it was successfully reused four times in various delamination processes without any decrease in its activity or reaction time. In the coper-nickel leaching process, a UV-visible spectroscopy analysis was used to determine the product concentration of leachate at various times at different conditions. Using beer's principle, a calibration graph was developed to aid kinetic study. An activation energy for the leaching of copper and nickel were found to be 129.8 J/mol and 34.8 J/mol, respectively. In all MW-assisted leaching process, enormous amounts of energy and reaction time were saved. According to SEM-EDS analysis, 100 wt% gold was obtained after the recovery process.

Table of Contents

List of Tables

List of Figures

Nomenclature

Symbols

ε	Complex permittivity
ε_o	Permittivity of free space
ε'	Dielectric constant
ε''	Dielectric loss factor
σ	Conductivity
δ	Skin depth
$\tan \delta$	Loss tangent
$\tan \delta_\mu$	Magnetic loss tangent
W_h	Hysteresis energy losses
D	Diffusivity
η	Viscosity
Z	Charge
n	Concentration
R	Universal gas constant
A	Pre-exponential factor
T	Temperature
k	Rate of reaction
E	Electric field
f	Frequency
μ	Permeability
B	flux density
M	Magnetization
H	Magnetic field intensity
I_{geo}	Index of geochemical accumulation
C_n	Measured concentration
B_n	Geochemical background concentration
C_{deg}	Degree of contamination
E_a	Activation energy

Acronyms / Abbreviations

PCB	Printed Circuit Board
WPCB	Waste Printed Circuit Board
TEPR	Thermosetting epoxy resin

VMS	Vacuum metallurgy separation
VOC	Volatile organic compound
FMR	Ferromagnetic resonance
TAE	Traditional acid extraction
MAT	Microwave-assisted treatment
S/L	Solid-liquid ratio
EC	Ethylene carbonate
DME	Dimethoxy ethane
SCAPE	School of chemical and process engineering
SEM	Scanning electron microscope
EDS	Energy Dispersive X-ray Spectroscopy
BSE	Backscattered electrons
DBSE	Diffracted backscattered electrons
ATR	Attenuated total reflection
IR	Infrared
FTIR	Fourier transform infrared
R&D	Research and Development
UV-Vis	Ultraviolet visible
UV	Ultraviolet
MHES	Microwave heating equipment setup
GAE	Gerling Applied Engineering
PNA	Performance Network Analyzer
FR4	Fire retardant 'grade 4'
IL	Ionic liquid
LMIC	Low and middle income countries
WS	Weighing site
DS	Dismantling site
RD	Road dust
SC	School compound
CA	Commercial area
CP	Church premises
HI	Hazard Index
WEEE	Waste electrical & electronic equipment
HH	Household
ICT	Information communication & technology
CE	Consumer equipment
E&E	Electrical and electronic
TV	Television

PC	Personal computer
DVD	Digital Video Disc
CPU	Central processing unit
ENIG	Electroless nickel immersion gold

Chapter 1

Introduction

1.1 Background

Electronic wastes, also termed e-wastes, are electronic products, or products containing electrical components, that have outlived their use or have reached the end of their shell life [1, 2]. E-wastes encompasses a broad and growing range of electronic devices ranging from large household appliances such as refrigerators, air conditioners, washing machines to small and portable devices like hand-held cellular phones, personal stereos and computers. In the European Union, approximately 8 million tonnes of e-wastes are generated every year with an annual increase of 3–5% [3] while approximately 20–50 million metric tonnes of e-wastes are generated worldwide [4]. The compositions of e-wastes cover most of the periodic table elements, with metals from the precious group (Au, Ag, Pd etc.), less valuable metals (Cu, Al, Fe, etc.), and heavy toxic metals (Pb, Cd, Hg, etc.) and other nonmetallic elements (Cl, Br, etc.) [5] . Waste printed circuit boards (WPCBs) found in e-wastes comprise a mixture of woven glass reinforced resin and multiple kinds of metals. Their special physical and chemical characteristics make it difficult to recycle them. Plenty of toxic materials including heavy metals, PVC plastics, and brominated flame retardants can be easily found in normal circuit boards. However, just like the two-sided coin, the scrap e-waste contains many kinds of metals, which remains as untapped metal resource in many parts of the world, where the waste management is poor. The essential parts of WPCBs have recently gained a lot of attention as the concentrations of the precious metals in them is at least 10 times higher than that of rich-content minerals [6, 7]. As a results, WPCBs have become an attractive secondary source of metals [8-12]. The extraction of these metals from electronic wastes could be both profitable and environmentally worthwhile.

Besides these valuable metals, WPCBs usually contain up to 70% non-metals including plastics, resin, glass fibers, ceramics and thermosetting epoxy resins

(TEPRs). TEPRs are a major component of WPCBs [13, 14] but because TEPRs are insoluble and infusible, the treatment and recycling of such solid wastes are very difficult. Therefore, after extracting the metals, a large number of TEPRs are sent to landfill sites for disposal or incinerated with other industrial waste to provide energy [15, 16]. Owing to many additives such as flame retardants containing halogens in TEPRs, the landfill and incineration result in serious environmental pollution such as emissions of persistent organic pollutants, and thus eco-friendly recycling gets more and more attention.

1.2 Current Treatment of E-Wastes

Chemical and mechanical methods are two traditional recycling processes for e-wastes. Chemical methods mainly include pyrolysis, combustion, leaching and electrolysis. Because of low cost and easy operation, currently, the majority of e-waste is processed in backyards or small workshops using primary methods such as open burning and acid washing [17]. Formal pyrometallurgy and combustion also generate atmospheric pollution through the release of dioxins and furans [18, 19]. For leaching and electrolysis techniques, large quantities of waste acid liquid are produced during the recycling process, which needs to be carefully disposed of. Many researchers have used various mechanical methods to separate metals from printed circuit boards such as shape separation [20], jigging [21], and density-based separation [22]. These tests, however, are time-consuming and expensive and emit waste to the environment. Corona electrostatic separation has been investigated extensively in the minerals processing industry. Both fundamental and practical aspects concerning the design of the electrode system have been investigated and developed by many researchers [23-26]. The extreme difference in the density and electrical conductivity between metallic and non-metallic materials provides an excellent condition for the application of a corona electrostatic separation in minerals recycling. However, the utilization of corona electrostatic separation in the recovery of metals from e-waste is still in its infancy.

A state of the art technique for e-waste separation and treatment by vacuum metallurgy separation is reported [27]. Vacuum metallurgy separation (VMS) means separating and recycling materials through several kinds of vacuum metallurgical methods; e.g. reduced pressure evaporation, sublimation, reduction, and pyrolysis, etc. Since inside the vacuum chamber no oxygen is present, the metal oxides are not generated, therefore the chances of polychlorinated dibenzo-p-dioxins and dibenzofurans generation are eliminated largely [27]. The metals with high vapour pressure as well as those easy to be oxidized can be evaporated and recycled at much lower temperatures under the vacuum pressure below 100 Pa, which is realized by mechanical pump. Though VMS consumes less energy than traditional metallurgy under atmosphere, the process requires more energy for heating and vacuum maintenance when compared with the hydrometallurgy and bio-metallurgy methods. VMS furnace must also meet the strict requirements, such as heat insulation and airtightness which makes the capital investment relatively high. While VMS has obvious environmental benefits, the economic benefits are not so obvious. The recovered materials after VMS treatment are mainly the metals with cheap values, pyrolysis gas/oil with low calories, and residues with complicated compositions. "The economic benefits will be a challenge for further promoting its application" [27].

1.3 Statement of the Problem

E-waste comprises a multitude of components, some containing toxic substances that can have adverse impact on human health and the environment if not handled properly. According to a recent report by the BBC [28], e-waste pollution is causing severe health concerns for millions of people around the world, mostly in the developing nations of Africa and Asia. In Ghana, like many other developing countries, the management of e-waste management assumes greater significance not only due to the generation of its own e-waste but also because of the dumping of e-waste from the developed countries [29]. This is coupled with the country's lack of appropriate infrastructure, advanced technology, safety measures and recycling procedures. As a results, the country suffers all the negative impacts that

comes along with waste electronic appliances. At Agbogbloshie, an e-waste damp site in Ghana, people make a living from these wastes by engaging in several indigenous processing steps to recover both base and precious metals. Open incineration, acid washing among other harsh methods are practiced by both able and vulnerable inhabitants including children. Open incineration results in the release of heavy metals and toxic fumes into the air such as lead, mercury, cadmium and brominated flame retardants. This dominant technique for waste treatment at Agbogbloshie poses severe health risks to the people most of who are children. The release of poisonous fumes into the air also results in severe air pollution which has replicative and extensive effects on the ecosystem. The metal scrap recovery workers at Agbogbloshie often use acid bath to dissolve lead and other metals contained in the e-waste in order to extract the gold and silver. Recovered parts are washed directly into the nearby rivers and other water bodies, thus polluting the water and endangering aquatic life.

E-waste is equally dangerous to deposit as solid waste at the landfill sites because of the risk of leaching of heavy metals into the soil and underground water. As a result there is a significant risk to health of animals, humans and the ecology of flora/fauna via contaminated soil and water.

1.4 Main Aim

This research aims to develop an energy efficient and environmentally friendly processing technique for the recycling and recovery of precious and non-ferrous metals, particularly gold, nickel and copper from waste PCBs connectors, also termed as the PCB fingers. The techniques investigated will be optimized in future for developing technology for countries like Ghana, where the resources, e.g. energy, chemicals, and heavy mechanical equipment are limited. An energy efficient chemical extraction technique, when fully developed as a technology, will not only pave ways for safe treatment of e-wastes by stopping the current environmentally polluting practices of e-waste treatment in emerging and developing economies. The reclamation of purer forms of valuable metals will be a resource for creating an environment of economic regeneration in the region.

In the proposed research the leaching media considered are diluted forms of mineral acid and ionic liquids as solvents for metals from PCB fingers. The interaction of microwave with the leaching media on metal extraction rate has been examined by adopting a range of reaction rate and materials characterization techniques.

1.4.1 Use of Ionic liquids

Ionic liquids (ILs) have attractive physical and chemical properties that make them useful for a variety of applications.; The salient properties of industrial importance include high thermal stability and, ionic conductivity, a large electrochemical window, low flammability and negligible vapour pressure [30, 31]. Ionic liquids exhibit good thermal stability, and tend to decompose above 200 °C [32]. The room temperature conductivities of ionic liquids are within a broad range of 0.1–18 $mScm^{-1}$. Generally, the ionic conductivity of the order of 10 $mScm^{-1}$ at room temperature is typically reported for imidazolium-based ionic liquids[33]. One of the primary driving forces behind research into ionic liquids is the perceived benefit of substituting traditional industrial solvents, most of which are volatile organic compounds (VOCs), with non-volatile ionic liquids. Replacement of conventional solvents by ionic liquids would prevent the emission of VOCs, which is a major source of environmental pollution [34]. Ionic liquids are not intrinsically "green", some are extremely toxic, but they can be designed to be environmentally benign, with large potential benefits for designing sustainable chemical processing techniques, e.g. the extraction of metals from a waste [35].

Ionic liquids are designed with large organic cation, such as imidazolium ($C_3N_2H_4$) or pyridinium (C_5H_5N), with alkyl chain (C_nH_{2n+1}) substituents and anions such as trifluoromethylsulfonyl imide (($CF_3SO_2)_2N^-$), chloride (Cl^-), nitrate (NO^{3-}), Bromide (Br^-), hexafluorophosphate (PF_6^-) and tetrafluoroborate (BF^{4-}) [36]. "The physicochemical properties of ILs are influenced by both their cationic and their anionic moieties" [37]. For example, the viscosity of 1-alkyl-3-methylimidazolium (C_nmim^+) cations with the same hexafluorophosphate (PF_6^-) anion increases as the length of the 1-alkyl chain of the cation increases. However, the density and surface tension decreases with increasing length of

the 1-alkyl chain [38]. Moreover, in an ionic liquid the anionic moiety affects its water solubility. For instance, bmim[Cl] and bmim[BF$_4$] are both soluble in water, whereas the bmim[PF$_4$] and bmim[NTf$_4$] ILs are immiscible in water [39]. Different arrangement of cations and anions may yield different properties, thus ILs are also termed "tailor-made" materials [40]

Ionic liquids are capable of virtually all possible types of interaction with solute [39]. In extractive metallurgy, the recovery of gold (Au) and silver (Ag) from mineral concentrates using ionic liquids was reported for the first time by Whitehead et al. in 2004 [41]. 1-butyl-3-methyl-imidazolium hydrogen sulphate ionic liquid, bmim[HSO$_4$], was mixed with iron (III) sulphate oxidant and thiourea to oxidize Au and Ag which were selectively extracted from the powdered ore at room temperature in 50 hours at ≥85% and ≥60% efficiency, respectively.

1.4.2 Microwaves

The reaction rate of chemical reactions are strongly dependent on temperature because of the need to overcome the chemical activation barrier. In this respect, there has been a number of studies on reducing the leaching reaction time using microwave irradiation [42-48]. The interaction of microwave offers a fast heating process, and thereby increases the dissolution rate than in a conventional resistive heating [49]. In an attempt to reclaim metallic values from the electronic printed circuit boards, Kuo et al adopted, leaching techniques to extract heavy metals from the sludge of the printed circuit board process. A traditional acid extraction (TAE) method demonstrated that 74% of copper can be leached out from a sludge of fine particle sizes using nitric acid after 18 hours treatment. By comparison, when the leaching was carried out by irradiating the medium with incident microwave powers of 400W and 800 W, respectively, the metal leaching efficiencies of 77% and 93%, were recorded for reactions lasting up to 30 mins. Evidence for enhanced kinetics of metal dissolution from the sludge is therefore indisputable in the presence of microwave radiation[50].

1.5 Justification

The proper recycling or treatment of e-waste would not only save the eco-system from harmful toxic and hazardous emissions, but the approach creates a waste management process from which the metallic values can be monetized by creating an industrial framework. There has been a lot of pressure from global environmental groups on electronics manufacturers. As a result, most of the manufacturers offer financial incentives to e-waste recycling facilities by buying the old electronics product that comes to them in large quantities. Also it helps in cutting the cost of raw materials at the manufacturer's end. As a result, the cost of the final product becomes more affordable.

The e-waste recycling process also makes the scarce resources available to manufacturers that not only supports sustainable development but also reduces the socio-economic and environmental burden on country's economy. The approach also averts the extraction costs in the form of mining and processing the extracted minerals and raw materials, which are quite energy demanding, when compared with the local management of e-waste.

1.6 A novel process

A novel route for the separation of plated gold, nickel and copper from the surface of PCB finger composites is explained in this thesis. More specifically, the role of microwave interaction with the selected leachate media (ionic liquid and mineral acid) for reducing the rate of reaction is discussed by characterising the chemical reaction kinetics and the reaction products thereof [48]. The microwave absorption properties of imidazolium ionic liquids were characterized at different microwaves frequencies (from 10 MHz to 10 GHz), together with the absorptive properties of PCB substrate. After the dissolution of metals into a leachate medium, the metallic values are subsequently reclaimed via electrowinning technique, as described below. Finally, the recycling of ionic liquid and spent acid is also discussed in order to minimise the waste generation. The remainder solid waste, which are usually the glass fibre and polymer, were also characterized for process description. A

schematic summary of the novel route, researched herein, is shown in Figure 1 below.
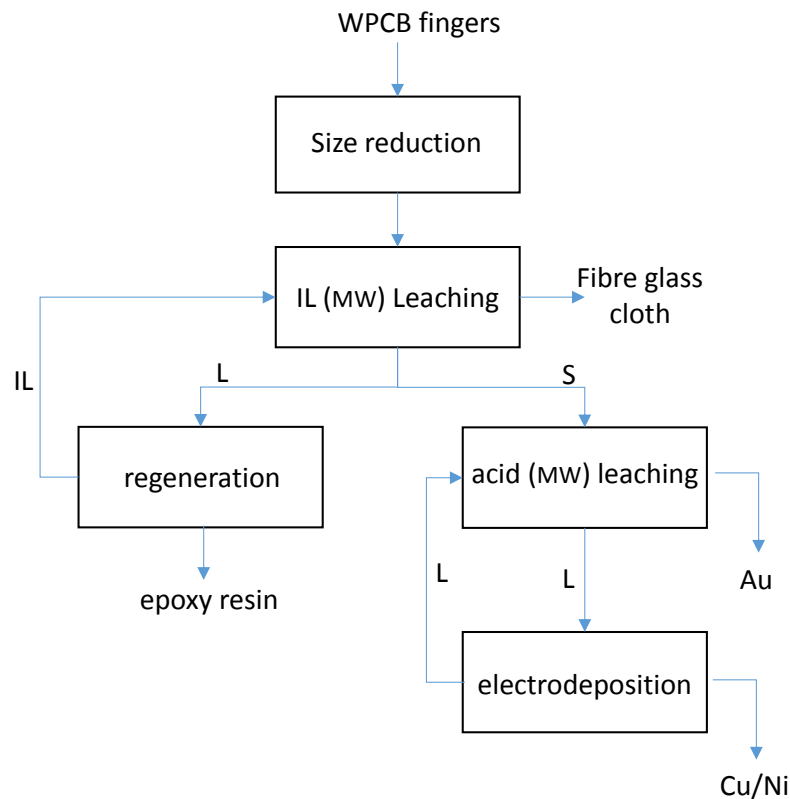
Figure 1: A green and novel route to separating waste PCB fingers.

1.6 Outline of thesis

This thesis brings to fore an alternative recycling technique well suited for the recovery of computer PCB wastes in the low and middle income countries where the resources are limited. Ghana is highlighted in this case study, because it accommodates the largest e-waste damp site on the planet, and also my PhD sponsorship was successful based on the research discussion I had with my supervisor before being accepted for the PhD study..

In the Literature Review (Chapter 2), a fairly extensive survey starting from the basic classification of electronic waste, and overview of the current recycling techniques employed in the developed countries are presented. Also reviewed are some applications of microwave and ionic liquids in relation to recycling and separation of electronic wastes, particularly PCB wastes.

In the Chapter Three (3), on Research Methodologies, a detailed description of the methods employed in this research is given. It begins with the sample preparation methods of the PCB fingers and the selected imidazolium-based ionic liquids and dilute HCl acid solution used. Analytical techniques which shed light on the microstructure and composition are described. Experimental setups using purpose-built and adapted equipment are described in detail with principles of operations.

Chapters 4 and 5 presents the results of my research investigations. Chapter 4 focusses on the structure and composition of the PCB samples. In this the IR spectroscopic analysis has been adopted for structural analysis of the selected ionic liquids. Chapter 4 explores the physical properties and the microwave dielectric properties of the ionic liquids. In chapter 5, a novel technique developed for the treatment (separation and recovery) of computer PCB wastes is presented and explained. The main reaction and chemical steps involved are also discussed.

In Chapter 6 (Conclusions), summarizes the results of the whole thesis, highlights the feasibility of the proposed technique in LMIC as relative to the objectives of this study and proposes areas of recommendations that may require more research for future development of an integrated process, which might be able to accommodate a range of e-waste materials with valuable precious and less-precious metals.

Chapter 2

Literature Review

2.1 E-waste

E-waste is divided into ten categories based on the European WEEE Directives 2002/96/EC and 2012/19/EU [51] as shown in Table 1. Printed circuit boards (PCBs) are found in electrical and electronics appliances (televisions, computers, mobile phones and laptops) irrespective of their category. Generally, PCBs are composed of 40% metals, 30% plastics and 30% ceramics.

Table 1 Waste from electrical and electronic equipment/ electronic waste categories according to the European directive on WEEE **[51]**.

No.	Category	Label
1	Large house hold appliances	Large HH
2	Small Household appliances	Small HH
3	IT and Telecommunications equipment	ICT
4	Consumer equipment	CE
5	Lighting equipment	Lighting
6	Electrical and electronic tools (with the exception of large scale stationary industrial tools)	E & E tools
7	Toys, leisure and sport equipment	Toys
8	Medical devices (with the exception of all implanted and infected products	Medical Equipment
9	Monitoring and control instruments	M & C
10	Automatic dispensers	Dispensers

PCBs are plastic platforms that mount nano-sized wires in complex electrical arrangements to aid in electronic control. These nano-circuits are formed by a thin layer of conducting materials deposited or printed on the surface of an insulating medium known as the substrate. Individual electronic components

are placed on the surface of the substrate and soldered to the interconnecting circuits. Contact fingers along one or more edges of the substrate act as connectors to other PCBs or to external electrical devices such as on-off switches. A printed circuit board may have circuits that perform a single function, such as a signal amplifier, or multiple functions.

2.1.1 Waste PCBs

There are three major types of PCB construction: single-sided, double-sided, and multi-layered. Single-sided boards have the components on one side of the substrate. When the number of components increases too much to accommodate all the components on a single-sided board, a double-sided board may be used. Electrical connections between the circuits on each side are made by drilling holes through the substrate in appropriate locations and plating the inside of the holes with a conducting material. The third type, a multi-layered board, has a substrate made up of layers of printed circuits separated by layers of insulation. The components on the surface connect through plated holes drilled down to the appropriate circuit layer. This greatly simplifies the circuit pattern.
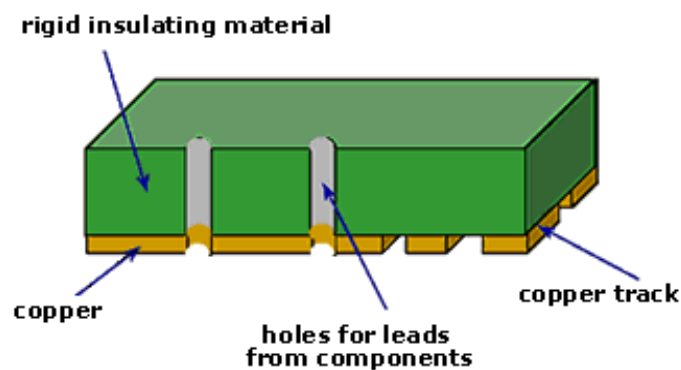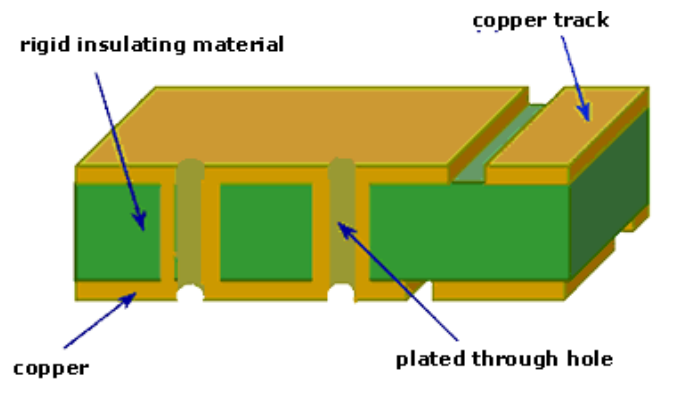
Figure 2 *A single-sided (top) and a double sided (bottom) PCB board types showing copper through holes and plating either or one side of the polymer substrate or on both sides [52].*

Components on a printed circuit board are electrically connected to the circuits by two different methods: the older "through-hole technology" and the newer "surface-mount technology." With through-hole technology, each component has thin wires, or leads, which are pushed through small holes in the substrate and soldered to connection pads in the circuits on the opposite side. Gravity and friction between the leads and the sides of the holes keeps the components in place until they are soldered. With surface mount technology, stubby J-shaped or L-shaped legs on each component contact the printed circuits directly. A solder paste consisting of glue, flux, and solder are applied at the point of contact to hold the components in place until the solder is melted, or "reflowed," in an oven to make the final connection. Although surface-mount technology requires greater care in the placement of the components, it eliminates the time-consuming drilling process and the space-consuming connection pads inherent with through-hole technology. Both technologies are used today.
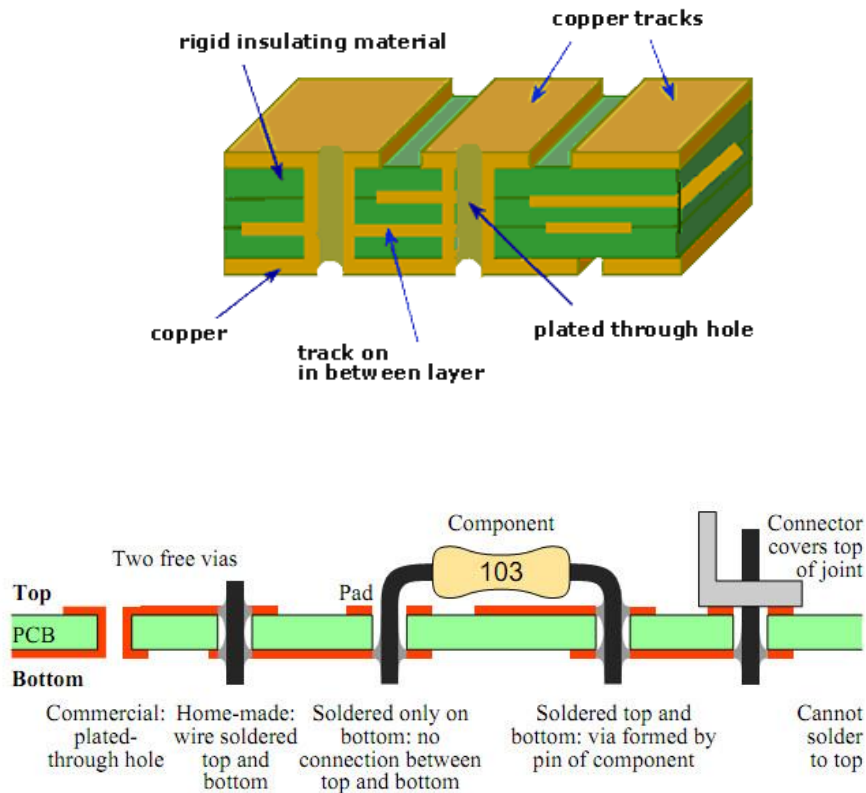
Figure 3*: (Top) A multi-layered PCB type showing copper plated holes, copper tracks embedded within polymer substrate and copper surface plates on both faces of the substrate [52]; (bottom) Cross-section of a double-sided printed circuit board showing free vias formed by a plated-through hole and a wire through a non-plated hole soldered top and bottom [53].*

The substrate most commonly used in printed circuit boards is a glass fiber reinforced (fiberglass) epoxy resin with a copper foil bonded on to one or both sides. PCBs made from paper reinforced phenolic resin with a bonded copper foil are less expensive and are often used in household electrical devices. The printed circuits are made of copper, which is either plated or etched away on the surface of the substrate to leave the pattern desired. The copper circuits are coated with a layer of tin-lead to prevent oxidation. Contact fingers are plated with tin-lead, then nickel, and finally gold for excellent conductivity. player, and Personal computers.

Table 2 shows a typical metallic composition of PCBs found in different electronic appliances. Precious metals, for example, Gold (Au), Silver (Ag) and Palladium (Pd) though lesser in quantity per board fetch much higher value than copper, nickel and other materials, used in much larger quantities. The lower part of Table 2 shows the value of each metal compared to its composition. Precious metals alone make more than 80% in value in TV-boards, DVD player, and Personal computers.

Table 2 Weight versus value distribution of metals in PCBs of different electronic appliances [54].

Weight-%	Fe (wt%)	Al (wt%)	Cu (wt%)	Plastics	Ag (ppm)	Au (ppm)	Pd (ppm)
TV-board	28%	10%	10%	28%	280	20	10
PC-board	7%	5%	20%	23%	1000	250	110
Mobile phone	5%	1%	13%	56%	1380	350	210
Portable audio	23%	1%	21%	47%	150	10	4
DVD player	62%	2%	5%	24%	115	15	4
Calculator	4%	5%	3%	61%	260	50	5
Value share	Fe	Al	Cu	sum PM	Ag	Au	Pd
TV-board	4%	11%	42%	43%	8%	27%	8%
PC-board	0%	1%	14%	85%	5%	65%	15%
Mobile phone	0%	0%	7%	93%	5%	67%	21%
Portable audio	3%	1%	77%	20%	4%	13%	3%
DVD player	13%	4%	36%	48%	5%	37%	5%
Calculator	0%	5%	11%	84%	7%	73%	4%

Recycling of waste PCBs is an important subject not only from the treatment for waste but also from the recovery of valuable materials. The typical metals in PCBs consist of copper (20 %), iron (8 %), tin (4 %), nickel (2 %), lead (2 %), zinc (1 %), silver (0.2 %), gold (0.1 %), and palladium (0.005 %) [55]. The purity of precious metals in waste PCBs is more than 10 times higher than that of rich-content minerals [56]. So waste PCBs are considered as an "urban

mineral resources". In addition, the non-metal portions of PCBs consist of thermoset resins and reinforcing materials. They also can be reused as fillers in composite materials.

In modern computers different types of electronic cards are used for: video, acoustic control, network interface, Ethernet card, accelerator card, video capture card, TV Tuner card etc. Some of them are essential cards while some others are inserted if needed. The main board of a computer is referred to as the motherboard or the system board. The mother board contains the CPU, memory, and basic controllers for the system. It has connectors for attaching devices and several other types of cards.

2.1.1.2 Gold Plating

The PCB fabrication industry offers two types of gold finish: Electroless Nickel Immersion Gold (ENIG) as a surface finish for the whole PCB, and hard plated gold over plated nickel for edge-connector fingers. Electroless gold gives excellent soldering properties, however as it is formed via the chemical deposition process, it means that it is too soft and too thin to withstand wear and abrasion in service. By comparison, the electroplated gold is thicker and harder making it ideal for edge-connector contacts for PCBs which will be repeatedly plugged in and removed.

2.1.1.2.1 Electroless Nickel Immersion Gold (ENIG)

In this technique, a 3 – 5 µm layer of electroless nickel is given a thin gold coating by immersion plating, an ion exchange process which coats the whole of the nickel surface.

A gold coating does not oxidize, its excellent wettability by molten solder does not degrade with time, and a plated finish maintains the flat surface of the copper lands. For these reasons a gold finish fulfils the requirements for boards designed for fine-line printing. However, with a thin gold immersion plating process, because nickel and gold ions are exchanged, a thick deposit (1.3–2 µm) can only be achieved when the gold is sufficiently porous to allow the underlying nickel to sustain the chemical reaction. But porous gold provides less protection for the nickel, which has an adverse impact on assembly. Current immersion gold processes plate 0.8–1.3 µm of gold and are

self-limiting, with reduced porosity compared with the earlier coatings. Gold readily dissolves in molten solder and will be present in the reflowed solder joint. Intermetallic gold-tin compounds formed cause joints to be brittle, and the gold film must therefore be thin (<<1 μm) to minimize the amount of intermetallics.

However, thin gold plating is porous, and does not protect the underlying copper against oxidation. Oxidized spots at the base of pores are a cause of dewetting, and copper can also diffuse into the gold surface during heat treatments, where it can oxidize and thus impair wettability. To prevent this, an electroless nickel underlayer is first deposited, to act as a barrier to copper diffusion: thickness specifications vary, but are usually in the 2–6 μm range.

2.1.1.2.2 Hard Plated Gold over Plated Nickel

For edge-connectors hard gold is electroplated. Electroplated gold is needed for edge connectors on printed circuit boards which will require repeated insertion and removal. Electroless gold gives good solderability but is too soft to withstand repeated abrasion. Therefore, for edge connectors 1 – 1.5 microns of gold is electroplated on a horizontal electroplating bath over 3 – 5 microns of plated nickel. This is done after a solder-mask process. The plated gold is not 100% pure; it contains some cobalt to increase the wear-resistance of the surface. The edge connectors are normally beveled to ensure easy insertion.

Figure 4: *Gold plated edge connector (PCB finger) [57].*

2.1.2 Global flow of e-waste

Africa records the largest inflow of used electrical appliances. These old and used appliances are mostly close the end of their useful life. Consequently, a much greater percentage of the world's e-wastes end up in Africa. Without doubt, most of the e-waste disposed of in developed countries eventually arrives in African countries through both legal and illegal means [29]. The exports of e-wastes from developed to developing countries includes everything from used TVs and refrigerators to computers and cell phones has caused concern. On one hand, this practice can help people in resource-poor countries acquire technology or earn income from selling re-usable parts and raw materials from the waste. But on the other, environmental regulations and enforcement in developing countries are often too weak to protect local people and their environment from the toxic wastes including lead and mercury.

Ghana, with its large and porous ports, proportionally records a very high inflow of used electronic appliances and thus records a high tonnage of electronic wastes inflow. The country's inability to collect, separate and properly dispose-off these electronic waste paves way for two common traditional treatments procedures, carried out by consumers or private waste collectors; landfilling and open incineration. In the scrap yards, unprotected workers, many of them children, dismantle computers and TVs with little more than stones in search of metals that can be sold. The remaining plastic, cables and casing is either burnt or simply dumped. Also in Pakistan, India, China and Nigeria, as shown in Figure 5, old waste often imported from abroad is broken up by unprotected workers and children to extract valuable components such as copper to sell [58].

Figure 5 *The electronic waste trail. E-waste is one of the fastest growing types of waste. Much of it ends up dumped in Africa and Asia. This map reveals these e-waste destination [59].*

In April 2008, following evidence that e-waste is being exported, often illegally, to Ghana from the EU and US, Greenpeace conducted the first investigation of workplace contamination from e-waste recycling and disposal in Ghana. The study extends the Greenpeace's global exposé of e-waste, which has previously documented environmental contamination from these practices in China and India [60]. In Ghana, Greenpeace experts collected soil and sediment samples from two e-waste recycling sites: the Agbogbloshie scrap market in the capital city, Accra, the main center for e-waste recycling in the country; and from a scrapyard in the smaller city of Koforidua, thought to be typical of the numerous small-scale e-waste recycling workshops in Ghana.

Figure 6 *Open incineration of e-wastes at Agbogbloshie, Ghana [61].*

At Agbogbloshie, e-wastes are manually dismantled at numerous small workshops within the market. Some parts are burned to remove plastics from valuable metals. Materials of no value are dumped along with other waste. Much of the work is carried out by children, some as young as five years old, with no protective equipment and using basic tools or bare hands. The study found that many samples contained numerous hazardous substances: including very high levels of the toxic metal lead; chemicals such as the phthalates DEHP and DBP, which are known to interfere with sexual reproduction; and chlorinated dioxins known to promote cancer. Injuries, such as burns, untreated wounds, eye damage, lung and back problems, go hand in hand with chronic nausea, debilitating headaches and respiratory problems.

Discarders of electronic goods expect them to be recycled properly. But almost all such devices contain toxic chemicals which, even if they are recyclable, make it expensive to do so. As a result, illegal dumping has become a lucrative business. The population of Agbogbloshie consists of economic migrants from northern and rural parts of Ghana. Living standards in the north and rural areas are growing worse, causing people to move to urban settings, such as Agbogbloshie. Inhabitants of Agbogbloshie live, eat, work and relieve themselves on the land and amongst the waste. The toxic smoke swirls around them and over Agbogbloshie, the roughly 20-acre scrap yard in the heart of

Accra, Ghana, where these men live and work [62].

2.1.3 Health and Environmental risks

In a research by Greenpeace, nearly all samples examined contained numerous hazardous chemicals, and very high levels of many toxic metals. Most toxic substances found in the samples were either used in electronic goods, or were formed when some hazardous materials in the products were burned. In some cases certain metals were present at concentrations over one hundred times higher than typical background levels for soils, including the highly toxic lead metal. Contamination with other toxic metals, such as cadmium and antimony, were also detected [58].

Also, in a study by Atiemo [63] where dust samples were collected from various points within the vicinity of Agbogbloshie scrap yard indicated a massive levels of contamination. Heavy metals such as Zn, Cu, Pb and Cd gave concentrations in the range of (10,575 - 30,384 mg/kg), (34 - 16,952 mg/kg), (351 - 5,105 mg/kg) and (2 - 72 mg/kg), respectively which were over thousand times more than the levels for which intervention is required. The scrap weighing site, the electronic waste dismantling site and the burning site (where electrical cables are burnt to retrieve metals) recorded the highest levels of heavy metals. Index of geo-accumulation (I_{geo}) which compares the levels of heavy metal obtained to background levels originally used with bottom sediments [64] was employed to determine the level of pollution of the various elements. The results gave values in the range of 6.7 - 8.2 for Zinc (Zn), 4.2 - 8.1 for lead (Pb) and 3.0 - 7.8 for Cadmium (Cd) indicating extreme pollution from all the sites. The index of geochemical accumulation is calculated using the equation 1 below:

$$I_{geo} = log_2 \frac{C_n}{1.5B_n} \qquad (1)$$

where C_n is the measured concentration of the heavy metal in road dust, B_n is the geochemical background concentration of the heavy metal [65]. This was also confirmed by contamination factor calculations. To assess the extent of

pollution of each of the site, degree of contamination (C_{deg}) was calculated which revealed that the most contaminated site is the Weighing Site (WS) which recorded C_{deg} value of 1482.93, followed by Dismantling Site (DS): 1221.6; Burning Site (BS): 1196.9; Road Dust (RD): 1061.9; School Compound (SC): 651.44; Commercial Area (CA): 618.6 and Church Premises (CP): 187.6, respectively. The results also indicate that children living around the scrap market face a very high risk from the ingestion of toxic metals such as Pb and Cd. The calculated cumulative risks expressed in terms of Hazard Index (HI) ranged from 15 to 205. The weighing site (HI = 205) at the scrap market by far pose the greatest cumulative risk followed by the dismantling site (HI = 130), road dust (HI = 88), burning site (HI = 60), school compound (HI = 52), commercial area (HI = 50) and church premises (HI = 15). These values are over many times more than the safe level of 1.

Table 3: Heavy metal concentrations in dust sampled from the vicinity of the e-waste damping site at Agbogbloshie, Accra. CP: Premises of ICGC headquarters; DS: Dismantling site; WS: Weighing site; BS: Burning Site; CA: Commercial Area; RD: Road dust; AT : Levels for which attention is required; IT: Levels for which intervention is required [63, 66].

Element		Fe	Mn	Cu	Zn	Cd	Cr	Ni	Pb
CP	Mean	16,743.1	90.7	34.4	10,575.0	2.4	21.6	26.3	351.1
	SD	193.8	10.5	5.2	347.2	0.5	2.1	4.2	30.9
DS	Mean	17,495.4	294.2	16,318.6	28,957.9	52.1	60.0	101.9	3,162.7
	SD	321.2	9.7	531.6	900.6	22.1	5.1	49.5	688.4
WS	Mean	17,920.2	293.5	16,951.7	29,720.7	68.5	114.5	191.4	5,105.4
	SD	279.4	8.2	641.8	442.7	2.1	19.7	33.6	895.3
BS	Mean	16,644.2	145.4	16,627.5	30,384.4	71.6	48.7	95.5	1,321.1
	SD	394.0	43.4	622.2	612.1	60.6	17.4	27.5	223.5
CA	Mean	16,493.1	189.8	11,589.4	20,847.2	4.4	34.6	28.7	1,149.1
	SD	54.9	22.6	3,318.5	1,727.7	1.0	3.9	5.4	218.2
RD	Mean	1,7118.0	269.7	31,028.2	22,256.0	5.1	72.4	49.2	1968.4
	SD	64.8	70.1	154.2	345.9	0.4	5.2	3.5	100.9
SC	Mean	17,543.6	197.4	10,099.1	22,052.3	12.1	105.6	29.9	1,195.2
	SD	168.2	35.5	2,614.2	1,216.5	4.7	10.6	4.5	179.3
	AT		1,500.0	100.0	300.0	3.0	100	75.0	50.0
	IT		2,500.0	200.0	600.0	5.0	300	150.0	100.0

All these undeveloped recycling techniques practiced by informal e-waste processers, on the one hand, aggravate the release of environmental toxins that pollute and contaminate landscapes, waters, and biota of Agbogbloshie. Waste left in fields and nearby bodies of water is ingested by animals and marine life, thus creating entry points for toxins into non-human ecological systems, while indirectly affecting humans via consumption of fish and seafood

that are dietary staples for coastal residents of Ghana, increasing their risk of cancer. On the other hand, very little or in most cases no protective measures in use, endanger not only the e-waste workers, but also local inhabitants, particularly children and infants. Due to the pervasive nature of environmental toxins in the local atmosphere, residents of the nearby settlements and those working and residing in the central business district are at risk of experiencing high exposure levels on a daily basis. Air samples from the Agbogbloshie Market have revealed heavy metals and polychlorinated naphthalene (PCN) congeners.

Blood samples of e-waste workers have been shown to exhibit elevated concentrations of heavy metals and flame retardants. Indeed, heavy metals and chemical compounds found within electronic devices have been linked to neurodevelopmental disorders and/or fetal perturbations [67, 68].

2.2 Recycling Techniques of PCBs

Recycling circuit boards is expensive. Only the metal parts of the boards have reusable value, so the nonmetallic parts must be separated out from the e-waste which is a costly process. Since the effects of PCB incineration in open causes a major risk to environment, plant and animal lives, it is essential to analyse the literature on recycling before a novel approach discussed herein may be able to offer an alternative solution which eliminates the above identified risks to human, animals, and flora/fauna due to high concentration of heavy metals such as cadmium, lead, copper and zinc [69].

The processes used for recycling PCBs may be divided into two categories: pyrometallurgical and non-pyrometallurgical methods discussed below. Dismantling, milling, mechanical separation and pyrolysis are typical pretreatment processes [70], as shown in Table 4 below.

Table 4 Comparison of the main processes for recovering metals from printed circuit boards (PCBs)**[70]**

Types	Thermal Processes	Non-Thermal Processes
Characteristics	– Non-metallic materials cannot be recovered – High investment in equipment and installation, including air-pollution control systems – Economic efficiency not proven for low-grade wastes	– Health risks for the milling operators, because of the possibility of inhaling fiberglass particles and heavy metals – Strong irritating odour generated by phenolic resin during the milling process – Large investment in equipment for waste-water treatment
Environmental impacts	– Generation of gaseous pollutants, including dioxins and lead fumes	– High water utilization and waste-water generation, with acidic residues – Noise pollution due to grinding equipment. – Generation of solid waste

2.2.1 Pretreatment Processes

Pretreatment of waste materials is one of the most important steps in the recycling chain. Waste electronic appliances are manually dismantled at the collection facility and individual components are isolated from the e-waste. The various steps are outlined in

Figure **7**. Hand dismantling involves the use of simple hand tools to disassemble waste electronic appliances into plastics, large metals, glass, small metals, cables, battery, and PCBs. All of these sub-sections are recycled or disposed of. The PCBs collected at this first stage are subsequently shredded using hand cutters and other hand shredding tools. Mounted electrical components like resistors, inductors, capacitors, wires, heat sinks, connectors and the like are removed from the board using hand pliers. After the clearing and the disconnection of all mounted electrical components, the

clean printed circuit boards are crushed using a hammer crusher or milled using a ball mill into fine powder.

Magnetic separation (Figure 8), a process in which magnetically susceptible material is extracted from a mixture using a magnetic force, is utilized at this stage to separate the ferrous metals from the crushed particles. The powder particles are allowed to fall on a rubber belt which moves horizontally over two rollers, one of which is magnetic. As the crushed particles roll over the belt, the magnetic component in it gets attracted towards the magnet.
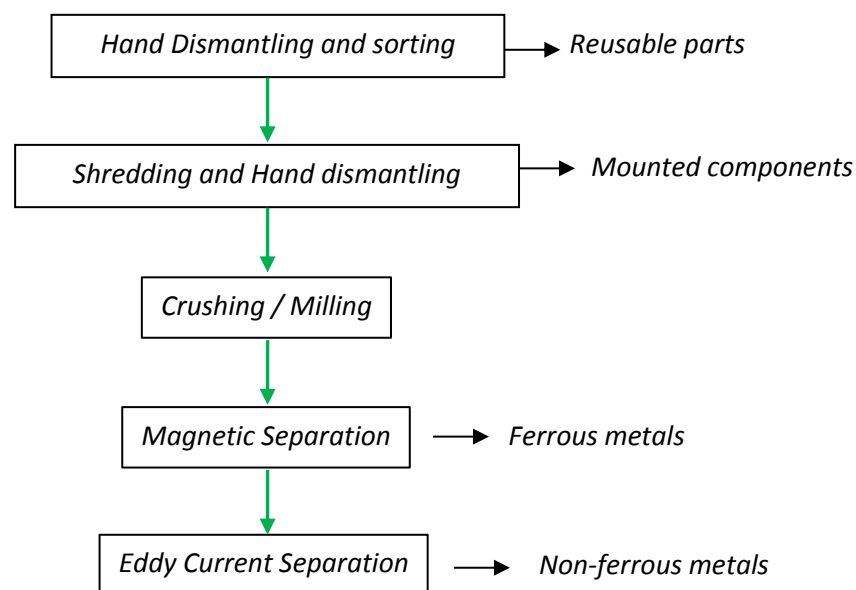
Figure 7 *The pre-processing of e-waste to separate the metal and non-metal fractions*

The magnetic component gets collected in a heap while the non-magnetic component forms a separate heap as indicated in Figure 8. Eddy current separation technique is used to separate the non-ferrous metals from the powder particles. Traditional eddy current separators have a problem in recovering non-ferrous particles with a diameter of less than 5 mm. Such machines rely on the eddy current force of the magnet rotor on the non-ferrous particles to create a separation. Unfortunately, this force scales as the fifth power of the particle size for small particles, whereas the mass of a particle scales only with the third power. The result is that frictional forces dominate

the separation for small particles [71].
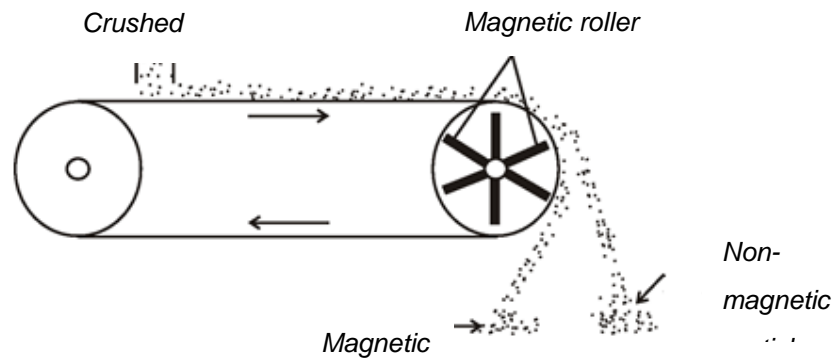
Figure 8 *Magnetic separation technique using a magnetic roller and a rubber belt.*

Inasmuch as pre-processing is a vital stage, it also has few negative environmental impacts including noise generation (130dB), dust production from shredding and mechanical attrition. Exposure to dust may cause damage to human health. In the shredding and smashing process of PCB, the temperature rise causes the decomposition of resin present, which then produce foul odour in a work environment. [72].

2.2.2 Thermal Processes (Pyrometallurgical techniques)

For the last 3 decades, the pyrometallurgical processes for recovering metals from various waste materials have been used. Smelting in furnaces, incineration, combustion and pyrolysis typically define e-waste pyrometallurgical recycling processes, during which the waste is heated in air well above the combustion temperatures above 1000ºC using controls to manage emission and exposure.

2.2.2.1 Pyrolysis

Pyrolysis is a thermochemical treatment, which can be applied to any organic (carbon-based) product. In this treatment, material is exposed to high temperature, and in the absence of oxygen goes through chemical and

physical separation into different molecules. Pyrolysis allows to receive products with a different, often more superior character than original residue. Thanks to this feature, pyrolysis has become increasingly important process for today's industry as it allows to bring far greater value to common materials and waste. In contrast with combustion and gasification processes, which involve entire or partial oxidation of material, pyrolysis bases on heating in the absence of air which makes it mostly endothermic process and ensures high energy content in the products received. Common pyrolysis by-products are solids (charcoal, biochar), liquid (pyrolysis oil and water) and non-condensable gases (H_2, CH_4, CO, CO_2 and N_2) [73].

Table 5: The main differences between incineration and pyrolysis adopted from Helsen et al [73]. Also shown is the chemical reaction equation for each process where '*Me*' represents a metal.

	Incineration	Pyrolysis
Temperature[°C]	250-900	800-1450
Pressure [bar]	1	1
Atmosphere	Air	inert/nitrogen
Gas phase	CO_2, H_2O, O_2, N_2	H_2, CO_2 H_2O, N_2, hydrocarbons
Solid phase	Ash, slag	Ash, coke
Liquid Phase		Pyrolysis oil, water
Chemical reaction	$xMe + {}^y\!/_2\, O_2 \rightarrow Me_xO_y$	$Me_{(s)} \rightarrow Me_{(l)}$

During pyrolysis of PCB, leads to the formation of gases, oils, and chars which can be used as chemical feed stocks or fuels. Pyrolysis degrades the organic part of the PBC wastes, making the process of separating the organic, metallic and glass fibre fractions of PCBs much easier and recycling of each fraction more viable. In elevated temperature pyrolysis above 800°C, the metallic values begin to melt and tend to separate away from the organic and inorganic parts of PCB. For the collection of metallic values, in some practice, waste copper metal scrap is used so that the cast copper plates can be used for electro-winning of metallic values. Polymer in PCB, has been widely investigated as a basis for pyrolytic recycling. In thermogravimetry, brominated

epoxy resins are thermally less stable than the corresponding unbrominated ones, and rapid decomposition above 300ºC leads to significant weight loss depending on the hardeners (e.g., aromatic amines and anhydrides) [74].

2.2.2.2 Smelting

Smelting is a unit process for pyro metallurgical extraction of metal in which gangue minerals are separated from the metal in liquid state. The waste materials are heated above the melting points so that they are separated in the liquid state. There are two types of smelting: reduction and matte smelting techniques. In reduction smelting, both the metallic charge fed into the smelter and the slag formed from the process are oxides whereas in matte smelting, the slag is an oxide while the metallic charge is a combination of metallic sulphides that melt and recombine to give a homogeneous metallic sulphide called matte. One advantage of matte smelting is its low melting point which makes it possible to smelt sulphide ores at lower temperatures than required for metals. Thus a matte with equal amounts of copper and iron sulphide melts below 1000ºC, whereas an alloy of Fe and Cu would melt at around 1400ºC. This leads to lower thermal energy requirements and gangue minerals can be separated easily as slag.
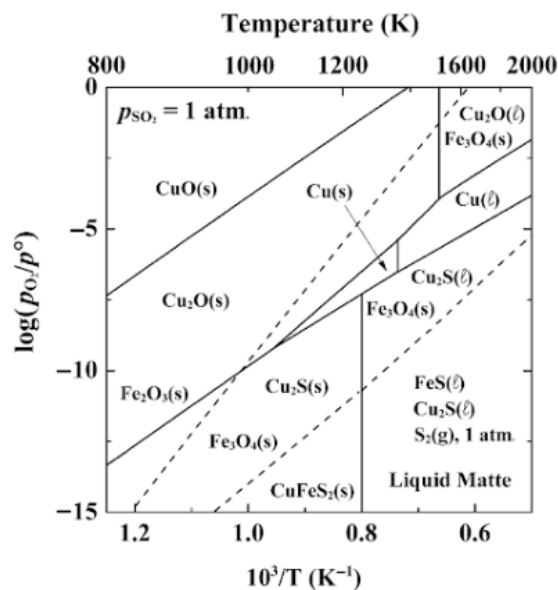
Figure 9: *Predominance-area diagram system showing principal compounds formed by oxidation of chalcopyrite at various temperatures and oxygen pressures [75].*

For example, if sulphide ores containing iron and copper are to be smelted, an understanding of both the iron and copper systems is needed. From Figure 9, chalcopyrite ($CuFeS_2$) decomposes to Cu_2S and FeS liquid mixture and S_2 gas at 1 atmosphere pressure at about 1250 K. Thus, the right-hand border of its stability region is the isotherm for this temperature. Fe_3O_4 forms upon the oxidation of FeS on the top border line representing equilibrium of the following reaction:

$$3FeS_{(l)} + 5O_2 = Fe_3O_{4(s)} + 3SO_2$$
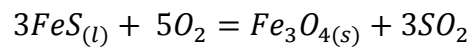
A further increase in oxygen pressure causes Cu_2S to form Cu_2O below about 1023 K. AT higher temperatures, Fe_2O_4 is the stable iron phase, while Cu_2S is converted to Cu liquid above 1358 K, which is the lowest temperature at which copper production by smelting would be possible. Above 1358 K, solid Fe_2O_4 floats on liquid copper. Flux is added to enable the iron oxide to dissolve in a slag as a liquid for easy separation. Addition of more oxygen results in the conversion of Cu to Cu_2O and finally to CuO while all the iron ends up as Fe_2O_3 [75].

State-of-the-art smelters and refineries can extract valuable metals and isolate hazardous substances efficiently. Such recycling facilities can close the loop of valuable metals and reduce environmental impact arising from large quantities of e-waste [51]. In thermal processing, metals are liberated by smelting at high temperatures. After Fe and Al, Cu and Pb are the main constituents of a typical e-waste. Iron and aluminium are easily separated at the pre-processing stage because they form bulky parts of the e-waste, for example, the body of most appliances are made from iron or aluminium.

Traditionally, pyrometallurgical technology has been used for recovery of precious metals from PCB to upgrade mechanical separation which cannot efficiently recover precious metals. In the pyrometallurgical processing the crushed PCBs scraps are burned in a furnace or in a molten bath to remove

plastics, and the refractory oxides form a slag phase together with some metal oxides. Further, recovered materials are retreated or purified by using chemical processing. Energy cost is reduced by combustion of plastics and other flammable materials in the feeding.

Despite differences in the plants, general electronic scraps are treated together with other metal scraps by pyrometallurgical processes. Recently a modified pyrometallurgy to recover metals from PCBs has been proposed [9] showing that addition of NaOH as slag-formation material promotes the effective separation of metals from slag, the remaining slag in the blowing step was found to favour the separation of Cu from other metals and allow noble metals to enter the metal phase to the greatest extent. Additionally, the resulting slag was shown to be very effective in cleaning the pyrolysis gas. Eventually Cu, Ag and Au recovery could be achieved in this process, confirming preliminarily the feasibility of modified pyrometallurgy in recovering metals from PCB. [76].

2.2.2.3 Limitations of Thermal Processes

Pyrometallurgical routes are generally more economical, eco-efficient and maximize the recovery of precious metals, however, they have certain limitations that are summarized here [51]:

1. Recovery of plastics is not possible because plastics replace coke as a source of energy;
2. Iron and aluminium recovery is not easy as they end up in the slag phase as oxides;
3. Hazardous emissions such as dioxins are generated during smelting of feed materials containing halogenated flame retardants. Therefore special installations are required to minimize environmental pollution;
4. A large investment is required for installing integrated e-waste recycling plants that maximize the recovery of valuable metals and also protect the environment by controlling hazardous gas emissions;
5. Handling the process of smelting and refining is challenging due to complex feed materials. The expertise in process handling and the thermodynamics of possible reactions will be difficult.

2.2.3 Non-Thermal Processes (Electro/hydrometallurgical processes)

In hydrometallurgical separation, acid or caustic leaching medium is often used for selective dissolution of precious metals (PMs) from e-waste. The metal-ion loaded leachate is separated and purified for the enrichment of metal content thereby impurities are removed as gangue materials. The isolation of metal of interest is conducted through solvent extraction, adsorption and ion exchange enrichment processes. Finally, metals are recovered from solution through electro-refining (electrometallurgy) or chemical reduction processes [77-79]. Hydrometallurgical techniques have potential toxic emissions that accompanies them. Gases from acids are not only hazardous when they come into contact with the human skin but also emit toxic fumes that are detrimental to the respiratory system of the human body. These techniques require appropriate safety precautions to be followed. Furthermore, after leaching and/or recovery, acidic solvents have to be disposed of carefully and in a more environmentally friendly manner.

Leaching is the process of extracting a soluble constituent from a solid by means of a solvent. Electronic wastes leaching involve acid and/or halide treatment due to the fact that acid leaching is a feasible approach for removing of base metals so as to free the surface of precious metals.

In a study by Park and Fray [77], aqua regia was used as a leachant and the ratio between metals and leachant was fixed at 1/20 (g/ml). Silver is relatively stable so the amount of about 98 wt% of the input was recovered without an additional treatment. Palladium formed a red precipitate during dissolution, which were consisted of $Pd(NH_4)_2Cl_6$. The amount precipitated was 93 wt% of the input palladium. A liquid–liquid extraction with toluene was used to extract gold selectively. Also, dodecanethiol and sodium borohydride solution were added to make gold nanoparticles. Gold of about 97 wt% of the input was recovered as nanoparticles.

A bench-scale extraction study was carried out on the applicability of hydrometallurgical processing routes to recover precious metals from PCBs in mobile phones [80]. An oxidative sulphuric acid leach dissolved copper and

part of the silver, an oxidative chloride leach dissolved palladium and copper, and cyanidation recovered the gold, silver, palladium and a small amount of the copper. To recover the metals from each leaching solution, precipitation with NaCl was preferred to recuperate silver from the sulphate medium, palladium was extracted from the chloride solution by cementation on aluminium, and gold, silver and palladium were recovered from the cyanide solution by adsorption on activated carbon.

Recently a general approach for recycling of scrapped PBC by hydrometallurgy has been proposed [81]. First the crushed PCB scraps are leached in the NH_3/NH_5CO_3 solution to dissolve copper. After the solution are distilled, the copper carbonate residue is converted to copper oxide by heating. The remaining solid residue after copper removal is then leached with hydrochloric acid to remove Sn and Pb. The last residue is used as a filler in PVC plastics which are found to have the same tensile strength as unfilled plastics, but has higher elastic modulus, higher abrasion resistance and are cheaper. Table 6 summarizes several hydrometallurgical recovery techniques of precious metals from e-wastes.

In a recovery of gold from computer circuit board research done by Sheng and Etsell, the computer circuit board scrap was first treated for 1 hour at 70°C in a nitric acid medium diluted with water in a 1:2 ratio.. Acid leaching step dissolves the base metals, thereby liberating the chips from the boards. After solid-liquid separation, the chips, intermixed with some metallic flakes and tin-oxide precipitate, were mechanically crushed to liberate the base and precious metals contained within the protective plastic or ceramic chip cases. The base metals in this crushed product were dissolved by leaching again with the same type of nitric acid-water solution. The remaining solid constituents, crushed chips and resin, plus solid particles of gold, were leached with aqua regia at various times and temperatures. Gold was precipitated from the leachate with ferrous sulphate [82].

Table 6 Summary of hydrometallurgical recovery of PMs from e-waste [51].

Investigators	Leaching agent	Process conditions	Recovered metals
Park and Fray [77]	Aqua regia	Ratio of metals to leachant = 1:20 g/mL	Au, Ag and Pd
Sheng and Estell [82]	HNO_3 (1st stage), epoxy resin (2nd stage), and aqua regia (3rd stage)	Extraction was carried out in the three stages (self-agitation)	Au
Quinet et al. [80]	H_2SO_4, chloride, thiourea and cyanide leaching	Leaching & metals recovery by cementation, precipitation, ion exchange and carbon adsorption	Au, Ag, Pd and Cu
Chielewski et al. [83]	HNO_3 and aqua regia	Roasting of e-waste in the presence of carbon; leaching with HNO3 and aqua regia; and solvent extraction with diethyle malonate	Au
Zhou et al. [84]	HCl, H2SO4 and $NaClO_3$	Combustion of e-waste at 400–500 °C followed by leaching	Ag, Au and Pd
Kogan [85]	HCl, MgCl2, H_2SO_4 and H_2O_2	Dissolution of e-waste in different solvents and leaching conditions; and recovery of metals in stages	Al, Sn, Pb and Zn (1st stage), Cu and Ni (2nd stage), Au, Ag, Pd and Pt (last stage)
Veit et al. [86]	Aqua regia and H_2SO_4	Mechanical processing and then dissolution of e-waste in different solvents	Cu

Mecucci and Scott [87]	HNO$_3$	Electrochemical deposition of Cu at cathode from solution	Pb and Cu

In a reclamation study of copper from PCB scraps, carried out by Veit et al [86], mechanical separation was firstly employed to concentrate fractions of mainly Cu, Pb and Sn metals. The copper content reached more than 50% in mass in most of the conductive fractions. At the second stage, the fraction concentrated in metals was dissolved with acids and treated in an electrochemical process in order to recover the metals separately, especially copper. The results demonstrate the technical viability of recovering copper using mechanical processing followed by an electrometallurgical technique. The copper content in solution decayed quickly in all the experiments and the copper obtained by electrowinning was above 98% in most of the tests.

2.2.3.1 Limitations of Non-Thermal Processes

Hydrometallurgical routes have been successfully used to recover PMs from e-waste. However, certain disadvantages that limit their application on the industrial scale. Some common limitations of hydrometallurgical methods for recovering PMs from e-waste are listed here [51]:

1. Overall, the hydrometallurgical routes are sometimes slow and time consuming and unfavourably impact recycling economy.

2. Mechanical processing of e-waste takes longer to reduce size for efficient dissolution. It is reported that 20% PM is lost by mechanical force during the liberation process that contributes to a significant loss in the overall revenue.

3. Cyanide is a dangerous leachant and should, therefore, be used with high safety standards because of the risks of contamination of rivers and seawater, especially near gold mines, which poses serious health risks to the inhabitants.

4. Halide leaching is difficult to implement due to strong corrosive acids and oxidizing conditions. Specialized equipment made of stainless steel and rubbers is required for leaching of gold using halide agents from e-waste.

5. The use of thiourea leachant is limited in gold extraction due to its high cost and consumption. Moreover, further developments are required to improve the current technology of thiourea-based gold leaching.

6. The consumption of thiosulfate is comparatively higher and the overall process is slower, which limits its application for gold extraction from ores as well as from e-waste.

7. There are risks of PM loss during dissolution and subsequent steps, therefore the overall recovery of metals will be affected.

2.3 Microwave Application

The most prominent characteristic of microwave heating is volumetric heating, which is quite different from conventional heating where the heat must diffuse from the surface into the material. Volumetric heating means that materials can absorb microwave radiation absorption homogeneously throughout the volume, and transfer the absorbed energy uniformly into the bulk via molecular or phonon vibrations, which is the cause of heating.

In microwave heating of dielectric materials such as polymers, glass and ceramics, the molecular motion is induced via vibrational of chemical bonds absorbing the electromagnetic radiation in the range of 300MHz to 300GHz.

"Microwave heating is usually applied at the most popular of the frequencies allowed for ISM (industrial, scientific and medical) applications, namely 915 MHz (896 MHz in the UK) and 2450 MHz" [49]. Domestic microwave ovens are a familiar example operating at 2450 MHz. The way in which a material will be heated by microwaves depends on its shape, size, dielectric constant and the nature of the microwave equipment used.

2.3.1 Loss mechanisms

The two main loss mechanisms for non-magnetic materials are dielectric (dipolar) losses and conduction losses. Conduction losses dominate in metallic, high conductivity materials and dipolar losses dominate in dielectric insulators. Magnetic materials also exhibit conduction losses with additional

magnetic losses such as hysteresis, domain wall resonance and electron spin resonance [88].

2.3.2.1. Losses due to the Oscillating Electric Field

In dielectric (electrically insulating) materials such as industrial ceramics, the microwave power absorbed by dielectric material is related with the complex permittivity ε, of a dielectric materials shown in eq.1.

$$\varepsilon = \varepsilon_0(\varepsilon' - i\varepsilon'')$$ (1)

Where ε_0 is the permittivity of free space (ε_0= 8.86 x 10^{-12} F/m), the real part ε' is the relative dielectric constant and the imaginary part ε'' is the effective relative dielectric loss factor. When microwaves penetrate and propagate through a dielectric material, the internal field generated within the effected volume induces translational motions of free or bound charges such as electrons or ions, and rotates charge complexes such as dipoles. "Inertial, elastic and frictional forces resist these induced motions and cause losses, a consequence of which is volumetric heating" [89]. The loss mechanisms are combined together for convenience to give the one electric loss parameter ε''. The loss tangent (tan δ) is also commonly used to describe these losses, which is defined in eq. 2.

$$\tan \delta = \frac{\varepsilon''}{\varepsilon'} = \frac{\sigma}{2\pi f \varepsilon_0 \varepsilon'}$$ (2)

Where σ is the total effective conductivity (S/m) caused by ionic conduction and displacement currents and f is the frequency. The power P that is absorbed per unit volume (W/m^3) of the sample at any instant of time can be described by eq.3.

$$P = \sigma |E|^2 = 2\pi f \varepsilon_0 \varepsilon' tan\delta |E|^2$$ (3)

Where $|E|$ (V/m) is the magnitude of the internal electric field. It has been assumed that the power is uniform throughout the volume and that thermal equilibrium has been achieved. This is not always the case and in addition E, tan δ, ε' and f are all in fact interdependent. However, it does provide a useful

approximation for the power absorbed and describes the basic relationships between the four variables. It can be seen that the power absorbed varies linearly with frequency, the relative dielectric constant, and the loss tangent, and varies with the square of the electric field.

2.3.2.2 Losses due to the Oscillating Magnetic Field

The permeability µ, of a material is defined as shown in eq.4.

$$B = \mu H = \mu_0 (H + M) \tag{4}$$

Where B is the flux density (T), H is the magnetic field intensity (A/m), M is the magnetisation (A/m) and μ_0 is the permeability of free space ($4\pi \times 10^{-7}$ H/m). For small fields the magnetisation is proportional to the field intensity which means that the initial relative permeability, μ_r, is a constant.

$$\mu_r = \frac{\mu}{\mu_0} = 1 + \frac{M}{H} = 1 + \chi \tag{5}$$

In an analogous way to the electric losses, the losses that occur due to a time varying magnetic field can be described by a complex relative permeability

$$\mu_r = \mu' - i\mu'' \tag{6}$$

where µ' is the permeability and µ" describes all the magnetic losses. An analogous magnetic loss tangent, tan δ_μ can also be defined where

$$tan\delta_\mu = \frac{\mu''}{\mu'} \tag{7}$$

In a similar way, the power P that is absorbed per unit volume (W/m^3) of the sample at a given instant in time can be described by eq. 8 [90]:

$$P = 2\pi f \mu_0 \mu'' |H|^2 = 2\pi f \mu_0 \mu'' tan\delta |H|^2 \tag{8}$$

It can be seen that the power absorbed varies linearly with frequency, permeability, and the loss tangent and with the square of the magnetic field.

"For a ferrite the loss tangent can be expressed in terms of three main contributors:

$$tan\delta_\mu = tan\delta_h + tan\delta_e + tan\delta_r \qquad (9)$$

in which $tan\delta_h, tan\delta_e$ and $tan\delta_r$ are the hysteresis, eddy current and 'residual' loss tangents respectively" [91]. The processes that contribute to the residual losses include the resonance losses and at high frequencies these will often dominate.

2.3.2.2.1 Hysteresis Losses

As a result of hysteresis, energy is dissipated as heat in a magnetic material as it travels around a B - H hysteresis loop. The hysteresis energy loss W_h per unit volume of material is

$$W_h = \oint BdH \qquad (10)$$

This loss is controlled by factors that control low frequency permeability and coercivity such as porosity, grain size and impurities as well as the intrinsic properties.

2.3.2.2.2 Eddy Current Losses

The conductivity of the material is important as it determines the extent of losses due to eddy currents. For ferrites, which have both magnetic and dielectric properties, the conduction mechanism is believed to be electron hopping between ions of the same type on equivalent lattice sites, known as valence exchange. Magnetite is one of the most conductive oxides with conductivity, σ, approximately 104 S/m at room temperature [91]. The skin depth, δ, in a conductive material is the depth of penetration of the magnetic field (as well as the current density) at which its value decreases by 1/e of its surface value. (This is similar to the penetration depth for a dielectric in which case it is the electric field that penetrates.) When the skin depth is large compared to the sample size the influence of eddy currents on the magnetic field is entirely negligible.

2.3.2.2.3 Domain Wall Resonance Losses

The resonance phenomena can in general be divided into two distinct mechanisms; domain wall resonance and those due to electron spin (ferromagnetic resonance, FMR). Domain wall resonance occurs at approximately one tenth of the frequency of FMR [91]. The small displacements of a pinned domain wall with an applied field introduces restoring forces. The other resonance phenomenon (in addition to domain wall resonance) is ferromagnetic resonance. This is the mechanism by which palaeomagnetic samples are demagnetised as the microwave energy first reduces the magnetic moment and then the energy is subsequently lost to the system as heat. The appropriate frequency of microwaves has to be used so that FMR can occur in all magnetic particles present in a particular sample. If only a few magnetic particles are in resonance, then higher powers will be needed for demagnetisation so that heat from the relaxation process along with any eddy current heating occurring can demagnetise the rest of the magnetic minerals.

2.3.3 Microwave Interaction with matter

Microwave heating of a material depends to a great extent on its `dissipation' factor, which is the ratio of dielectric loss or `loss' factor to dielectric constant of the material. The dielectric constant is a measure of the ability of the material to retard microwave energy as it passes through; the loss factor is a measure of the ability of the material to dissipate the energy. In other words, `loss' factor represents the amount of input microwave energy that is lost in the material by being dissipated as heat. Therefore, a material with high `loss' factor is easily heated by microwave energy.

Microwaves are reflected from the surface and therefore do not heat metals. Metals in general have high conductivity and are classed as conductors. Conductors are often used as conduits (waveguide) for microwaves. Materials which are transparent to microwaves are classed as insulators (Figure 10). Insulators are often used in microwave ovens to support the material to be heated. Materials which are excellent absorbers of microwave energy are easily heated and are classed as dielectrics.

	Material Type	Penetration
	Transparent (insulator) (no heating)	Total transmission
	Conductor (no heating)	None
	Absorber (dielectric) (Materials are heated)	Partial to total absorbtion
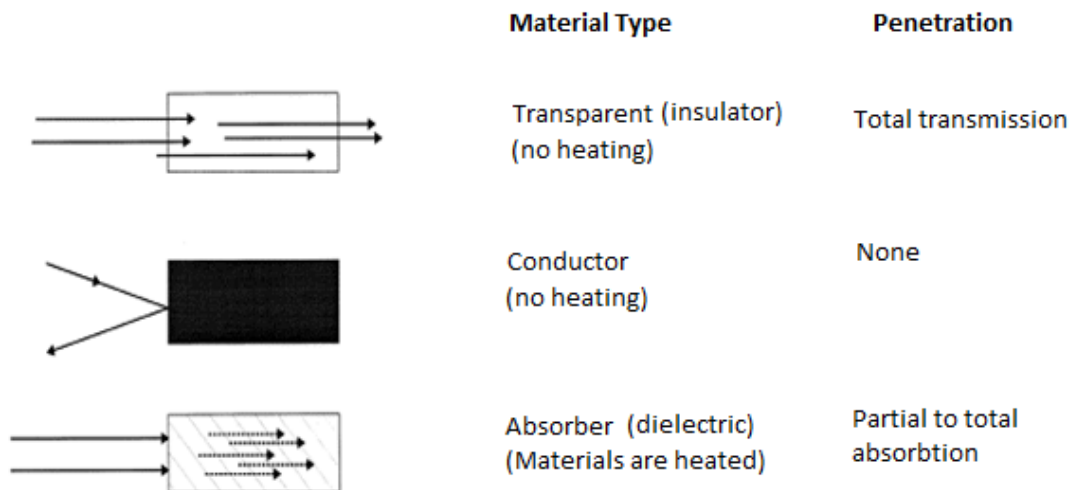
Figure 10 Interaction of microwave with materials *[49]*

The extent of microwave heating is also dependent on the size of the material; for example, a metal (i.e., conductor) in fine particle size can be heated by microwaves through a micro-arcing process. In addition, insulator materials can be heated with a microwave heat facilitator, such as, magnetite, silicon carbide or carbon. Microwave energy first heats the facilitator, which subsequently heats the insulator [92].

A microwave heating system is made up of four basic components: power supply, magnetron, applicator (i.e., oven) for the heating of the target material and waveguide for transporting microwaves from the generator to the applicator. Figure 11 shows a simplistic diagram of the microwave heating system.
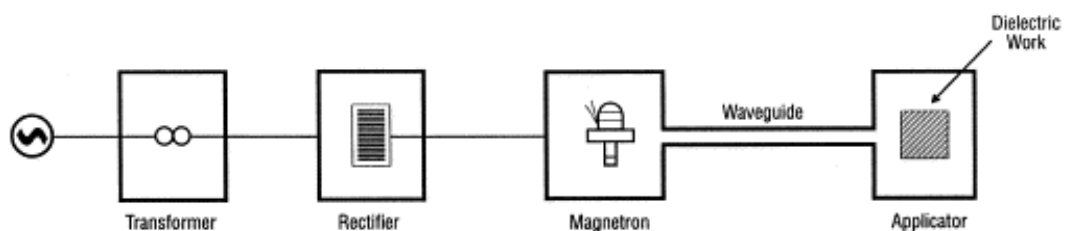
Figure 11 Microwave heating system *[49]*.

2.3.3.1 Microwave – Metal Interaction

Microwave heating in metals is different from that observed in dielectric materials. In dielectric materials, the microwaves penetrates and propagates through the material causing an internal electric field (E) within a specific volume, which in turn induces polarization and movement of charges. The resistance to these induced motions due to internal, elastic, and frictional forces attenuates the electric field. These losses result in volumetric heating. However, no internal electrical field is induced in metals. The induced electrical charge remains at the surface of the metal. Consequently, monolithic metals reflect microwaves; hence, no bulk absorption or heating occurs [93]. Microwave interaction with metals is restricted to its surface only. This depth of penetration in metals, also known as skin depth (δ), is defined as the distance into the material at which the incident power drops to 1/e (36.8 %) of the surface value. The skin depth is mathematically expressed as follows:

$$\delta = \frac{1}{\sqrt{\pi f \mu \sigma}} = 0.029\sqrt{\rho \lambda o} \qquad (11)$$

Where f is the microwave frequency (2.45 GHz), μ is the magnetic permeability, σ is the electrical conductivity, ρ is electrical resistivity, and λ_o is the incident wavelength (12.24 cm for 2.45 GHz waves). The skin depth in metals typically varies between 0.1 and 10 µm [94].

The microwave field allows the loosely bounded electrons to move and concentrate at surfaces, edges and points which results in two possible consequences; one is the heating effect since the induced eddy current on the metal surface is responsible for the Joule heating and the other is the discharge of the energy in the form of arcing [95].

For microwave heating of metallic materials, the skin depth of microwaves at a given frequency is an important parameter since it constitutes an upper limit to the thickness of the material which can be heated directly by microwaves. According to eq. 12, the skin depth depends on the electrical and magnetic properties (μ and σ) of the material. Materials with high conductivity and permeability present a lower penetration depth for a given frequency [96].

Joule heating is a process by which the passage of an electric current through a conductor produces heat. Induced eddy current created by incident microwaves creates an electric field that accelerates charge carriers (e.g. electrons) in the direction of the field by energizing them by gaining kinetic energy. When the energized electrons collide with the ions in the conductor, they scatter in order to conserve energy at the resonant condition. The inelastic scattering (no momentum conservation) of electrons causes them to lose the direction of alignment with the incident electric field of microwave, which results into heating. In other words, it is the surface or skin resistance effect of current which causes heating in metals.

"Microwave fields also alter the distribution of the positive and negative charges on the conducting material and an additional unique phenomenon may take place when metals with sharp edges, tips or submicroscopic irregularities are subject to microwaves irradiation. This phenomenon is usually an electric spark or an electric arc, generally known as discharge" [93]. Due to the very low skin depth of metals, the microwave-induced charges move entirely on the surface of the metal and accumulates at sharp edges, tips and submicroscopic irregularities, when they are subjected to high-frequency electromagnetic wave. When some accumulated charges attains enough kinetic energy, they jump out of the material, resulting in the ionization of the surrounding medium, producing an electric discharge. As a direct consequence of these discharges, considerable heat is produced, leading to the formation of high-temperature local hotspots.

Due to the much larger mobility of the electrons with respect to ions, the heating and arcing process is sustained by the electrons as the heavier ions cannot respond to the rapid oscillation field of the microwaves, and in turn attempt to dampen the induced vibration of molecules, which may be explained the linear harmonic oscillator model, which is given by:

$$v = \frac{1}{2}\pi \cdot \left(\frac{f}{\mu}\right)^{0.5} \tag{12}$$

where the harmonic oscillator frequency, υ (cm^{-1}) is inversely related with square root of the size of the ions, defined by the reduced mass (μ) and directly related with the cation-anion force constant (f) of a linear harmonic oscillator. The energy dissipation is therefore determined by heat conduction by phonon (linear harmonic oscillator), which may be resonantly absorbed in the microwave.

When the resonant absorption by molecules (e.g. oscillator) gains energy by resonant absorption and exceeds the activation threshold to break the bond during the microwave heating, then the ionic species may momentarily leave the surface and cause surface ionization, and in this situation the relaxation of lost charge back into the surface produces plasma at the surface, which may be visible during the microwave heating of metallic materials. Plasma is an ionized gas consisting of positive ions and free electrons in proportions resulting in more or less no overall electric charge, typically at very high temperatures. Since the plasma represents a highly energetic state of matter, the relaxation of charged matter in plasma produce photons, which may be visible with naked eye. The continuum of plasma induced relaxation is maintained, as long as the microwave in on and this is particularly important when examining the chemical activation process in the microwave.

Wang et al reported the heat produced by discharge can melt the metal terminals and the energy conversion efficiency from the electric energy to heat by microwave-metal discharge can amount to 20%–60% during the microwave irradiation process [97, 98]. One the other hand, at a microscopic level, these discharge are actually plasma [93, 99].

Hussain et al. found the interaction of microwaves with iron led the temperature to rise up to 1100–1200 °C and even up to the melting point of iron [100], which is currently utilized in metal production on a pilot-scale.

Chen *et al.* described that audible and bright discharge accompanied by solvent decomposition and formation of considerable amounts of graphitized material were observed by adding metal particles of Mg, Zn, Cu to liquid benzene under microwave irradiation. "Since benzene is completely

microwave transparent, the decomposition reaction is attributed to microwave-metal discharge, indicating microwave heating can be extended into more fields through the introduction of electric discharge or plasma formation thus promoting the chemical reactions in microwave transparent solvents". [101].

2.3.3.2 Microwave heating of metal powders (Sintering)

The use of microwaves to process absorbing materials was studied intensively in the 1970s and 1980s, and has now been applied to a wide variety of materials.

In the study by Roy et al. [102], A wide range of standard powdered metals from commercial sources were sintered, using a 2.45 GHz microwave field, yielding dense products with better mechanical properties than those obtained by conventional heating. Powdered metal components of various alloy compositions, including iron and steel, copper, aluminium, nickel, molybdenum, cobalt, tungsten, tungsten carbide and tin, and their alloys, were sintered to obtain essentially fully dense bodies. All standard 'green' parts metal powders were cold pressed with a little addition of organic binder. The typical size range was 2–5 cm in the largest dimension, with a wide variety of rectangular and cylindrical cross-sections, including typical toothed gears in the 1–4-cm range. The microwave generators were operated at a frequency of 2.45 GHz, with power output in the range 1–6 kW, in both single- and multi-mode operation. Inside a typical microwave cavity was an alumina tube surrounded by ceramic fiber (typically mullite) insulation. The primary function of insulation is to preserve the heat inside the tube. At higher temperatures (above about 1,400 $^{\circ}$C) ZrO_2 insulation was used, though it is much more expensive. The 'green' commercial powdered-metal bodies were introduced into the microwave chamber and heated at 1,100 –1,300 $^{\circ}$C typically for times ranging from 5 minutes to one hour in flowing forming gas (N_2 and H_2) or in a pure hydrogen atmosphere. In a large number of cases, similar samples had been heated in conventional furnaces for direct comparison of the properties. The first few runs produced highly sintered bodies in a very short period of time. This was achieved in a controlled-atmosphere microwave system with 2.45 GHz frequency and a maximum 6 kW power: but only 1.4 kW of power

was used to attain the desired sintering temperatures. Figure 12 shows a diagram of a microwave system for sintering powdered metal samples studied by Roy et al. and Table 7 compares conventional sintering process to microwave sintering.
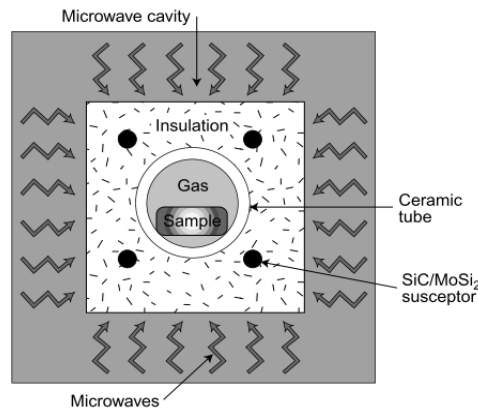
Figure 12 *Diagram of microwave system for sintering of powdered-metal samples. The system consists of a 2.54 GHz microwave oven (cavity) and a ceramic (alumina) tube which is inserted into the cavity and surrounded by ceramic fiber blocks. Inside the insulation, SiC or $MoSi_2$ susceptor rods are inserted. The sample is placed inside the ceramic tube. The system is capable of achieving temperatures up to 1,600 °C, and any desired atmospheres (such as H_2, N_2, Ar) can be used* **[102]**.

Table 7 Properties of microwave and conventionally processed powder metal samples. MW, microwave processed; conv., conventionally processed. The modulus of rapture (MOR) of most microwave-processed samples is higher than that of the conventional samples. The densities of many microwaved processed samples are also higher than those of conventional samples.

Sample	Process	Green Density (g/cm^3)	Sintered density (g/cm^3)	Rockwell hardness	MOR (10^3 lb/in^2)
Fe-Ni	MW	7.11	7.15	B82	177
(industrial part)	Conv.		7.10	B77	109
Fe- Cu	MW	6.81	7.17	B96	142
(industrial part)	Conv.		6.84	B80	118
Fe-Cu	MW	6.95	6.96	B75	134
(lab. Sample)	Conv.		6.95	B64	122

2.3.3.3 Microwave Heating of thin metal films

Bulk metal is excellent reflector of microwave energy and in general is not heated significantly by microwave. Therefore, few application have been conducted so far on heating of bulk metal. On the other hand, recently there has been much interest in microwave heating and sintering of metal powder. This is because metal powder has a large specific surface area compared to bulk metal. Thin metal film is similar to metal powder from a view point of specific surface area. However, microwave characteristics of thin metal film may differ from those of metal powder. For example, as the thickness of a thin metal film is decreased to that of a few atomic layers conductivity drops below that of the metal bulk.

Sueyoshi and Kakiuchi investigated the heating of gold thin films, and it was found out that thin gold film is continuously heated during microwave irradiation, regardless of the history of thin film fabrication. In the experiment, Thin Au film was prepared by sputtering and evaporation methods with a quartz substrate, followed by microwave irradiation in air (frequency of microwave: 2.45 GHz, incident flux of microwave: 563W, irradiation time: 600 s). As a result, it was confirmed that microwave heating of thin Au film is feasible. The growth of crystalline and particles due to microwave heating was confirmed from AFM observation. Microwave heating depends on the amount of microwave absorption on a thin Au film, which is related to the thickness and microstructure of the thin Au film. The rate of temperature rise depends on the ratio of a thickness to resistivity of thin Au film [103].

Figure 13 indicates the rate of change of temperature of gold thin films during microwave irradiation, for both sputtered and evaporated samples with 34.6nm and 29.5nm thickness respectively showing exactly similar heating rate patterns.
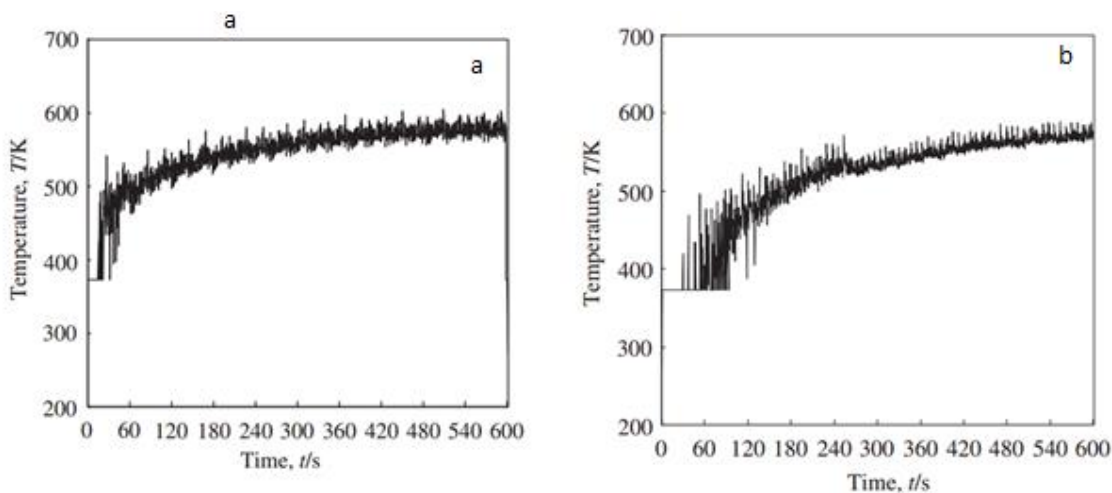
Figure 13 *Change in temperature of sputtered thin film of with a thickness of 34.6 nm during microwave irradiation. b) Change in temperature of evapourated Au film with a thickness of 29.5 nm during microwave irradiation.***[103]**

2.3.3.4 Microwave assisted dissolution

Microwave energy has the potential for application in mineral treatment and metal recovery processes such as heating, drying, grinding, leaching, roasting, smelting, carbothermic reduction of oxide minerals, pretreatment of refractory gold concentrate or ore, spent carbon regeneration and waste management. Usually, microwave energy is more expensive than electrical energy, mainly due to the low conversion efficiency from electrical energy. However, the efficiency of microwave heating is often much higher than conventional heating and overcomes the cost of the energy. Microwave heating is material specific, offers a faster heating rate and consequently a faster dissolution rate than conventional heating [49].

In a study by Kuo et al. [50], various leaching technologies were applied to extract heavy metals from sludge from the printed circuit board process. These methods included traditional acid extraction (TAE) and microwave assisted treatment (MAT). The target heavy metal was copper. Experiments were performed to determine the leaching efficiency by changing operating conditions, including acid type and concentration, leaching time, microwave

power, and solid to liquid ratio (S/L). The TAE method demonstrated that copper leaching from a sludge of fine particle sizes (d<150 µm) was 74 % efficient at an S/L of 1/6, a leaching time of 18 hours, using nitric acid in the leaching solution. Alternatively using a microwave assisted irradiation of 800W and 400W, the leaching time was 30 mins, with leaching efficiency of 93% and 77 %, respectively. The Microwave assisted treatment procedure reduced the leaching time and improved the leaching efficiency above that obtained by TAE. Table 8 and Table 9 gives more comparative results between the two methods when parameters like type of leachant, particle size and solid-liquid ratio are altered.

Table 8 Comparisons with TAE and MAT of leaching efficiency. TAE, Traditional acid extraction; MAT, Microwave-assisted treatment; d < 150 µm; S/L (solid to liquid ratio): 1/6 **[50]**.

Leachant	TAE		MAT	
	Leaching time (h)	**Copper leaching (%)**	**Leaching time (min)**	**Copper leaching (%)**
Nitric Acid	48	81	10	85
Sulphuric Acid	48	76	10	79

Table 9 Comparisons with size of sludge and leachant of leaching copper during different leaching time. Microwave power: 800 W; S/L: solid to liquid ratio **[50]**.

	Leaching time (min)	Copper leaching (%) at S/L: 1/20		Copper leaching (%) at S/L: 1/6	
		d<9.5mm	**d<150µm**	**d<9.5m m**	**d<150µ m**
Nitric Acid	5	78	85	63	74
	30	96	96	93	96
Sulphuric Acid	5	73	74	92	48
	30	95	94	92	93

From Table 8, for a leaching efficiency of more than 80 % using HNO_3, a leaching time of 48 hours is needed with the TAE method as compared to a leaching time of 10 minutes when microwaves are used in a MAT method. The time saved is comparable when sulphuric acid is used as the leachant but with a slightly lesser leaching efficiency. Table 9 compares the leaching efficiency in an 800 W MAT method when the particle size and the S/L ratio are altered. Leaching efficiency is increased when the particle size and the S/L ratio are both decreased.

The decomposition of pyrite and marcasite in a nitric acid medium heated by microwave energy has been investigated [104]. It was found that microwave exposure could effectively improve the leaching kinetics of both minerals. Marcasite had a substantially higher decomposition rate than pyrite. The decomposition rate increased with an increase in leaching temperature and concentration of acid and with a decrease in particle size. Only 5 – 7 % of the dissolved Sulphur was transformed into elemental Sulphur. A kinetic study showed that the decomposition of both minerals was controlled by chemical reactions on the surfaces of particles.

The effect of microwave on the rate of dissolution of metal oxide (CeO_2 and CO_3O_4) in 7 M nitric acid was investigated to elucidate whether microwaves have a non-thermal effect upon this type of dissolution reaction. From preliminary experiments performed with conventional heating, the activation energy of the dissolution process was found to be approximately 102 kJ/mol and 110 kJ/mol for CeO_2 and Co_3O_4 respectively. The results obtained showed that the action of the microwaves was purely thermal in nature and thus did not provide any detectable specific activation. However, the use of microwaves was highly interesting because it provided a convenient way of transferring energy to a given system and, chiefly, gave rise to an apparent acceleration of the chemical reactions as a result of a 'superheating' phenomenon [48].

In a study by Hinds et al. [105], a closed-vessel microwave dissolution procedure has been shown to reduce the time and amount of aqua regia (3 parts HCl + 1 part HNO_3) required to dissolve platinum in comparison with conventional open-vessel hot-plate dissolution. Four types of platinum

samples were used in the study. These were termed: foil (0.2 mm thickness); chunk (1 mm thickness); wire (0.5 mm diameter); and scrap (variously shaped and sized bits). The results are summarized in Table 10. From the results, it is apparent that microwave dissolution takes between 2 and 3 hours despite wide variations in platinum sample type and mass. Hot-plate dissolution appears to be strongly affected by sample shape and only somewhat affected by sample mass. Nevertheless, it is evident from the study that, in general, microwave sample dissolution requires less time than hot-plate dissolution and is independent of sample mass and shape. Chunk samples required 50% more time on the hot-plate than in the microwave system. The volume of aqua regia needed was twice (20 cm^3) that used in the microwave system (10 cm^3).

Table 10 A comparison of conventional hot-plate dissolution and microwave assisted dissolution of Pt in aqua regia. Effects of sample shape and size on dissolution time **[105]**.

	Samples	Mass (g)	Dissolution time	
			Hot plate (h)	**Microwave (h)**
1	Foil (0.2 mm thickness	0.1	3.4	2.2
		0.2	2.1	2
2	Chunk (1 mm thickness)	0.2	4.5	3
3	Wire (0.5 mm diameter)	0.1	5	2
4	Scrap (various shaped and sized bits)	0.3	>22	2
		0.4	22	2
		0.5	23	2
		0.7	24	2
		1	28	2

2.4 Ionic Liquids

Ionic liquids are composed entirely of ions. For example, molten sodium chloride is an ionic liquid; in contrast, a solution of sodium chloride in water (a

molecular solvent) is an ionic solution. The term "ionic liquids" has replaced the older phrase "molten salts" (or "melts"), which suggests that they are high-temperature, corrosive, viscous media (like molten minerals). Ionic liquids can be liquid at temperatures as low as −96 °C. Furthermore, room-temperature ionic liquids are frequently colourless, fluid, and easy to handle.

As noted above, ionic liquids have no detectable vapour pressure, and therefore contribute no VOCs to the atmosphere. But that is not the only reason for using ionic liquids. There are numerous potential possible binary and ternary ionic liquids. This diversity enables the solvent to be designed and tuned to optimize yield, selectivity, substrate solubility and product separation. Ionic liquids can also be highly conducting.

2.4.1 Ionic Liquids as electrolytes

From Table 11, the specific conductivity of aqueous KOH (29.4 wt%) solution, applied in alkaline batteries, is 540 mS/cm. The electrolyte applied in lead-acid batteries, 30 wt% aqueous H_2SO_4, shows a conductivity at the level of 730 mS/cm. However, non-aqueous solutions show one order of magnitude lower conductivity. One of the most conductive is Et_4NBF_4 solutions, in acetonitrile, for application in double-layer capacitors, characterised by conductivity of 60 mS/cm. Lithium ion containing solutions, for use in lithium-ion batteries, show a conductivity at the level of 10 mS/cm, similar to that characteristic for some ionic liquids. The conductivity of a solution of $LiPF_6$ (1 mol/dm^3) in a mixture of ethylene carbonate with 1,2-dimethoxyethane (EC+DME) is 16.6 mS/cm. A dilution of neat ionic liquids with solvents (molecular liquids) also brings about an increase in conductivity. For example, the specific conductivity of neat [EtMeIm][BF_4] is 14 mS/cm, while its 2 mol/dm solution in acetonitrile shows a conductivity of 47 mS/cm. This is not unexpected, as an ionic liquid + molecular liquid mixture is a solution of a salt in a solvent, and therefore, ions are separated by solvent neutral molecules. However, at high salt concentrations all solvent molecules are involved in the ions primary salvation shell and the resulting system, called 'solvent in salt solution' may show properties rather characteristic for ionic liquids than that typical of classical solutions [33].

Table 11 Examples of conductivity of classical electrolytes in various electrochemical applications [33].

Electrolyte	Solvent	σ [mS/cm]	Application
H_2SO_4 (30 wt.%)	H_2O	730	Lead-acid battery
KOH (29.4 wt.%)	H_2O	540	Alkaline battery
NH_4Cl (25 wt.%)	H_2O	400	Leclanche battery
$[Et_4N]^+[BF_4]^-$ (1 mol/dm^3)	AN	60	Double-layer capacitor
$LiN(CF_3SO_2)_2$ (1 mol/dm^3)	EC+ DME (1:1)	13.3	Lithium-ion battery
$LiN(CF_3SO_2)_2$ (1 mol/dm^3)	EC+ DC (1:1)	6.5	Lithium-ion battery
$LiCF_3SO_3$ (1 mol/dm^3)	EC+ DME (1:1)	8.3	Lithium-ion battery
$LiPF_6$ (1 mol/dm^3)	EC+ DME (1:1)	16.6	Lithium-ion battery
$[Et_4N]^+[BF_4]^-$ (0.65 mol/dm^3)	PC	10.6	Double-layer capacitor
$[EtMeIm]^+[BF_4]^-$ (2 mol/dm^3)	AN	47	Double-layer capacitor
$[EtMeIm]^+[BF_4]^-$ (2 mol/dm^3)	PC	16	Double-layer capacitor

2.4.2 Ionometallurgy

An innovative approach as alternative to conventional mineral acid leaching that can have significant impact to waste valorisation is ionometallurgical leaching. Ionometallurgy is the term that describes the use of ionic liquids as solvents in the field of metal processing. ILs, are room temperature molten salts, constituted by ions, generally an organic cation and an inorganic/organic anion. These solvents have superior properties against organic solvents such as negligible vapour pressure, low volatility, wide electrochemical window, non-flammability and high thermal stability. From the vast number of combinations of the cation and anion during synthesis, ILs properties can be tuned for the needs of the application rendering them as designer solvents. As such ILs have a wide range of application in extractive metallurgy since they can be used either as electrolytes for electrodeposition of reactive metals, as solvents for liquid-liquid metal extraction or separation as well as lixiviants [106].

Several ILs have been studied as leaching agents in hydrometallurgical processes. In aqueous solutions, the oxidation of metals from their elemental state is usually carried out using strong oxidising agents such as sulphuric

acid, nitric acid or aqua regia. The digestion of metal oxides also requires the use of strong acids or bases, such as sulphuric acid or ammonia. One of the major issues associated with digestion is the solubility of the metals and metal oxides in the chosen ionic liquids. Very little work has been carried out into the factors that control solubility, mainly due to the lack of consistent data in a single ionic liquid with a given series of comparable solutes.

One of the first studies of the digestion of metal salts in ionic liquids was by Dai et al., who studied the dissolution of UO_3 in imidazolium chloroaluminate melts. The solubility of UO_3 was found to be within the range of 1.5 to 2.5 x10^{-2} mol dm^{-3} in Lewis basic melts and the main species was $[UO_2Cl_4]^{2-}$. Although chloroaluminate liquids might not be the most suitable choice for digestion because of their high water sensitivity and high initial metal ion concentration, they have provided the catalyst for all subsequent novel solvatometallurgical processes [107].

Huang et al., used an imidazolium $[PF_6]^-$ salt to study the recovery of nano-scale zinc particles from phosphor ashes [108]. Classical solubility models are more difficult to apply to these types of processes due to the current lack of data on the species formed. Speciation of metals in solution is a complex issue which is largely dependent on the Lewis acidity of the metal and the Lewis basicity of any possible ligands that are available in the ionic liquid. To determine the speciation of metals in ionic liquids a wide range of techniques have been previously employed, most of which have largely been centred on EXAFS, Raman, FAB-MS and UV-visible spectroscopy [109, 110].

The solvation of metal ions in ionic liquids is still poorly understood, mainly because of the complexity of the interactions between the solute and ionic components. Polarity parameters have been measured for ionic liquids [111, 112] and have been shown to be good at predicting kinetics of reactions in ionic liquids where hydrogen bonding interactions dominate [113]. However, these parameters are not an accurate measurement of Lewis acidity and basicity and are therefore less informative for metal oxide solubility.

The dissolution of metal oxides in an acid-saturated ionic liquid, followed by selective stripping of the dissolved metal ions to an aqueous phase is

proposed as a new ionometallurgical approach for the processing of metals in ionic liquids. The hydrophobic ionic liquid trihexyl(tetradecyl)phosphonium chloride (Cyphos IL 101) saturated with a concentrated aqueous hydrochloric acid solution was used to dissolve CaO, NiO, MnO, CoO, CuO, ZnO and Fe_2O_3. It was found that nickel(II) and calcium(II) could be separated from all other transition metals present in the ionic liquid phase by stripping at high chloride concentrations [114].

Extensive studies into the solubilities of a range of metals and their salts in a variety of Deep Eutectic Solvents (DESs) have been made by Abbott et al. [115]. These novel solvents have the ability to dissolve a wide range of metal oxides and the solubility of 17 metal oxides in the elemental series Ti to Zn has been reported in three different DES based on choline chloride [116]. A selection of this data is shown in Figure 14, with comparison made to the solubility of metal oxides in hydrochloric acid (HCl). Although HCl still provides the most solubility for the majority of the metals, it can be seen quite clearly that for some metals DESs have comparable solubility strength. Due to the high anionic concentrations in DES, these liquids will often form complexes with the metal ions in solution [109]. By judicious choice of the hydrogen bond donor, selectivity for the extraction of specific metals from a complex matrix can then be obtained [117].
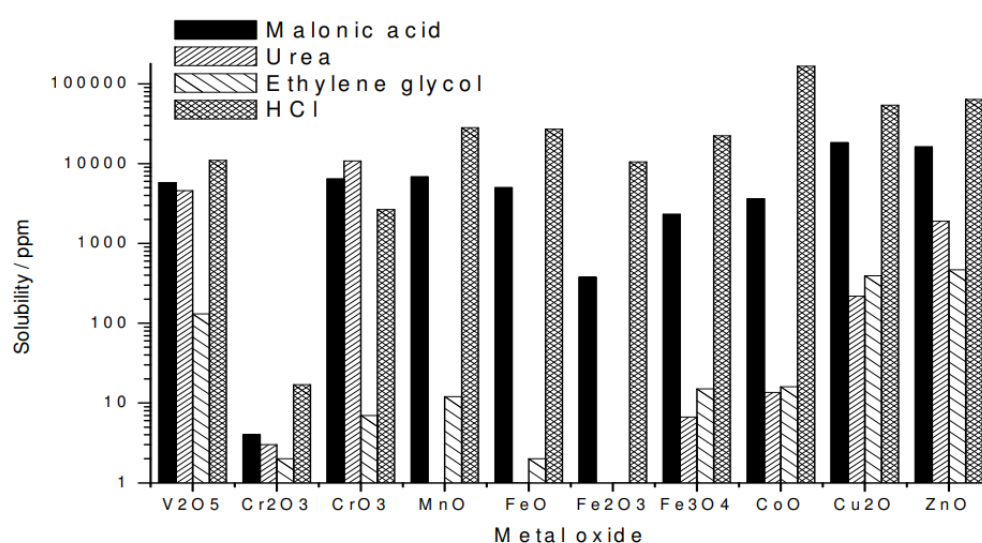
Figure 14: Graph showing the solubility of a range of d-block metal oxides dissolved in three different DESs, compared to HCl [118].

The recovery of gold and silver from ore in an ionic liquid is reported for the first time by Whitehead et al. in 2004 [41]. 1-butyl-3-methyl-imidazolium hydrogen sulphate ionic liquid bmim[HSO$_4$] was employed, with iron (III) sulphate oxidant and thiourea added. Selective extraction of gold (Au) and silver (Ag) from powdered ore (of dominantly chalcopyrite/ pyrite/ pyrrhotite/ sphalerite mineralogy) was achieved at room temperature in 50 hours at ≥85% and ≥60% respectively, with other lower-value metals present in the ore (Cu, Zn, Pb, Fe) extracted to only low percentages. Gold extraction was similar to that achieved in aqueous H$_2$SO$_4$/ thiourea/ Fe$_2$(SO$_4$)$_3$, and silver extraction was significantly better. Moreover, the ionic liquid can be recycled following selective stripping of gold and silver on activated charcoal, with reuse in at least four successive treatments leading to neither ionic liquid degradation nor any loss in extraction efficiency.
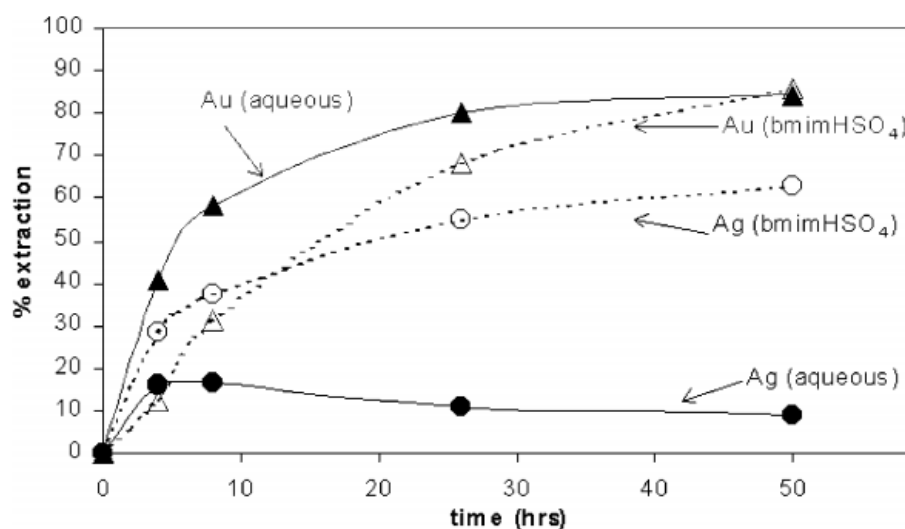
Figure 15 *Comparative leaching of gold and silver from ore using aqueous H$_2$SO$_4$ or bmim+HSO$_4$- in the presence of Fe(III) and thiourea **[41]**.*

As illustrated in Figure 15, for the extraction of gold, an equivalent extraction is achieved for the bmim[HSO$_4$] leaching system (86 % extraction) compared with the aqueous system (85 % extraction). For silver, the aqueous system gives a very poor result with a maximum extraction of less than 20%. The concentration of silver in the aqueous system reaches a maximum before

slowly decreasing over time. The bmim[HSO$_4$] leaching system proved to be more promising for the recovery of silver from the Perseverance ore, with high selectivity for silver giving a 60% extraction at 50 hours. Also, no decrease in the concentration of silver was observed during the extraction time frame.

2.4.3 Ionic liquid used to dissolve PCB substrate

A feasibility study was conducted to dissolve bromine epoxy resins of waste PCBs using the ionic liquid, 1-ethyl-3-methylimizadolium tetrafluoroborate emim[BF$_4$], a non-aqueous green solvent for recovering copper foils and glass fibres [119, 120]. Experimental results indicated that there was initial delamination when the PCBs were heated in the IL at 240 ^{o}C for a duration of 30 min (Figure 16). When temperature was increased to 260 ^{o}C for a duration of 10 min, the bromine epoxy resins substrate of the PCBs were throughout dissolved in the IL and the separations of copper foils and glass fibres from PCBs were completed (Figure 17).

Figure 16 *Photograph (A) and metallographic photograph (C) of cross section untreated WPCBs as well as photograph (B) and metallographic photograph (D) of cross section the WPCBs treated by the emim[BF$_4$] at 240°C after 30 min* ***[119]***.
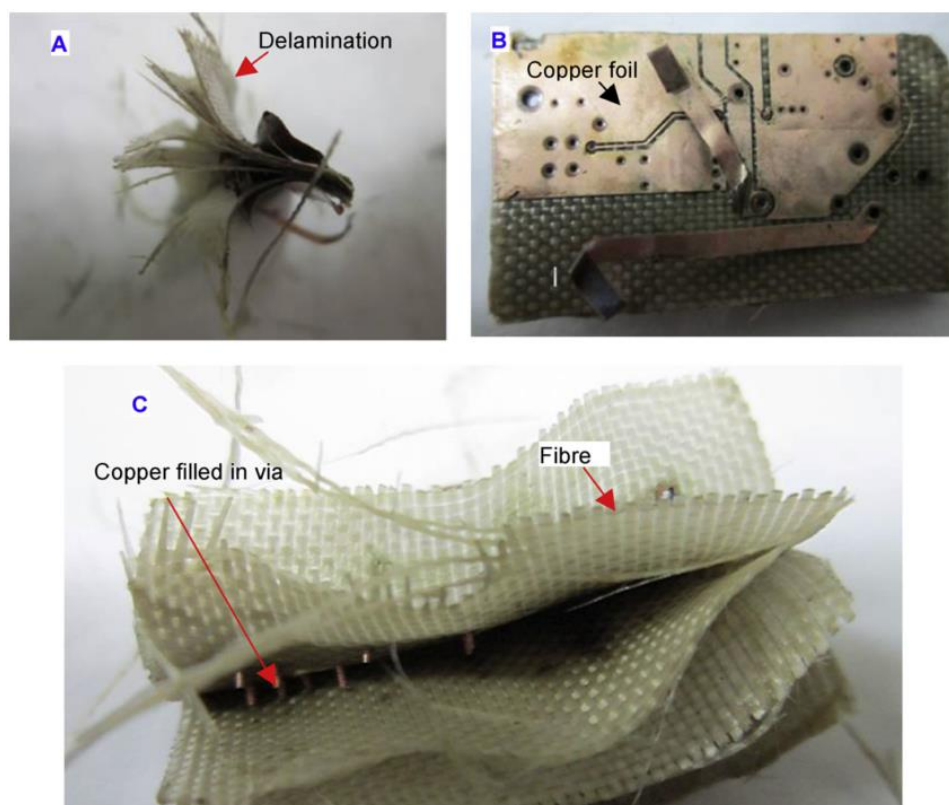
Figure 17 Photograph of waste PCB treated by the emim[BF$_4$] at 260°C after 20 min [119].

2.4.4 Conductivity and viscosity in ionic liquids

Recently research shows that ionic liquids could have conductivities and viscosities approaching those of aqueous electrolyte solutions [121], although to date few studies have been carried out to comprehend the fluid properties of these media. In contrast numerous models have been developed to account for the motion of ions in high temperature ionic liquids (molten salts), which are based on the observation that the liquid volume increases upon melting and the free volume of the liquid increases. These models can in general be split into three types: Schottky-vacancy models, where a lattice exists in the fluid and the ions influence the sizes and positions of the vacancies, hole theory models, where the vacancies are randomly distributed and gas-oriented models, where the ions are assumed to occupy a space surrounded by a free volume [122-124]. Each of these models has limitations, but the most

commonly applied model is the Hole theory approach of Fürth because of its more quantifiable analysis [125].

Hole theory assumes that on melting, an ionic material contains empty spaces that arise from thermally generated fluctuations in local density. The holes are of random size and location and undergo constant flux. The radius of the average sized void, $\langle r \rangle$, is related to the surface tension of the liquid, γ, by Equation 13 [126]

$$4\pi \ \langle r^2 \rangle \ = 3.5 \text{kT}/ \gamma \qquad (13)$$

Where k is the Boltzmann constant and T the absolute temperature. "It has previously been shown that the average size of the holes in a molten salt (1.5–2.5 Å) is of similar dimensions to that of the corresponding ion (1–2.6 Å) [126]. Hence, it is relatively easy for a small ion to move into a vacant site and accordingly the viscosity of molten salts is similar to that for molecular liquids (1–5×10^{-3} Pa s). The surface tension for room temperature ionic liquids is comparable with high-temperature fused salts and Equation (1) shows that the average size of holes will be smaller in the lower temperature system. This, coupled with the larger ion size will make ion mobility considerably more difficult and this explains why viscosities of room temperature ionic liquids can be as high as 10^1–10^3 Pa s" [123].

To quantify the viscosity of ionic fluids it is necessary to account for these differences between ion and void dimensions. To date, attempts have only been made to quantify the mobility of ions in terms of thermodynamic constrains on the formation of cavities [127]. In the current analysis it will be assumed that cavities are not formed; they simply exist and move in the opposite direction to solvent ions/molecules. At any moment in time a fluid will have a given distribution of cavity sizes and an ion will only be able to move if there is a cavity volume of suitable dimensions adjacent to it to permit motion. It can therefore be assumed that at any moment in time only a fraction of solvent molecules is capable of moving and this gives rise to the inherent viscosity of the fluid. It is, therefore, necessary to determine the distribution of

hole sizes to determine the likelihood of movement. The probability, P, of finding a hole of radius, r, in a given liquid is given by Equation (14).

$$Pdr = \frac{16}{15\sqrt{\pi}} a^{7/2} r^6 e^{-ar^2} dr \tag{14}$$

Hence the probability of finding a hole of sufficient dimensions to accommodate an ion can be obtained by integrating Equation (14) over the limits $r=R_{+/-}$ to $r=\infty$. This was achieved using commercial mathematical software[128] and yielded Equation (15)

$$P = 0.602a^{7/2} \left[-\frac{r^5 e^{-ar^2}}{2a} + 2.5 \left\{ -\frac{r^3 e^{-ar^2}}{2a} + \frac{1.5\left(\frac{re^{-ar^2}}{2a} + \frac{0.443erf\sqrt{ar}}{a^{\frac{3}{2}}} \right)}{a} \right\} /a \right] \tag{15}$$

Figure 18 shows the probability distribution for NaCl at 1000 K and butyl methyl imidazolium (bmim) [PF$_6$] cation at 298 K, and also shows the average ion radius ($R_{+/-}=(R_+R_-)^{1/2}$) as vertical lines in each distribution. It is immediately apparent that the probability of finding an ion-sized hole in a high temperature salt is orders of magnitude larger than in its low temperature counterpart.
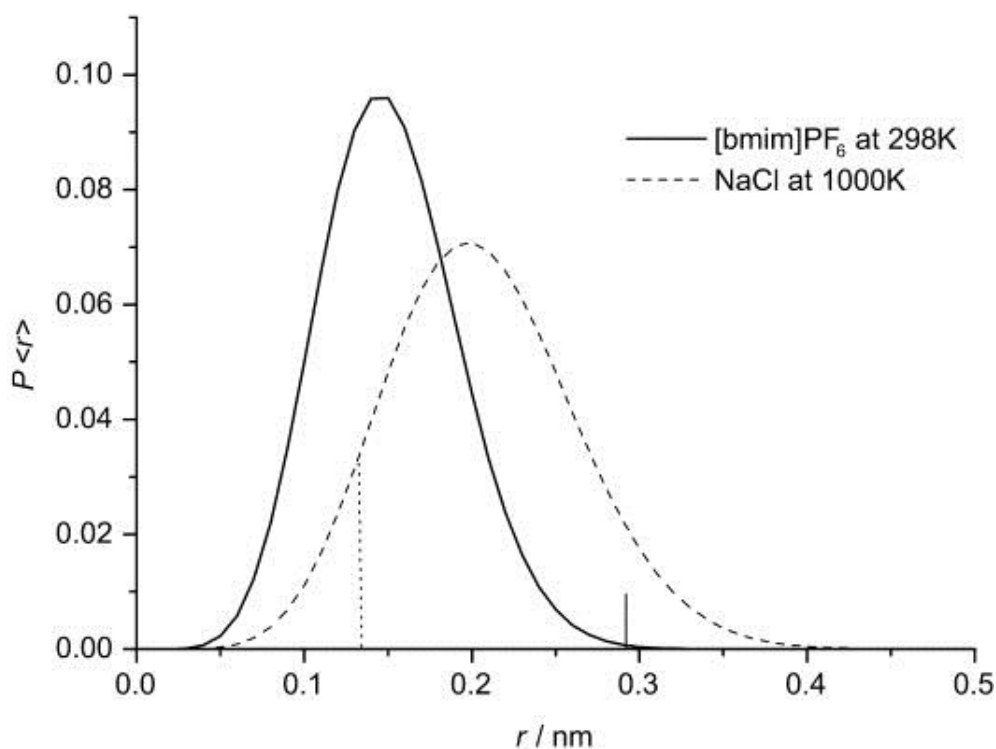
Figure 18: Probability distribution for holes in [bmim]PF$_6$ at 298 K and NaCl at 1000 K. Vertical lines show the average ionic radius of the ions.

2.5 Research Objectives

There exit several e-wastes recycling and treatment techniques, all of which are too expensive to run, polluting to the environment or both. Developing countries are the most venerable as they do not have adequate resources to treat these electronic waste. PCBs forms an integral part of all electronic wastes because they contain or house most metals such as Zn, Cu, Pb, Cd, Ni, etc which contribute to environmental pollution and poses severe risks to health.

The main objective of this research project is to develop a novel technique for the treatment of PCB finger wastes that adapts the use of an ionic liquid as leaching solvent and microwaves to assist leaching reactions. Goals of my PhD are divided into two high-level objectives: a) design a process for preventing the release of toxic and harmful gas; and b) consider process safety

and design considerations that will enable application in LMICs; e.g. in Ghana. Specific objectives include:

1.   Application of low-cost Ionic liquids in the recycling of PCBs: Since the ionic liquids actually exhibit good thermal stability with onset of decomposition well above 200 $^{\circ}$C [32], the main aim in this thesis is to demonstrate the use of a suitable ionic liquid for recycling of gold, nickel and copper from PCB fingers. The demonstration of proposed approach will remove the risk of toxic and hazardous fume generation.

2.   Once an ionic liquid is identified for reclamation of valuable metals from PCB, our goal is to demonstrate the reuse of derived ionic liquids for the extraction of valuable metals. Under this objective the goal is to demonstrate the regeneration of selected ionic liquid for enhancing the opportunity for low-cost process development. By demonstrating this objective, the risk of reuse of mineral acids and wastes generated from such acids will be reduced significantly.

3. For enhancing process efficiency, energy saving is essential and this true in LMICs where the cost is high. For this reason, the use of microwave energy for delivering power efficiently during the leaching process will be analysed. Especially, the efficient use of microwave energy will be demonstrated by using the domestic ovens, operating at low power (<400 watt specification). In this respect the use of ionic liquid and mineral acid media will be compared for analysing the extraction efficiency of three main metals (gold, nickel and copper). The comparison of power consumed using domestic microwave and hot plate will be compared in this thesis.

4. The penultimate objective is to compare the salient chemistry of extraction process of metals (gold, nickel, and copper) using mineral acid and ionic liquid when irradiated with domestic microwave.

5. To analyse the product derived after electrowinning of metals from the leachate solution and reclamation. This step is important for the economic analysis.

Chapter 3

Experimental

3.1 Materials and Sample Preparation

3.1.1 PCB fingers

PCBs exist in all electrical and electronic appliances. In this study however, waste computer PCBs, commonly referred to as PC cards, were used due to their availability and abundance. Broken down computers were collected from the inventory of broken components at the IT center of School of Chemical and Process Engineering (SCAPE) at the University of Leeds, UK. The IT center at SCAPE provides service and repairs to computers that belong to the university. From time to time broken down and faulty computers that end up there are collected by a third party for recycling.

a) A computer card	b) PCB finger samples
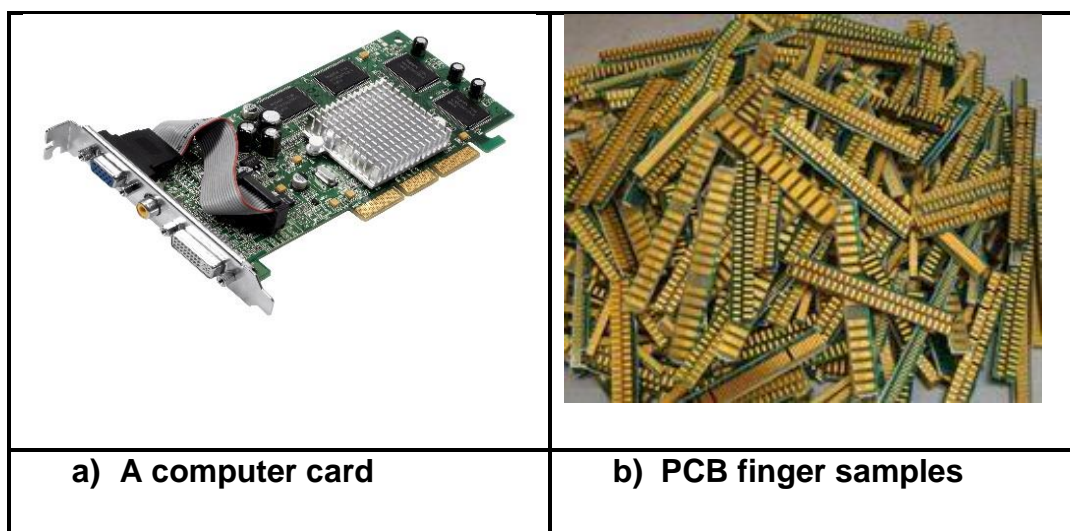
Figure 19 (a) A typical computer PCB card; (b) PCB fingers ripped off from several computer cards.

Some of these scrapped computers were collected and taken to the lab to salvage for computer cards. The computer cards were manually taken out with

the aid of simple hand tools such as screw drivers and pliers. A typical computer PCB card is shown in Figure 19a. The bulk scrap computers were re-assembled and returned to the IT center after the cards were taken out, to be recycled.

PCB mounts and attachments like aluminium heat-sinks, resistors, inductors, capacitors, cables, transistors and so on were either unscrewed or simply ripped off using a hand plier. The edge connector also termed 'fingers' were shredded, using a plier or a hand cutter, from the green board to populate a concentrate sample of gold plated fingers (Figure 19b). The rough edges were carefully smoothened using a hand file and the samples were stored in a desiccator for subsequent experimental work. The populated finger samples, when ready to be used were cut into smaller pieces using a hand cutter. These smaller pieces are termed 'PCB chips'.

3.1.2 Ionic Liquids

Four imidazolium-based ionic liquids were employed in this study namely:

1. 1-methyl-3-propylimidazolium bis trifluoromethylsulfonyl imide, >98% (mpim[N(CF$_3$SO$_2$)$_2$]),

2. 1-ethyl-3-methylimidazolium thiocyanate, 99%, (emim[SCN]),

3. 1-butyl-3-methylimidazolium hydrogen sulphate, >95% (bmim[HSO$_4$]) and

4. 1-Ethyl-3-methylimidazolium hydrogen sulphate, 95% (emim[HSO4]).

These liquids were purchased from the Ionic Liquids Technologies (IOLITEC) GmbH, Germany and were used and analysed in the as-received form. To prevent water hydration, the ionic liquids were kept in a desiccator inside the packaging with air tight bottles.

3.2 Analytical Techniques

3.2.1 Scanning Electron Microscope (SEM)

The scanning electron microscope (SEM) uses a focused beam of high-energy electrons to generate a variety of signals at the surface of solid specimens. The signals that derive from electron-sample interactions reveal information about the sample including external morphology (texture), chemical composition, and crystalline structure and orientation of materials making up the sample. In most applications, data are collected over a selected area of the surface of the sample, and a 2-dimensional image is generated that displays spatial variations in these properties. Areas ranging from approximately 1 cm to 5 microns in width can be imaged in a scanning mode using conventional SEM techniques (magnification ranging from 20X to approximately 30,000X, spatial resolution of 50 to 100 nm). The SEM is also capable of performing analyses of selected point locations on the sample; this approach is especially useful in qualitatively or semi-quantitatively determining chemical compositions (using EDS) [129]. Sample preparation can be minimal or elaborate for SEM analysis, depending on the nature of the samples and the data required. Minimal preparation includes acquisition of a sample that will fit into the SEM chamber and some accommodation to prevent charge build-up on electrically insulating samples.

The PCB chip samples were held in a plastic resin, and polished to reveal a cross section of the sample. Most electrically insulating samples are coated with a thin layer of conducting material, commonly carbon, gold, or some other metal or alloy. The choice of material for conductive coatings depends on the data to be acquired: carbon is most desirable if elemental analysis is a priority, while metal coatings are most effective for high resolution electron imaging applications. Carbon was thus used to coat the plastic resin within which the PCB chip sample was embedded.

3.2.1.1 Fundamental Principles of SEM

Accelerated electrons in an SEM carry significant amounts of kinetic energy, and this energy is dissipated as a variety of signals produced by electron-sample interactions when the incident electrons are decelerated in the solid sample. These signals include secondary electrons (that produce SEM images), backscattered electrons (BSE), diffracted backscattered electrons (DBSE that are used to determine crystal structures and orientations of minerals), photons (characteristic X-rays that are used for elemental analysis), visible light (cathodoluminescence), and heat. Secondary electrons and backscattered electrons are commonly used for imaging samples: secondary electrons are most valuable for showing morphology and topography on samples and backscattered electrons are most valuable for illustrating contrasts in composition in multiphase samples. X-ray generation is produced by inelastic collisions of the incident electrons with electrons in discrete orbitals (shells) of atoms in the sample. As the excited electrons return to lower energy states, they yield X-rays that are of a fixed wavelength that is related to the difference in energy levels of electrons in different shells for a given element. Thus, characteristic X-rays are produced for each element in a mineral that is "excited" by the electron beam. SEM analysis is considered to be "non-destructive"; that is, X-rays generated by electron interactions do not lead to volume loss of the sample, so it is possible to analyse the same materials repeatedly. Essential components of all SEMs include the Electron Source ("Gun"), Electron Lenses, Sample Stage, Detectors for all signals of interest, Display / Data output devices. SEMs always have at least one detector (usually a secondary electron detector), and most have additional detectors. The specific capabilities of a particular instrument are critically dependent on which detectors it accommodates [129-131].

3.2.1.2 Energy-Dispersive X-Ray Spectroscopy (EDS)

Interaction of an electron beam with a sample target produces a variety of emissions, including X-rays. An energy-dispersive (EDS) detector is used to separate the characteristic X-rays of different elements into an energy spectrum, and EDS system software is used to analyse the energy spectrum

in order to determine the abundance of specific elements. EDS can be used to find the chemical composition of materials down to a spot size of a few microns, and to create element composition maps over a much broader raster area. Together, these capabilities provide fundamental compositional information for a wide variety of materials.

EDS systems are typically integrated into an SEM instrument. EDS systems include a sensitive x-ray detector, a liquid nitrogen dewar (a double-walled flask of metal or silvered glass with a vacuum between the walls) for cooling, and software to collect and analyse energy spectra. The detector is mounted in the sample chamber of the main instrument at the end of a long arm, which is itself cooled by liquid nitrogen. An EDS detector contains a crystal that absorbs the energy of incoming X-rays by ionization, yielding free electrons in the crystal that become conductive and produce an electrical charge bias. The x-ray absorption thus converts the energy of individual X-rays into electrical voltages of proportional size; the electrical pulses correspond to the characteristic X-rays of the element.

3.2.2 Infra Red (IR) Spectroscopy: The VERTEX 70

Infrared (IR) spectroscopy is one of the most common and widely used spectroscopic techniques. Absorbing groups in the infrared region absorb within a certain wavelength region. The absorption peaks within this region are usually sharper when compared with absorption peaks from the ultraviolet and visible regions. In this way, IR spectroscopy can be very sensitive to determination of functional groups within a sample since different functional group absorbs different particular frequency of IR radiation. Also, each molecule has a characteristic spectrum often referred to as the fingerprint. A molecule can be identified by comparing its absorption peak to a data bank of spectra. IR spectroscopy is very useful in the identification and structure analysis of a variety of substances, including both organic and inorganic compounds. It can also be used for both qualitative and quantitative analysis of complex mixtures of similar compounds.

The VERTEX 70 offers an extensive line of sampling accessories for the internal sample compartment for transmission, ATR, diffuse reflectance and additional types of measurements. Certain applications, however, need to be carried out using accessories that can only be mounted externally, e.g. for space reasons or to keep the internal compartment free for more routine measurements.
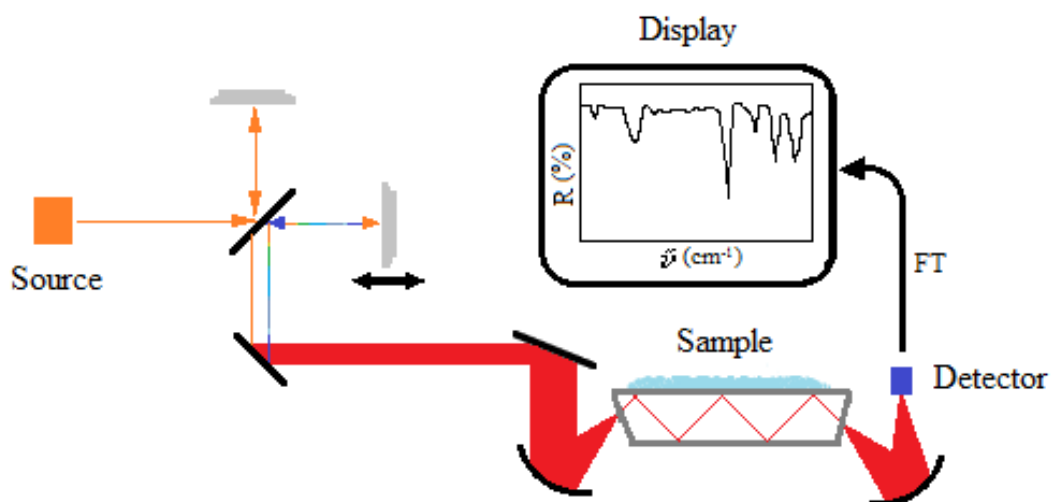
Figure 20: *Schematic of ATR-FTIR spectrometer showing how the IR beam interacts with the surface of the sample without penetrating into it [132].*

Bruker's OPUS is an easy-to-use, powerful, all-in-one spectroscopy software which is part of the VERTEX delivery. It includes the most comprehensive collection of data acquisition, processing, and evaluation functions optimized for applications in the fields of routine laboratory analysis, advanced R&D applications, and reaction monitoring. The OPUS interface is completely customizable and easy to use. In this research, the ATR mode was adopted where the sample is in direct contact with an ATR crystal. As the IR beam reaches onto the ATR crystal, it extends beyond the crystal surface and protrudes into the sample at a shallow depth (0.5-5 µm). The sample absorbs some of the energy of the IR beam as the wave is internally reflected between the ATR crystal and the sample. The attenuated wave at the exit end is collected by the detector and shown in Figure 20.

3.2.2.1 IR Analysis

IR spectroscopy is a great method for identification of compounds, especially for identification of functional groups. Therefore, we can use group frequencies for structural analysis. Group frequencies are vibrations that are associated with certain functional groups. It is possible to identify a functional group of a molecule by comparing its vibrational frequency on an IR spectrum to an IR stored data bank. Infrared spectroscopy can also be applied in the field of quantitative analysis, although sometimes it's not as accurate as other analytical methods, like gas chromatography and liquid chromatography. The main theory of IR quantification is Beer's law or Beer-Lambert law, which is written as

$$I = I_o \exp(-\epsilon l c) \qquad (16)$$

$$A = \log\left(\frac{I}{I_o}\right) = -\epsilon l c \qquad (17)$$

Where A is the absorbance of the sample, I is the intensity of transmitted light, I_o is the intensity of incident light, l is the path length, ϵ is the molar absorptivity of the substance, and c is the concentration of the substance. Absorption is the property of the material of transferring energy from the photons to its atoms and molecules. The ratio of the energy transferred to the matter from the incident light to the total incident energy is called absorptance (A), which can be expressed in terms of the reflection (R) and transmission (T) as shown in eq. 18 [133].

$$A = 1 - T - R \qquad (18)$$

From the Beer's Law, we could figure out the relation between the absorbance and the concentration of the sample since the analytes have a particular molar absorptivity at a particular wavelength. Therefore, we could use IR spectroscopy and Beer's Law to find the concentration of substance or the components of mixture.

3.2.3 UV-Vis Spectroscopy: The LAMBDA 950

The LAMBDA 950 is one of our highest performance UV/Vis system designed for analysis of coatings, high performance glass, and components in both research and manufacturing. The instrument meets industry standards for ultra-high performance, flexibility, and convenience. Its operation wavelengths ranges from 175 - 3,300 nm. Absorption of visible and ultraviolet (UV) radiation is associated with excitation of electrons, in both atoms and molecules, from lower to higher energy levels.

Since the energy levels of matter are quantized, only light with the precise amount of energy can cause transitions from one level to another will be absorbed. In each possible case, an electron is excited from a full (low energy, ground state) orbital into an empty (higher energy, excited state) anti-bonding orbital. Each wavelength of light has a particular energy associated with it. If that particular amount of energy is just right for making one of these electronic transitions, then that wavelength will be absorbed. The larger the gap between the energy levels, the greater the energy required to promote the electron to the higher energy level; resulting in light of higher frequency, and therefore shorter wavelength, being absorbed. All molecules will undergo electronic excitation following absorption of light, but for most molecules very high energy radiation (in the vacuum ultraviolet, <200 nm) is required. Consequently, absorption of light in the UV-visible region will only result in the transition shown in Figure 21b. Therefore in order to absorb light in the region from 200 - 800 nm (where spectra are measured), the molecule must contain either bonding pairs of electrons or atoms with non-bonding orbitals. A non-bonding orbital is a lone pair on, say, oxygen, nitrogen or a halogen.
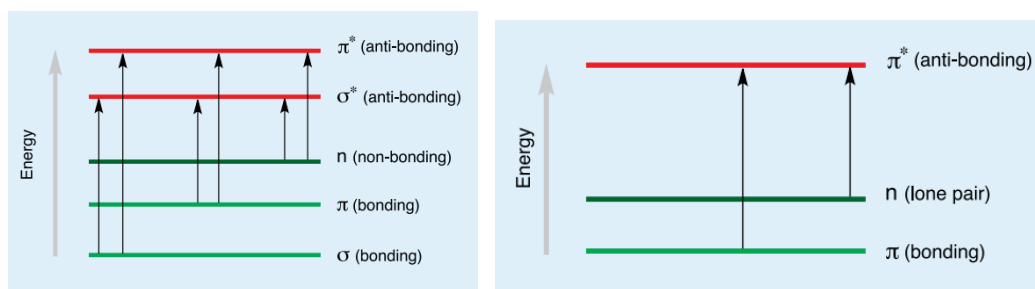
Figure 21: (a) The possible electronic transitions that light might cause, (b) electronic excitation following absorption of light, for which very high energy radiation (in the vacuum ultraviolet, <200 nm) is required.

UV-visible spectrometers can be used to measure the absorbance of ultra violet or visible light by a sample, either at a single wavelength or perform a scan over a range in the spectrum. The UV region ranges from 175 to 400 nm and the visible region from 400 to 3200 nm. The technique can be used both quantitatively and qualitatively. The light source (a combination of tungsten/halogen and deuterium lamps) provides the visible and ultraviolet radiation. The output from the light source is focused onto the diffraction grating which splits the incoming light into its component colours of different wavelengths, like a prism. For liquids the sample is held in an optically flat, transparent container called a cell or cuvette. The reference cell or cuvette contains the solvent in which the sample is dissolved and this is commonly referred to as the blank. For each wavelength the intensity of light passing through both a reference cell (I_o) and the sample cell (I) is measured. If I is less than I_o, then the sample has absorbed some of the light. The absorbance (A) of the sample is related to I and I_o according to equation 1. The detector converts the incoming light into a current, the higher the current the greater the intensity. The chart recorder usually plots the absorbance against wavelength (nm) in the UV and visible section of the electromagnetic spectrum as indicated in Figure 22.
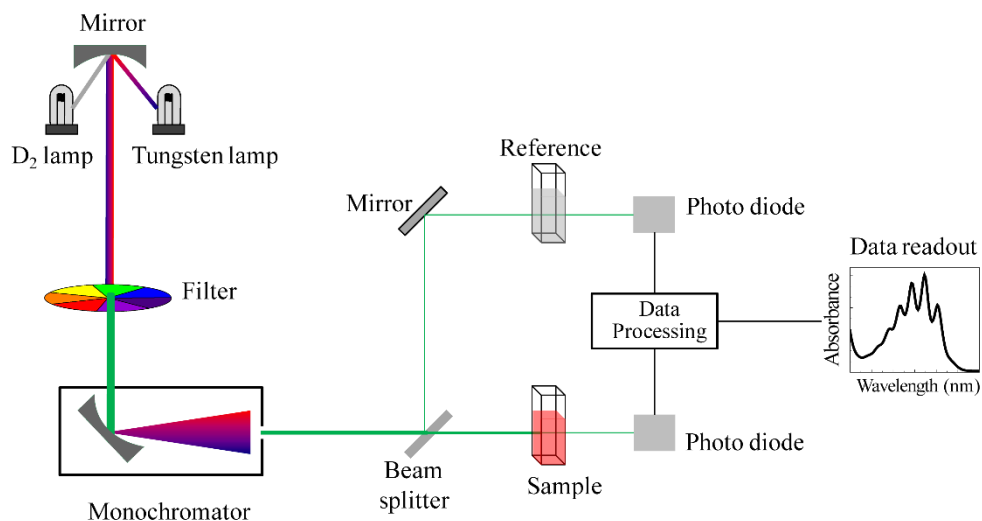
Figure 22: *Schematic of UV-visible spectrometer showing the working principle [134].*

3.2.3.1 Beer-Lambert Law

According to the Beer-Lambert Law the absorbance is proportional to the concentration of the substance in solution and as a result UV-visible spectroscopy can also be used to measure the concentration of a sample. If the absorbance of a series of sample solutions of known concentrations are measured and plotted against their corresponding concentrations, the plot of absorbance versus concentration should be linear if the Beer-Lambert Law is obeyed. This graph is known as a calibration graph. A calibration graph can be used to determine the concentration of unknown sample solution by measuring its absorbance. Since the absorbance for dilute solutions is directly proportional to concentration another very useful application for UV-visible spectroscopy is studying reaction kinetics. The rate of change in concentration of reactants or products can be determined by measuring the increase or decrease of absorbance of coloured solutions with time. By plotting absorbance against time, one can determine the orders with respect to the reactants and hence the rate equation from which a mechanism for the reaction can be proposed.

Both FTIR and UV-visible use Lambert-Beer's law. Please consolidate and write in the context of characterising the concentrations of Ni, Cu and gold, provided these elements have absorption in the UV-to-IR region.

3.4 Experimental Setups

3.4.1 Conductivity Cell

Electrical Conductivity is a parameter used to measure the ionic concentration and activity of a solution. The more salt, acid or alkali in a solution, the greater its conductivity. The unit of electrical conductivity is S/m, often also S/cm. The scale for aqueous solutions begins with pure water at a conductivity of 0.05 µS/cm (25 °C). Naturally occurring waters such as drinking water or surface water have a conductivity in the range 100 - 1000 µS/cm. At the upper end of the chart some acids and alkalines can be found. Conductivity cell measurements are used for a wide range of applications such as the production of ultrapure water or determining the salinity of sea water.

Conductivity is measured by using a conductivity cell to make a measurement of the electrical resistance. The kind of measuring cell used in this study consists of two similar electrodes. An alternating voltage applied to one of the conductivity electrodes causes the ions in the solution to migrate towards the electrodes. The more ions in the solution, the greater the current which flows between the conductivity electrodes. The conductivity meter measures the current produced by the conductivity cell and uses Ohm's law to calculate first the conductance of the solution and then by taking the cell data into account the conductivity.

The conductivity of the ionic liquid was characterised using this home-made apparatus, shown below in Figure 23, in which two copper electrodes with dimensions (25 mm x 25 mm x 1.5 mm) spaced 10 mm apart, were positioned in a T-glass tube, with wall thickness of 3 mm and internal diameter of 38.1 mm. The cell was subsequently filled with ionic liquid and closed with 35mm x 40.5 mm x 38.5 mm silicone rubber bung stoppers to contain the ionic liquid

inside the glass tube. The terminals of the Cu wire were connected to an electrical circuit, as shown in the Figure 23.
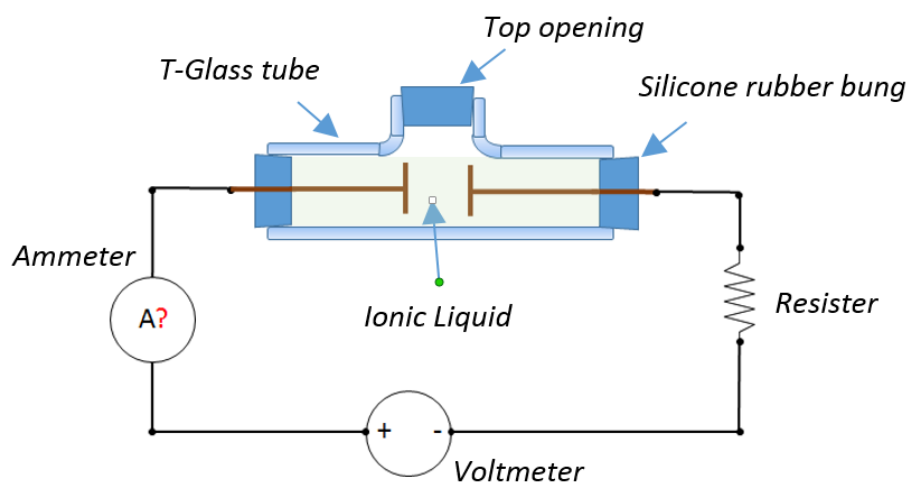
Figure 23*: A T-glass tube with electrical circuit used to measure the electrical conductivity of the ionic liquids*

3.4.2 Microwave Heating Experimental Setup (MHES)

A 1.8 KW continuous wave microwave waveguide heating experimental setup (MHES) designed in the lab was used to in heating experiments of the imidazolium-based ionic liquids. MHES was originally designed by a postgraduate researcher in the Institute of Microwaves and Photonics at the University of Leeds, to measure microwave dielectric properties of powder samples. It consists of a power supply, a generator, isolator, directional coupler, waveguide, water load, fibre optic thermometer, digital video recorder and digital power meters. Basically, generated microwaves at a set power is guided to irradiate a sample in the 'waveguide applicator'. The block diagram of the in-line heating equipment is shown in Figure 24.

The MHES was used to determine the thermal behaviour of the ionic liquids under microwave irradiation. It was also used to determine the absorption behaviour of the liquids at particular microwave powers and frequencies.
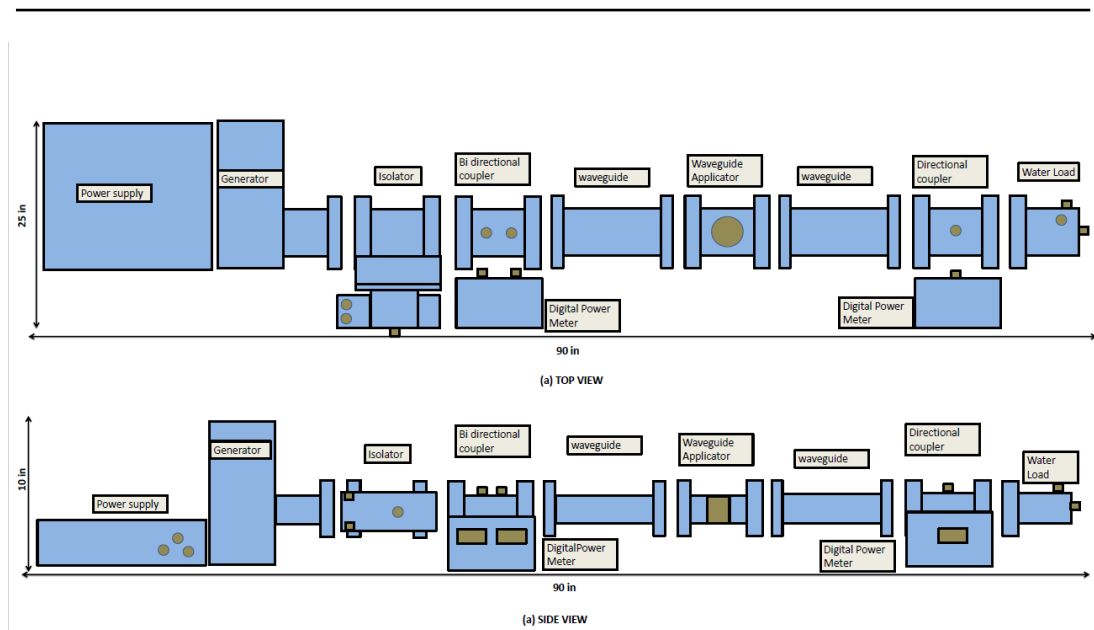
Figure 24: *1.8 KW microwave heating equipment block diagram*

An SM 845 microwave power magnetron head and power supply from MKS instruments ltd was used to generate continuous microwave power up to 1.8KW at 2450 MHz. The output power generated from the magnetron was taken via WR-340 waveguide flange. Stable output power was adjustable from 100W to 1.8 KW by using DC (0-10 V) reference signal.

Microwave isolator was a 2-port microwave device which allowed electromagnetic waves to travel in one direction only. Its purpose was to protect magnetron from the damaging effects of reverse microwave power due to mismatched load. A 6KW microwave isolator (GA116) from Gerling Applied Engineering (GAE) was connected to the output of microwave power generator. Microwave power generated from magnetron travelled in the forward direction and was delivered to the load. The reflected power signal travelling in the opposite direction was dissipated in the water load connected to the isolator.

A bidirectional digital microwave power meter from GAE was connected at the output port of the isolator. This device measured the electromagnetic signals travelling in both forward and reverse direction. Bi-directional power meter consisted of a bi-directional waveguide coupler, diode detector and a digital voltage meter.

The waveguide tuner GA1002 from GAE was used to maximize the forward power by matching the load impedance. The 3-stub waveguide tuner consisted of a waveguide section with 3 movable tuning stubs placed at a distance of quarter wavelength from each other.

GA6004A universal waveguide applicator from GAE was used for the experiments. It was a standard WR-340 waveguide section with 5cm diameter removable adapter ports on the top and bottom walls and a mounting boss on one side for attaching an IR sensor head or a camera. This allowed the used of the applicator either in batch mode or continuous flow applications. There existed a number of 3mm diameter holes in one side wall of the applicator. These were used to insert fibre-optic temperature probes in the sample. There was a 2cm diameter gooseneck pipe connected to the other side wall of the applicator. This was used to position the digital video recorder cam.

At the end of the waveguide setup a waveguide dummy water load was connected. It consisted of a short circuited waveguide with a flowing water glass pipe through it. This unit was connected to dissipate all of the remaining microwave power which was not being utilized by the sample. This helped to minimize reverse power in order to protect the magnetron.

A four channel (FOB-100) from Omega engineering is used to continuously monitor the temperature of the sample when exposed to microwave radiations. Fibre-optic probe was placed inside the sample through a 3mm hole in the side wall of the applicator as indicated in *Figure 26*.
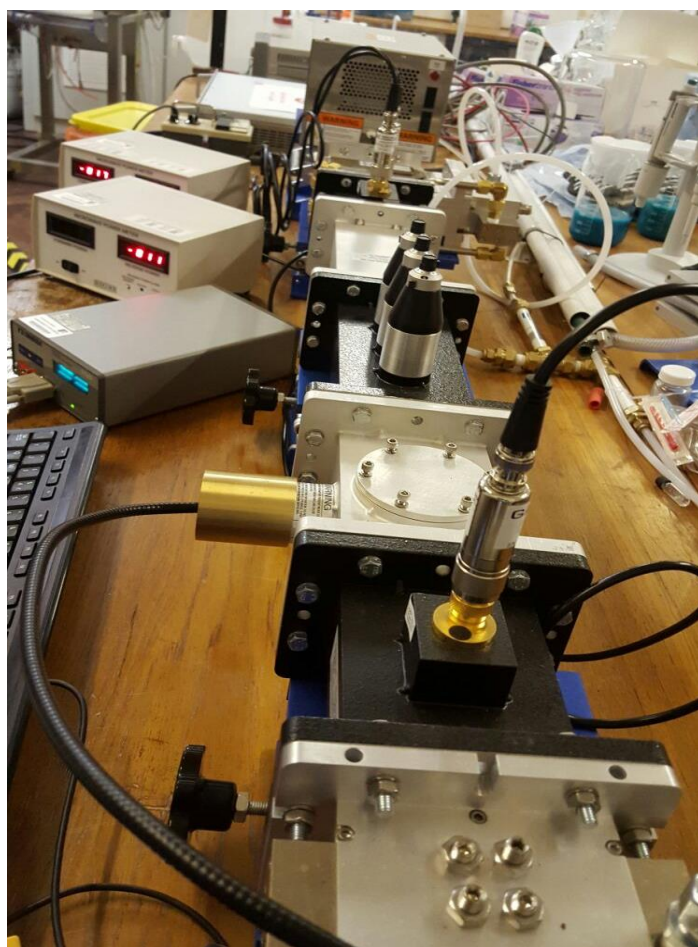
Figure 25: The photograph of the complete MHES

The MHES was adapted to liquid samples to enable measurements on the ionic liquids by introducing a cylindrical Teflon holder. A 4.5 cm diameter Teflon holder was used to hold approximately 20 mL of ionic liquid in the waveguide applicator. The fibre optic thermometer wire was gently immersed in the liquid such that it touched the bottom of the Teflon container. After setting the chamber cover in place, a camera was inserted through the side opening and held in place with the aid of a flexible gooseneck arm tube (see Figure 25 and *Figure 26*).
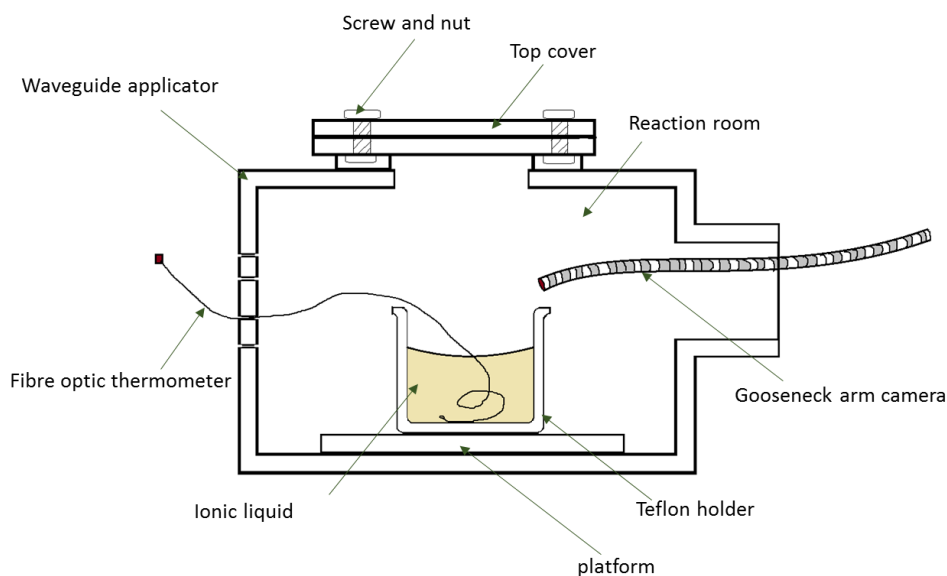
Figure 26: *Microwave applicator setup showing the Teflon holder.*

3.4.3 Performance Network Analyzer (PNA)

A network analyzer is an instrument used for characterising or measuring the response of devices at RF or even microwave frequencies. By measuring the response of a device or network using an RF network analyzer, it is possible to characterise it and in this way understand how it works within the RF circuit for which it is intended. It is possible to use RF network analyzers for measuring a variety of components ranging from filters and frequency sensitive networks, to devices such as transistors, mixers and any RF orientated device. Typically RF network analyzers are more usually associated with microwave type frequencies. However the RF network analysers that are available cover down to much lower frequencies than this, and some are even able to make measurements at frequencies down to 1 Hz.

The frequency sweep measurement of the ionic liquids under study was carried out to determine the dielectric properties (loss factor and dielectric constant) using Agilent Technologies E8361A Performance Network Analyzer (PNA) which offers a combination of speed and precision, with an operating coverage from 10 MHz to 67 GHz, capable for evaluating a wide range of microwave and millimetre wave component [135].

The experimental set up is presented in Figure 27, where a 25 ml glass beaker containing 10 ml of IL was placed on a digital hot plate. The PNA high temperature dielectric probe was positioned to just touch the IL on the surface, making sure that no bubbles were trapped underneath it. The hot plate was used to heat the IL to enable isothermal readings at 25, 50, 100 and 125 °C. At each temperature, a microwave frequency sweep from 10 MHz to 10 GHz was measured and analysed.
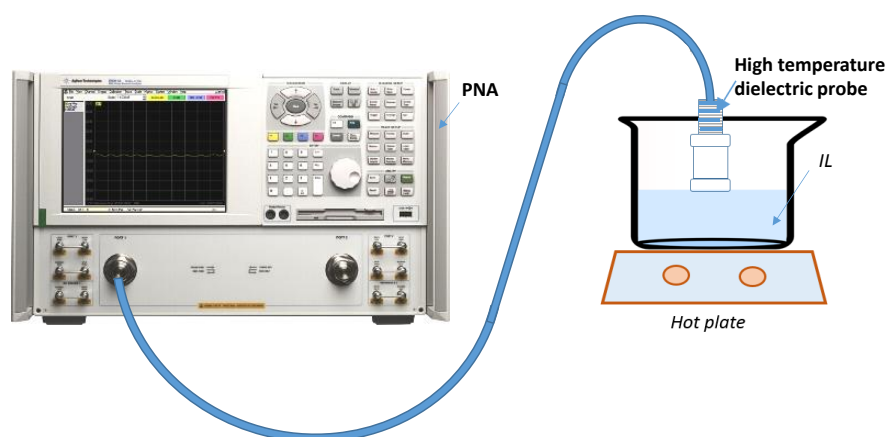
Figure 27*: PNA frequency sweep mode of measurement; A hot plate is used to vary the temperatures (25, 50, 100 and 125 °C) of the ILs as the measurement is conducted. The probe just touches the surface of the liquid.*

3.4.4 MW-Assisted Leaching Setup

MW-assisted leaching method requires microwave transparent and reagent resistant materials such as fluorocarbon polymers (examples are PFA or TFM), borosilicate glass (Pyrex) or quartz to contain acids and samples. For higher pressure capabilities the vessel may be contained within layers of different microwave transparent materials for strength, durability, and safety. The internal volume of the vessel should be at least 45 mL, and the vessel must be capable of withstanding pressures of at least 30 atm (435 psi), and capable of controlled pressure relief. These specifications are to provide an appropriate, safe, and durable reaction vessel [136].

A 21 litres, 2.45 GHz frequency Maestrowave MW10 Microwave oven, with 10 variable output power levels of up to 1000 W was utilized. The solution (leaching solution and solute) was held in a 160 mL capacity Pyrex vessel and air-tight sealed using a Pyrex glass stopper and scotch tape (see Figure 28). The solution is heated in the microwave unit for a specified period of time. After cooling, the vessel contents are allowed to settle, filtered, diluted to volume and analysed by an appropriate determinative method.
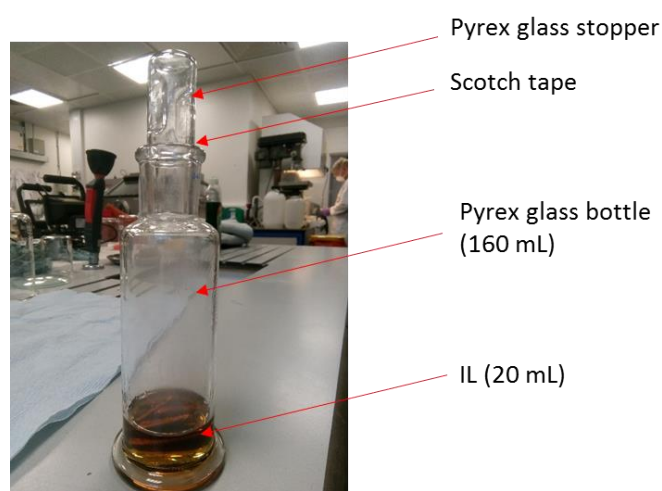
Figure 28: *MW-assisted leaching setup for the leaching of epoxy resin from WPCB chips using bmimHSO$_4$ ionic liquid.*

A 'Clas Ohlson' Multimeter temperature probe was used in a similar setup (where an open Teflon container is utilized) to calibrate the temperature of each liquid inside the microwave oven as a function of time. The temperatures measurements of the liquids were swiftly but carefully taken by dipping a temperature probe into the liquid immediately after the set resident time in the microwave oven. A time-dependent calibration curve was thus developed for each liquid.

3.5 Leaching & Electrowinning Processes

Leaching is a process of extracting a substance from a solid material that is dissolved in a liquid. This process is commonly referred to as extraction, particularly in the chemical industry. Three basic steps are involved in the

leaching process: contact, separation, and extraction. First, the solvent comes into contact with the solid matrix. A solvent is usually a liquid that functions to dissolve the solute. A solute is the substance being dissolved by a solvent. Next, the solvent travels through the solid matrix, separating the substance from the matrix so that it can be subsequently collected using techniques such as filtration and/or electrowinning.

Electrowinning is a widely used technology in modern metal recovery, mining, refining and waste water treatment applications. Electrowinning is one of the oldest electrolytic processes known which is based on the principle of electrolysis. Electrically conductive solution is created when an electrolyte is dissolved in water or other polar solvent. Electrolytes consist of positively and negatively charged ions (cations and anions). When a DC voltage is applied to the solution the positively charged ions (cations) move towards the cathode, while negatively charged ions (anions) move towards the anode. Processes like this are called electrolysis and electrowinning is based on this principle. In electrowinning the electrolyte includes dissolved metals that have to be recovered. Another similar process is electrorefining which is strictly used in refining applications to improve the purity of the metals.

Four main sub-sections are written here describing the leaching, separation and electrowinning setups utilised to absolutely separate the PCB finger composites namely; (i) leaching of epoxy resin (FR4 substrate), (ii) the regeneration process for $bmimHSO_4$ ionic liquid (iii) leaching of Cu/Ni layers of the surface multi-layered surface plates, and (iv) the electrowinning of Cu-Ni alloy from the leachate solution.

3.5.1 Delamination process of PCBs

The purpose of these sets of experiment was to completely delaminate the PCB fingers in a TEPR leaching process. These experiments would both enable kinetic study and determination of microwave influence on the reaction. 20mL $bmimHSO_4$ ionic liquid, used as the leaching solvent, was poured into a 160mL Pyrex glass vessel to completely submerge a known mass of PCB chip samples already introduced in the vessel. The vessel was capped and sealed

in place with the aid of a glass stopper and scotch tape. The vessel was then put into the microwave oven, and heated at the set power of 200 W over a specified period of time. Visual observation was made at time intervals. After specific resident times of reaction, samples were brought out, allowed to cool and filtered. With a syringe, a small amounts (~1 mL) of the filtrate were collected and prepared for FTIR and/or UV-Visible spectroscopy. The experiments were repeated on hot plates, without microwave-assistance, using a Corning PC-4200 heating plate.

3.5.2 Regeneration of BmimHSO$_4$

The purpose of this regeneration step is to purify the 'epoxy-resin' pregnant ionic liquid after delamination reaction to enable reuse of the liquid. To achieve this the following apparatus were employed; a 500 mL beaker, glass funnel, filter papers, separating funnel, volumetric flasks, condenser, thermometer, VWR vacuum gas pump (P_{max}: 100kPa or 1.0 bar), hot plate and magnetic stirrer.

Firstly, the fluidity of the pregnant solution was enhanced by diluting it with distilled water to a ratio of 1:10. The solution was stirred at 300rpm for about 5 mins to allow complete dissolution of the ionic liquid in water. The epoxy resin due to its water immiscibility property is undissolved and remains suspended in the solution. After allowing the solution to sit for at least an hour, a complete decanted solution is achieved which is subsequently easily separable by the use of separating funnel and/or filter papers.

After separating the epoxy resin from the solution, the next step was to separate the water from the solution. A vacuum distillation setup sketched in Figure 27 was constructed. Evaporation of water was achieved at 90 °C at a reduced pressure of approximately 100 kPa.
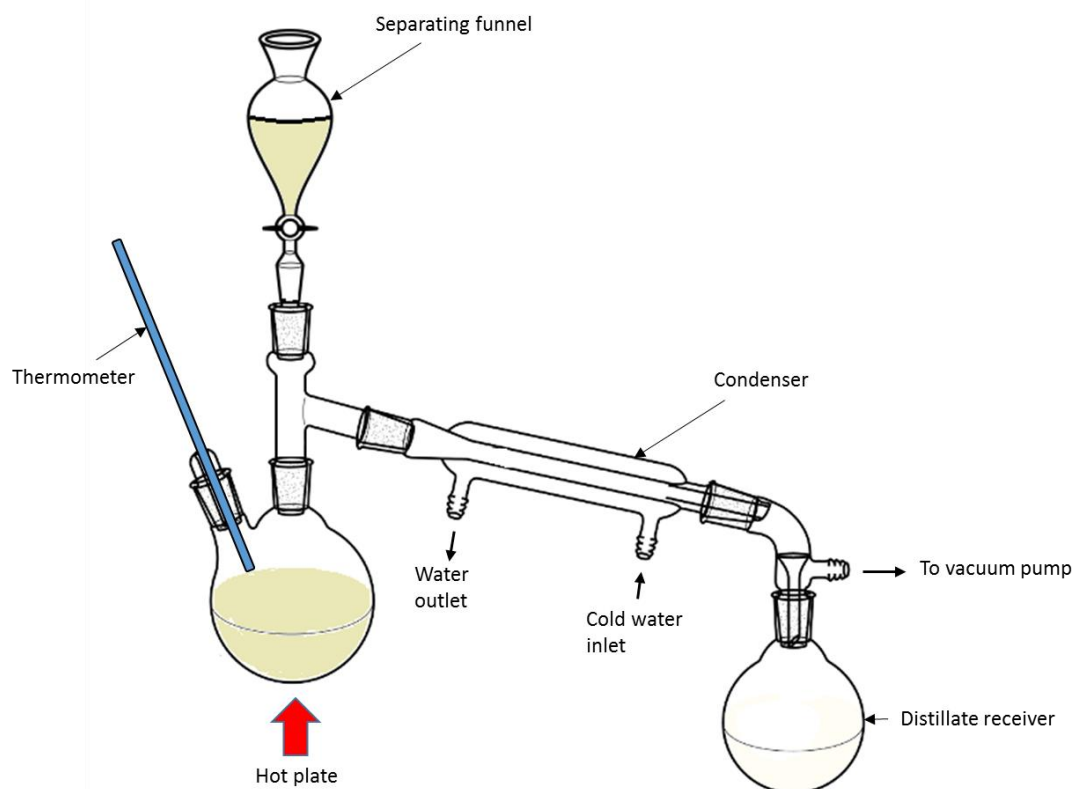
Figure 29: *Vacuum distillation setup for the regeneration of BmimHSO$_4$ ionic liquid after delamination reaction process.*

3.2.3 Leaching of Cu/Ni layers

The multi-layered surface plate samples, products of the delamination process, were used as the solute for this set of leaching experiments. All room temperature leaching experiments were performed in a 25 mL Pyrex vessels whereas high temperature and microwave-assisted experiments were performed in a 160 mL Pyrex vessel.

Firstly, hydrochloric acid solution (20 mL) of a known concentration was introduced into a Pyrex vessel to cover a known mass of PCB chips. Unless stated otherwise, 1g of ammonium chloride powder (NH$_4$Cl) was added to the acid to act as oxidant after which it was stirred at a constant speed of 300 rpm during the leaching tests. Stirring was not possible in microwave-assisted leaching tests. A 1 ml of leach solution was sampled periodically at specific time intervals by a syringe, filtered and sent for chemical analysis to enable

the determination of product concentrations and reaction rates using UV-Visible spectroscopy. After the leaching experiment was over, the solution was decanted and filtered through a paper using vacuum pump. The residue was washed three times with distilled water. The percentage leaching of metals was calculated based on the copper concentration in the leach liquor including the wash liquor. Hot plate heating and magnetic stirring was performed using a Corning PC-4200 heating plate.

3.3.3 Electrodeposition of Cu/Ni

Electrowinning is the recovery of metals, in this case copper-nickel alloy, from solution by passing a current through the solution. Electrons from the current chemically reduced the copper and/or nickel ions, to form a solid metal compound on the cathode. The current was supplied and controlled by a PS3003 power supply which operates at 0-30V, 0-3A. All the experiments used a 250 mL Pyrex glassware beaker as the cell vessel and were conducted at room temperature. The solution was stirred with a magnetic stir bar and external stirring plate using Corning PC-4200 heating plate. For each of the experiments performed, 150 mL of electrolyte was used. Two different electrode assemblies were used. The first utilized a 20 mesh cathode woven from 0.41 mm diameter copper wire (25 mm wide, 38 mm height) circled around a single graphite rod anode, 4 mm thick and 38 mm height. These were immersed 30 mm into the electrolyte. A wooden holder maintained the electrode spacing at 20 mm. The second assembly used two graphite electrodes, one as a cathode and the other as an anode. These twin electrodes were 4 mm thick and 38 mm in height, immersed 30 mm, and spaced 20 mm from each other. Experiments with both assemblies used $CuCl_2$/$NiCl_2$ leachate as the electrolyte. A voltage of 3.0 V was applied to the cell for a period of 3 mins after which the voltage was cut. The electrowinning process was repeated several times per solution to ensure that a large fraction of the copper-nickel metal alloy had been extracted. This was evident from the change in colour shade of the solution after several steps. UV-Vis was

performed of the electrolyte after each some counted number of voltage pulse to check the concentration reduction of the leachate.

3.6 Chapter summary

The experimental chapter outlines the experimental techniques and processes followed in this research project.

The PCB fingers were shredded into chips whereas the ionic liquids were stored in tight bottles in a desiccator to prevent water hydration. Analytical methods adapted to determine the product concentration of IL leachates were UV-Visible and FTIR spectroscopy using beer's principle. SEM-EDS was utilized to determine the structure and composition of the PCB finger samples. Experimental setups were developed, sometimes as attachments to existing setups or equipment. The conductivity of the ILs were measured using a home built conductivity cell. Already existing equipment like the Microwave Heating Experimental Setup (MHES) and Performance Network Analyzer, NPA E861A were utilized to enable the determination of microwave absorption properties of the ILs.

Finally, individual processes adapted in the development of the recycling technique for the separation and recovery of gold and copper-nickel alloy from PCB finger wastes have been outlined in this chapter.

Chapter 4

Materials Characterization

The physical properties of the ILs namely density, viscosity and electrical conductivity are compared and discussed. Fourier transform infrared spectroscopy (FTIR) was utilised to analyse the ionic liquids. All four selected ionic liquids were scanned to confirm their structure and composition based on IR peaks which correspond to internal molecular stretching and vibrations. The microwave dielectric properties of the ILs were measured using 'Agilent Technologies' PNA over a range of frequencies at different temperatures and their results discussed.

The PCB finger samples were analysed for their microstructure and elemental composition using SEM-EDS analytical equipment. With the aid of mainly the backscattered detector which gives information about the elemental contrast and the EDS attachment which utilizes characteristic X-rays to identify elements, the composition of the PCB sample was determined. A conceptual structure was developed to aid the determination of mass fraction and value share analysis of each constituent.

4.1 Properties of ILs

4.1.1 Physical properties

Density is a unit used to measure the compactness of a substance, and it is mostly calculated in kilograms per cubic meter (Kg/m^3) or grams per cubic centimetre (g/cm^3). Therefore, the density of every object can be averagely equated with the summation of its mass divided by the aggregated volume of the object. Viscosity is a measure of a fluid's resistance to flow under applied force. It describes the internal friction of a moving fluid. A fluid with large viscosity resists motion because its molecular makeup gives it a lot of internal friction. A fluid with low viscosity flows easily because its molecular makeup results in very little friction when it is in motion. The formula for measuring viscosity is fairly simple:

$$viscosity = \frac{shear\ stress}{shear\ rate} \tag{19}$$

The result is typically expressed in centipoise (cP), which is the equivalent of 1 mPa s (millipascal second). Shear stress is the force per unit area required to move one layer of fluid in relation to another. Shear rate is the measure of the change in speed at which intermediate layers move with respect to one another, The Newtonian viscosity of a fluid would remain constant regardless of changes to the shear rate. Fluids, such as water and honey in which the viscosity does not change with the shear rate, which is why such fluids are called the Newtonian fluids. Most fluids, however, have viscosities that increase or decrease, depending on the shear rate, and are called the non-Newtonian fluids.

Electrical conductivity defines the property of a material ability to conduct electricity either using electron or ions. There are therefore two type namely electronic conductivity and ionic conductivity. In electronic conduction, conductivity depends on the movement of electron into the conduction band such as in metals. Ionic conductivity, depends on the activation energy for diffusion of ions. With a suitable applied voltage, the jump over the energy barrier can be reached to achieve conductivity.

Table **12** below shows the physical properties (molar mass, density and viscosity) of the ionic liquids obtained from literature. The ionic conductivity of the liquids however was measured using the T-glass tube conductivity cell described in the Figure 23. These measured conductivity values are also compared with the literature values, so that a reliable calibration can be established for the ILs used in this investigation [137-141].

Table 12 : A comparison of the physical properties of the four imidazolium ionic liquids. Ab[C] format: A is the measured/referenced value, b is the temperature and [C] refers to the referencing source. An inverse relationship is apparent between conductivity and viscosity of the conducting medium.

Ionic Liquids	Measured (25°C) σ (mS/cm)	Referenced σ (mS/cm)	M (g/mol)	Density, ρ (g/cm^3)	Viscosity, η (cP)
emim[SCN]	22.00	21 [142]	169.25	1.12 [139]	21^{25} [142] 22^{25} [139]
mpim[N(CF$_3$SO$_2$)$_2$]	4.40	4.35 [137]	405.34	1.47 [137, 138]	43.7^{25} [138] 43.94^{25} [137]
emim[HSO$_4$]	1.38	-	208.24	1.36 [141]	101.2^{80} [141]
bmim[HSO$_4$]	1.34	1.4 [140]	236.29	1.32 [140]	164^{80} 1572^{24} [140]

Table 12, it is evident that the ionic conductivity decreases with increasing viscosity of the ionic liquids, which may be explained by using the Stoke-Einstein viscosity model and the Nernst-Einstein law [143]. In the Stoke-Einstein model expressed in equation 20, the molecular viscosity (η, P) is inversely related with the ionic or molecular diffusion coefficient (D, m^{2}s^{-1}). Here k is the Boltzmann constant and T is the temperature in absolute scale. The ionic diffusion, however, is inversely dependent on the average spherical diameter (a, nm) of the molecule. On the basis of the Stoke-Einstein model, a relationship between the apparent electrical conductivity of ILs and viscosity may be explained at a given temperature by using the classical ionic conductivity or diffusivity.

$$D = \frac{kT}{6\pi\eta a} \tag{20}$$

$$\sigma T = A(n_1 Z_1^2 e^2 D_1 + n_2 Z_2^2 e^2 D_2 + \cdots) \tag{21}$$

The Nernst-Einstein law relates the total ionic conductivity (σ, S/m) of a conducting solvent with the diffusion coefficient (D, m^2/s) of the constituent ions, as expressed in equation 21, where A is a numerical factor and n and Ze, are, correspondingly, concentrations (ions/m^3) and charges (Coulombs) of constituent ions. In equation 22, which is obtained by comparing equations 2

and 3, an inverse relationship is apparent between conductivity and viscosity of the conducting medium irrespective of its composition and particular properties of the constituent ions [143].

$$\sigma T = \frac{kTAe^2}{6\pi\eta}\left(\frac{n_1 Z_1^2}{a_1} + \frac{n_2 Z_2^2}{a_2}\right)$$ (22)

As the apparent viscosity of an ionically conducting medium increases the conductivity is expected to decrease, in accordance with the Stoke-Einstein and Nernst-Einstein models. The molecular thermal vibration (kT) in equations 21 and 22, therefore contributes to dispersion of molecular vibration modes contributing to overcoming the ionic conduction. Amongst the four ILs investigated, as evident in that the Bmim[HSO$_4$] IL has the highest viscosity of 164 cP at 80 ^{o}C, and consequently the lowest electrical conductivity of 1.34 mS/cm at room temperature. On the other end, the IL emim[SCN] exhibits high electrical conductivity of 22 mS/cm and low viscosity of 21 cP at 25 ^{o}C.

Also from Nernst-Einstein law, the electrical conductivity of a liquid depends upon the number of ions per unit volume and upon their drift velocity expressed as diffusivity. This can be understood by considering sodium chloride; in its solid state, positively charged sodium ions and negatively charged chlorine ions occupy adjacent places in the crystal lattice. These ions are firmly anchored in position in the solid phase. Solid sodium chloride is a non-conductor of electricity. At high temperatures the ions have sufficient thermal energy to overcome the attractive forces holding them in place, and the substance melts. Molten sodium chloride is a good ionic conductor, depicting ~100 % ionic conductivity. The sodium and chlorine ions in molten sodium chloride drift under the action of the electric field. The sodium ions migrate toward the cathode, and the chlorine ions migrate toward the anode, so that pure sodium and chlorine may be separated in an electrolytic cell. Free electrons do not traverse the cell. A viscous liquids will exhibit greater reluctance to transverse the cell, and vice versa. Similarly, the conductivity of ionic liquids is dependent on the number of the ions and the viscosity of the liquid.

4.1.2 FTIR spectra analysis

When Infrared (IR) radiation is passed through a sample, some radiation is absorbed by the sample and some passes through or is transmitted. The resulting signal at the detector is a spectrum representing a molecular 'fingerprint' of the sample. The usefulness of infrared spectroscopy arises because different chemical structures (molecules) produce different spectral fingerprints.

Upon first inspection, a typical infrared spectrum can be visually divided into two regions. The right half, above 2000 cm^{-1}, usually contains relatively few peaks, but some very diagnostic information can be found here. First, alkane C-H stretching absorptions just below 3000 cm^{-1} demonstrate the presence of saturated carbons, and signals just above 3000 cm^{-1} demonstrate unsaturation. A very broad peak in the region between 3100 and 3600 cm^{-1} indicates the presence of exchangeable protons, typically from alcohol, amine, amide or carboxylic acid groups. The frequencies from 2800 to 2000 cm-1 are normally void of other absorptions, so the presence of alkyne or nitrile groups can be easily seen here.

In contrast, the left half of the spectrum, below 2000 cm^{-1}, normally contains many peaks of varying intensities, many of which are not readily identifiable. Two signals which can be seen clearly in this area is the carbonyl group, which is a very strong peak around 1700 cm^{-1}, and the C-O bond with can be one or two strong peaks around 1200 cm^{-1}. This complex lower region is also known as the "fingerprint region" because almost every organic compound produces a unique pattern in this area, therefore identity can often be confirmed by comparison of this region to a known spectrum.

IR spectra of all the IL samples were recorded on the Vertex 70 FTIR equipment described in the experimental chapter using an ATR inset.

4.1.2.1 Bmim[HSO$_4$]

The FTIR spectrograph of bmim[HSO$_4$] is displayed in

Figure 30 below. Noticeable from the fingerprint region are 1334 and 1160 which are representing S=O stretching and SOH bending of the anion [144]. Also the 840 peak represents C-N stretching of the cation. The presence of both saturated and unsaturated C-H stretch are seen in peaks just below and above 3000cm^{-1}. Peak 2872 and 2965 represents saturated C-H stretch of sp^3 hybridized group, meanwhile, the peaks 3095 and 3153 represents C-H

stretch of sp^2 hybridized groups, all of which are evident in the imidazole cation. Within the double bond region are two peaks (1589, 1636) representing C=C, C=N stretching vibrations. Finally in the diagnostic ring is a broad peak at 3430 cm^{-1} which is due to O-H stretching. This is clearly evident in the [HSO$_4$] anion.
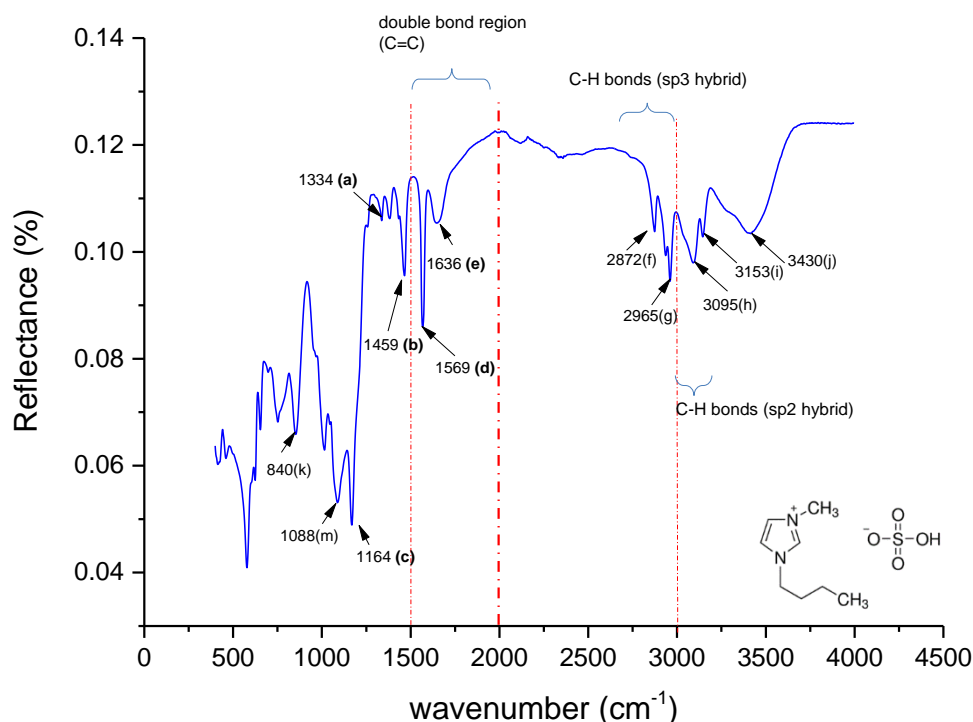
Figure 30: *Fourier Transform Infre-red (FTIR) spectra for Bmim[HSO$_4$]. (a) S=O stretching (b) antisymmetric SO$_2$ stretching (c) SOH bending.*

4.1.2.2 Mpim[(CF$_3$CF$_2$SO$_2$)$_2$N]

In the diagnostic region above 2000cm-1, there are three noticeable set of peaks as evident in *Figure 31*. First is a twin peak 'd' and 'e' representing asymmetric vibrations of alkene in the imidazole ring. The other two sets are found below and above 3000 cm^{-1}. The peaks just below 3000cm^{-1} are aliphatic symmetric and asymmetric stretching vibrations due to methyl groups (C-H) at 2889 and 2965 cm^{-1}. The last set of peaks at 3118 and 3161 are due to C-H bending of unsaturated carbon groups. Below 1500 is the fingerprint region. Between 1500 cm^{-1} and 2000 cm^{-1} is the double bond region where a

single peak at 1570 cm^{-1} is seen. This like the bmim[HSO4] liquid is representative of C=C stretching vibrations at the cation.
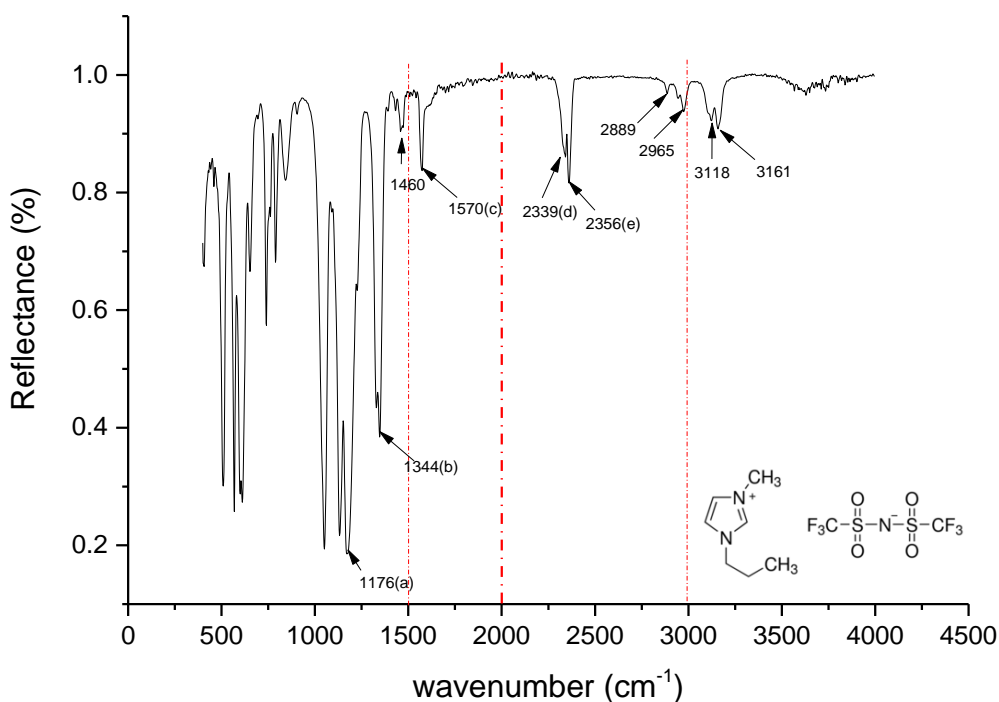
Figure 31: Fourier Transform Infre-red (FTIR) spectra for Mpim[(CF$_3$CF$_2$SO$_2$)$_2$N]. (a) S=O stretching, (e) C=C stretching vibrations Compare all these spectra with the literature data

4.1.2.3 Emim[SCN]

"Nitrile-containing compounds normally have a sharp absorption in the region 2260-2200 cm^{-1}. Inorganic cyanides absorb over a wide range, 2250-2000 cm^{-1}, as do coordination complexes 2150-1980 cm^{-1}" [145]. A strong sharp band in the region 2050 cm^{-1} is therefore characteristic of the SCN group, as evident in *Figure 32*. Left to the 2054cm^{-1} SCN characteristic peak is the 1566 cm^{-1} peak representing C=C stretching vibrations in the imidazole ring. Also the three peaks below and above 3000 cm^{-1} namely 'c', 'd', 'e' are sp^2 and sp^3 hybridized C-H bond stretching. Sp^2 hybridised characteristic peaks above the 3000 cm^{-1} wavenumber and sp^3 hybridized characteristic peak below.
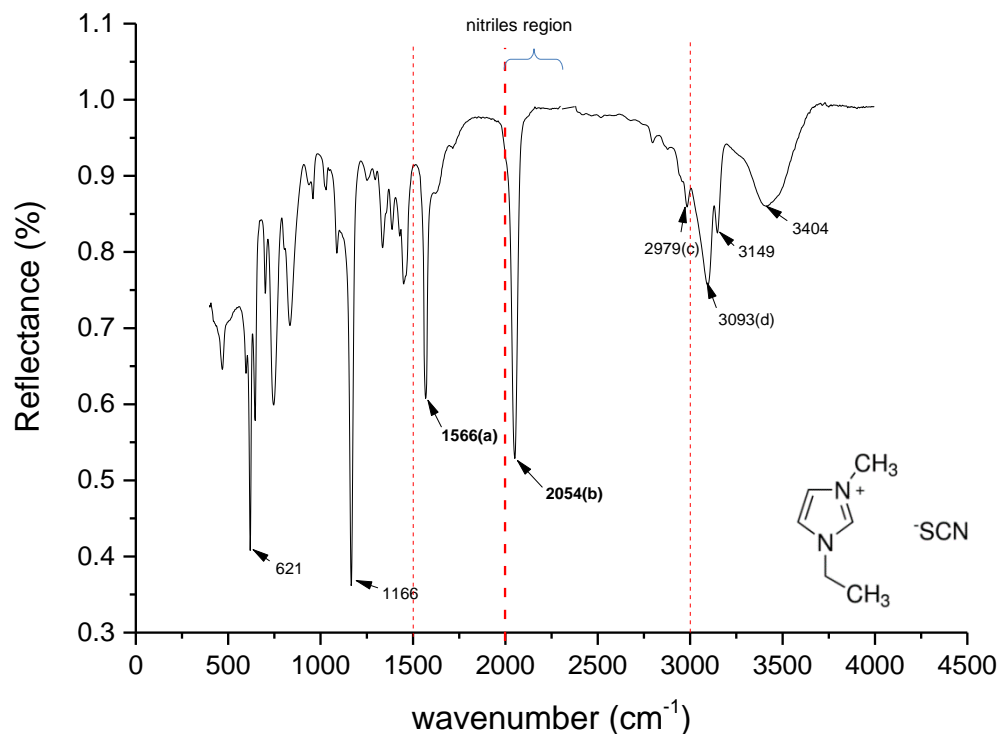
Figure 32: *Fourier Transform Infre-red (FTIR) spectra for Bmim[HSO₄]. (a) C=C stretching vibrations (b) SCN group stretching (c) C-H stretching from imidazole ring.*

4.1.2.4 Emim[HSO₄]

Noticeable from the fingerprint region of *Figure 33* are 1348 and 1172 which represents S=O stretching and SOH bending of the anion [144]. Peaks located at 2965-2873 cm^{-1} are stretching C-H of CH_2 and CH aromatic and aliphatic meanwhile, the peaks 3107 and 3153 cm^{-1} represents C-H stretch of sp^2 hybridized groups, all of which are evident in the imidazole cation. The broad band at 3430 cm^{-1} is assigned to O-H stretching of hydroxyl groups, revealing the presence of [HSO₄] anion. Within the double bond region are two peaks (1569, 1604) representing C=C, C=N stretching vibrations. Stretching of C=C aromatic rings is seen at 1604 cm^{-1} whiles C-C stretching is observed at 1569 cm^{-1}.
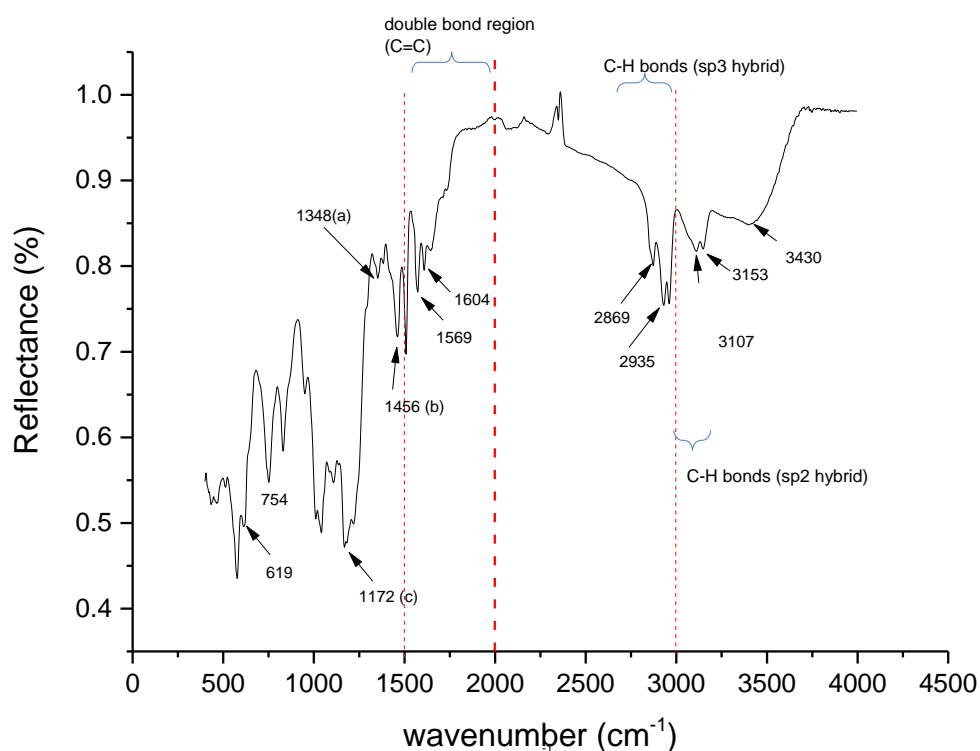
Figure 33: Fourier Transform Infre-red (FTIR) spectra for emim[HSO$_4$]: (a)
S=O stretching; (b) antisymmetric SO$_2$ stretching; (c) SOH bending.

4.1.3 Microwave dielectric properties

In order for a chemical reaction to take place, the reactants must collide. The collision between the molecules in a chemical reaction provides the kinetic energy needed to break the necessary bonds so that new bonds can be formed. For a successful collision to occur, the reactant molecules must collide with enough kinetic energy to break original bonds and form new bonds to become the product molecules. This energy is called the activation energy for the reaction; often referred to as the energy barrier. The temperature is a measure of the average kinetic energy of the molecules; raising the temperature increases the kinetic energy available to break bonds during collisions.

This research adapts the efficient use of microwave energy to provide enough kinetic energy to reactants for dissolution reactions to occur. The microwave dielectric properties of the four selected ILs, one of which would serve as leaching solvent in TEPR dissolution reaction were investigated and their results presented herein.

4.1.3.1 Effect of frequency on Dielectric properties

Microwaves interact with dielectric materials either through conduction process or by polarization. Conduction involves the translation motion of free charges such as ions due to the internal field generated by the microwaves in the ionic liquid. Conduction losses occur when the moving ions collide with other species in the liquid. Polarization occurs when the charge complexes such as dipoles are induced to align in the direction of the microwave field. Polarization losses occur when frictional forces resist induced motions by the microwaves. Both conduction and polarization loss mechanisms dissipate heat into the system which results in volumetric heating.
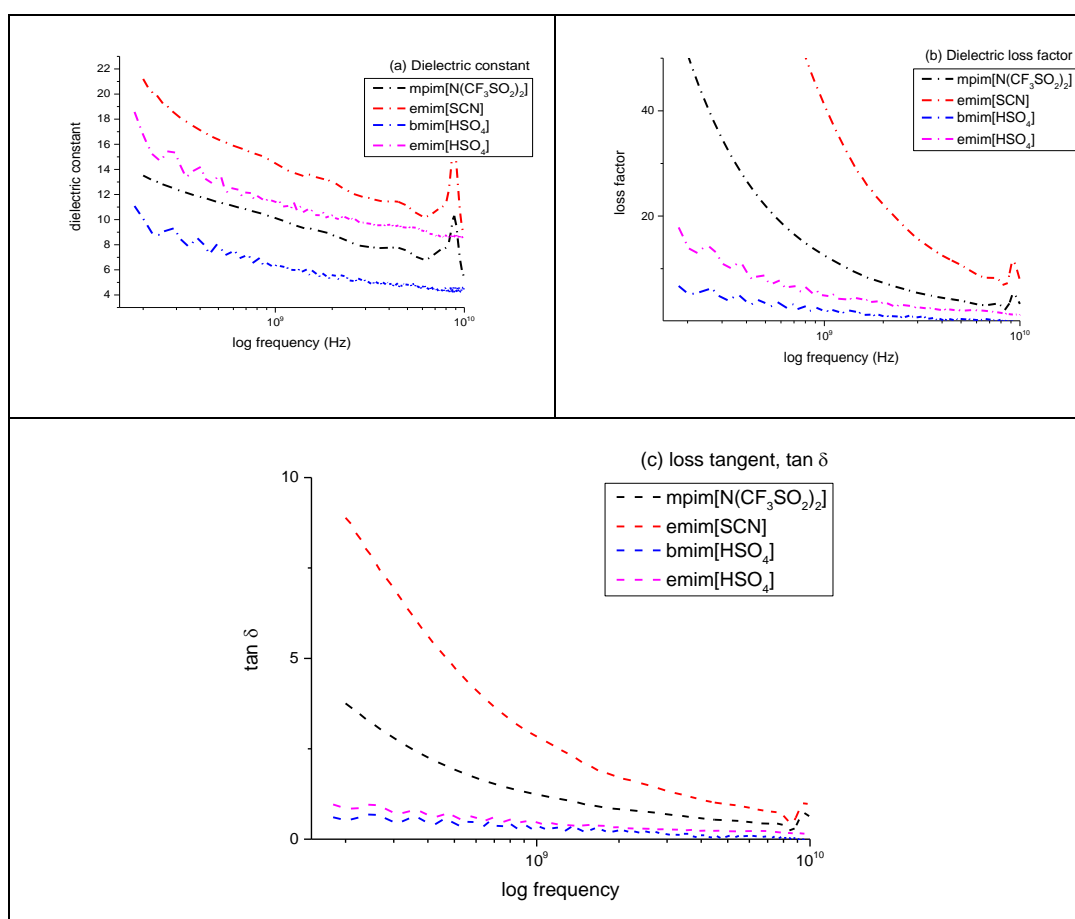
Figure 34: *Measured frequency sweep data for four imidazolium-based ionic liquids at room temperature, showing the frequency dependence of microwave absorption and permittivity dispersion. The loss tangent distribution is also shown in fig (c).*

From Figure 34, it is obvious that the measured dielectric properties decrease with frequency, which is in agreement with equation 2 where the loss tangent is inversely proportional to the microwave frequency. Various polarization mechanisms contribute to the total polarization effect of microwave irradiation. The most dominant is dipole rotation, also referred to as orientation polarization. Other polarization processes include electronic polarization, which results from the realignment of electrons around specific nuclei; atomic (ionic) polarization, which arises from the relative displacement of nuclei due to the unequal distribution of charge within the molecule; and interfacial polarization, also referred to as space charge or Maxwell-Wagner polarization, which occurs when there is a build-up of charges at the interfaces normally observed in amorphous or polycrystalline solids. These polarization mechanisms have frequency dependence and that is because of the mass associated with the charge dipoles and hence inherent inertia to movement.

a) Electronic polarization   b) Atomic (Ionic) polarization

c) Dipolar (orientation) polarization
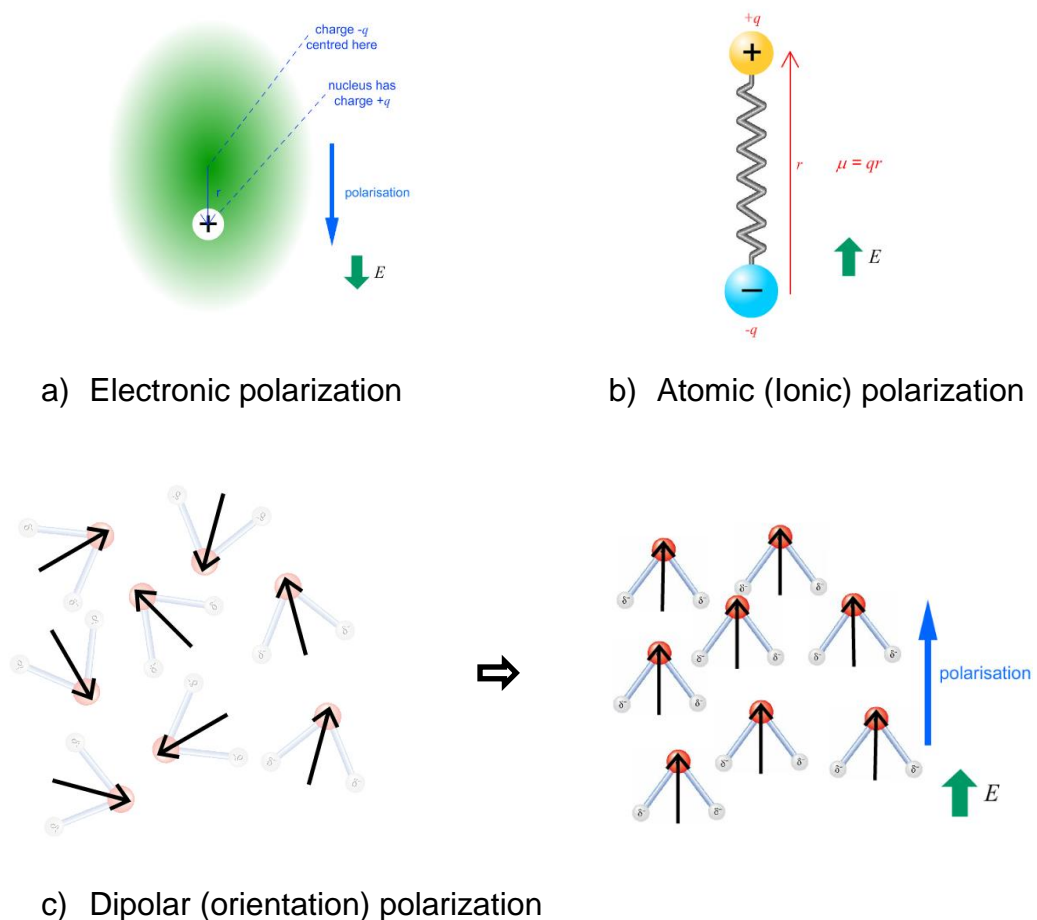
Figure 35 *Schematic of mechanisms of polarization*

Atomic polarization is present in all materials by definition and hence any other mechanism would be an addition. While mathematical treatment of the first three mechanisms is rather straightforward, interface polarization is not easy to quantify.

Qualitatively, we can see that in the above mechanisms (Figure 35), the masses of the entities to be displaced are different, with mass getting larger from electronic to atomic to dipolar polarization. This has a direct relation with the frequency of the applied field (see Figure 36). Intuitively, we can mention that heavier the particular entity, more is the time spent in displacing it. As a result, electronic polarization is the fastest and typically persists at frequencies between $\sim 10^{13}$-10^{15} Hz. In contrast, ionic polarization is sluggish and typically occurs at frequencies between $\sim 10^9$-10^{13} Hz while dipolar polarization involving movement of molecules happens below 10^9 Hz. Interface or space charge polarization occurs at frequencies below 10 Hz. It is important to note that interfacial polarization is nil in the measured ionic liquids as it usually happens at the grain boundaries or any other interface such as electrode-material interface and at very low frequencies [146].
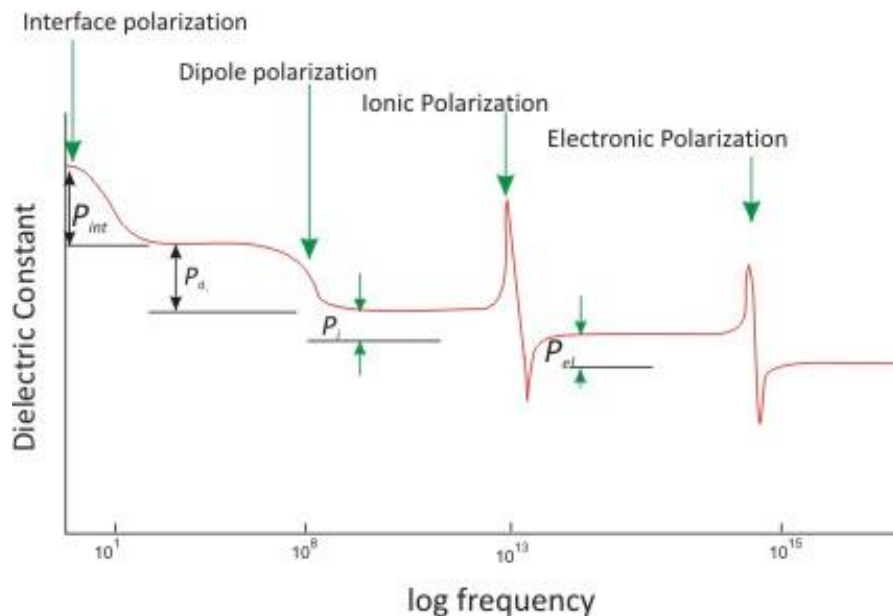
Figure 36: *Schematic figures between dielectric constant verses frequency showing various mechanisms [146].*

In case of electronic and ionic polarization, the charge dipoles can be considered behaving as mechanical oscillators where charges are connected with linear springs whose restoring force balances the force induced via the applied electric field. The characteristic of any such mechanically oscillating system is resonance at a certain frequency.

In case of dipolar (orientation) polarization, there is no direct mechanical restoring force. Instead there are many statistical events that respond in their average results to the driving forces of electrical fields. In other words, if a driving force is present, there is an equilibrium state with an average (net) dipole moment. If the driving force were to disappear suddenly, the ensemble of dipoles will assume a new equilibrium state (random distribution of the dipoles) within some characteristic time called relaxation time. This process does not show any resonance phenomena and is characterized by its relaxation time instead of a resonance frequency.

Given our measured frequency range (up to 10^{10} Hz) the two main mechanisms of polarizations taking place in the ionic liquid are dipolar and ionic polarization.

The timescales for the polarization and depolarization for electronic and atomic polarization is much faster compared to the timescale associated with the permanent dipoles moments in a molecules during orientation polarisation [147]. As a results, due to decreasing contributions of polarisation mechanisms as microwave frequency is increased, the total losses measured in all four liquids is seen to decrease with frequency as evident in Figure 34.

4.1.3.2 Effect of Temperature on Dielectric Properties

For materials that possess permanent dipoles, like the various ionic liquids under study, there is a significant variation of the dielectric constant with temperature. This is due to the effect of heat on dipolar or orientation polarization. As already seen, if a field is applied to the polar material, the dipoles in it will rotate to align with the electric field.

However, it's not that simple. In liquids, it is generally assumed that the dipoles can point in any direction and are continually changing due to thermal agitation

[148]. For a system at equilibrium there is as much random motion in any one direction as in the opposite direction, therefore the average positions of the molecules remain constant.

The dominant mechanism for dielectric heating is dipolar loss, also known as the re-orientation loss mechanism. When a material containing permanent dipoles is subject to a varying electromagnetic field, the dipoles are unable to follow the rapid reversals in the field. As a result of this phase lag, power is dissipated in the material [88]. Therefore, when the temperature of the ionic liquid is increased, the internal energy of the dipolar molecules also increases resulting in a stronger vibrational motion. This makes it even more difficult for the dipoles to follow up with the varying electromagnetic field of the microwaves and thus causes more dipolar losses. An increase in the dielectric constant and loss values is observed for all the measured ionic liquids as temperature is increased from room temperature to a maximum of 125°C as shown in *Figure 37*. Temperature increases the random motion of the liquid molecules which also decreases the relaxation time of polarization. The Debye model expressed in equation 18 directly relates the relaxation time of polarization (τ, s) and/or temperature (T, K) with the viscosity (η, P) of the medium:

$$kT\tau = 4\pi r^3 \eta \qquad (23)$$

Where k is the Boltzmann's constant (1.38×10^{-23} m^2 kg s^{-2} K^{-1}) and r is the radius of the dipolar molecule. The relaxation time of polarization measures the time it takes for a polarised dipole under an applied field to assume its original orientation when the applied field is removed. Assuming that the relaxation time of polarization is fixed in the Debye model, an increased temperature would directly increases the viscosity of the medium which would allow speedy movement of the both free and bound charges causing an increased conduction and number of collisions to result in conduction losses.
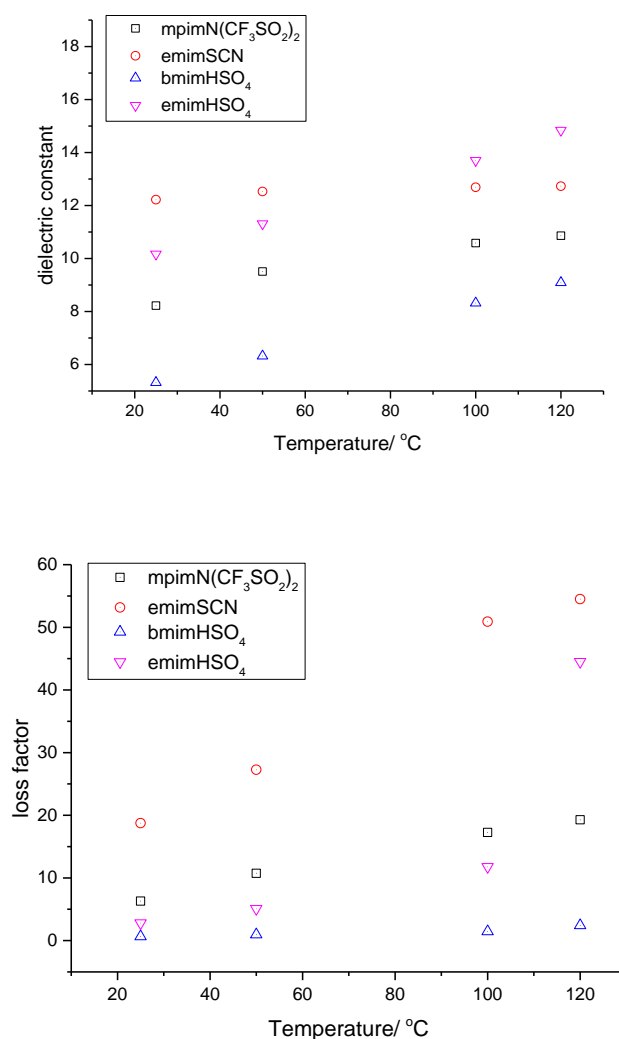
Figure 37: *Effect of temperature on the dielectric properties of the measured ionic liquids at 2.45 GHz frequency; (top) dielectric constant against temperature, (bottom) dielectric loss factor against temperature.*

The vibrational motion and internal kinetic energy of the dipoles would also increase to enhance phase lagging and polarization losses within the medium. An overall increase in microwave dielectric heating is therefore to be expected with temperature as evident in *Figure 37*.

Microwaves directly excite polar molecules and ions. On the macroscopic scale, the substance or substance mixture heats up, which is induced through friction of molecules and/or ions with each other. Therefore, the presence of ions and/or polar molecules is necessary for substances to be heated in the

microwave field [149]. Arrhenius plots were constructed for each liquid by plotting ln(dielectric property) versus 1/T as relative to equation 24 below:

$$\varepsilon = \varepsilon_0 \exp\left(\frac{E_a}{RT}\right) \tag{24}$$

Where E_a is the activation energy (J/mol) needed to be overcome to cause dielectric losses, R is the universal gas constant (8.3145 J.mol^{-1}.K^{-1}) and T is absolute temperature (K). The activation energy for each liquid calculated from Figure 38 has been presented in Table 13 where it is evident that bmimHSO4 liquid possesses the highest activation energy whiles emimSCN has the lowest.
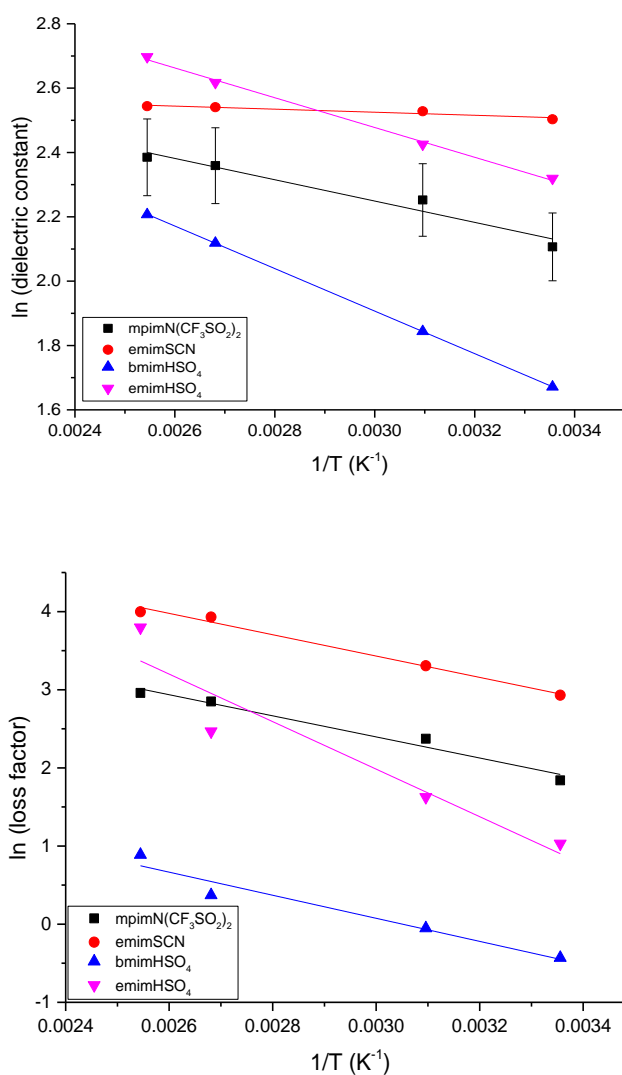
Figure 38: *Arrhenius plots of the dielectric properties of the imidazolium-based ionic liquids measured at 2.45 GHz.*

Table 13: Slopes from the Arrhenius plots (from **Figure 38**) and their derived activation energies (E_a) using the Arrhenius equation, for both dielectric constant and loss factor, Error analysis.

	dielectric constant, ε'		loss factor, ε''	
	slope	E_a (kJmol^{-1})	slope	E_a (kJmol^{-1})
mpim$N(CF_3SO_2)_2$	-331.26	2.8	-1349.74	11.2
emimSCN	-47.48	0.4	-1365.38	11.6
bmimHSO4	-661	5.5	-1476.09	12.3
emimHSO4	-462	3.8	-3040.9	25.3

4.2 Structural Properties of PCB fingers

4.2.1 SEM-EDS analysis

The edge connectors of the computer cards, also called PCB fingers, which were sampled were analysed under SEM-EDS to determine their structure and composition. A couple of micrographs taken are using the SEM equipment are shown in *Figure 39*. All sampled PCB fingers were revealed to be a multi-layered type which indicates that they had additional layers of metal plates embodied within the Thermosetting Epoxy Resin (TEPR) substrate in addition to the surface plates. Six internal metal plates were counted for all 15 randomly sampled fingers, each internal plate measuring an average thickness of 24 µm. Approximately 59 µm was measured as thickness for the surface metal plates which were later revealed by SEM line scan analysis to be laminated.
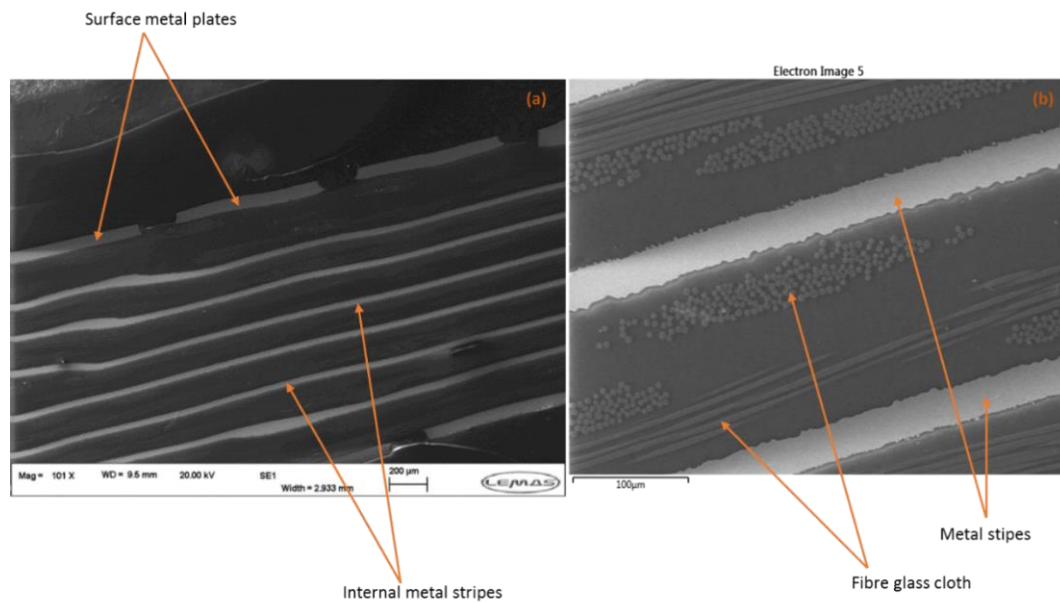
Figure 39: *a) cross-sectional image of a PCB finger indicating the surface metal plates and the internal metal plates. b) A zoomed-in image of the polymer substrate of a PCB finger showing the fibre glass reinforcement and internal metal stripes.*

A zoom-in image of the TEPR matrix presented in *Figure 39*b shows a cluster of bright grey circles and stripes. This is evident of the presence of woven structure of fibreglass cloth used as reinforcement in the TEPR substrate; the circles represent the horizontal cross section of the fibreglass threads and the stripes shows their vertical cross section. A cylindrical thread material can show more than one cross-sections based on the angle of the sectioning plane. *Figure 40* shows two possibilities that are seen in the PCB TEPR micrograph.
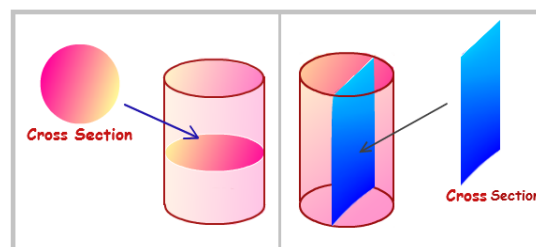
Figure 40: A schematic showing two types of cross sections possible for a cylindrical materials as evident in Figure 39 to represent fibreglass cloth used as reinforcement in TEPR substrate.

TEPR are the most commonly used materials for PCB substrate, because of their good mechanical and electrically insulating properties. From the PCB manufacturer's perspective, epoxy resins are generally relatively inexpensive, adhere well to both copper foil and electroless copper, bond well to glass fibre finished with epoxy-silane, drill easily, can be formulated to be flame-retardant. The term 'epoxy', which describes the type of chemical bond, covers a range of materials with widely differing characteristics and costs. The simplest epoxies are 'difunctional' blends, manufactured by reacting epichlorohydrin and bisphenol. For more demanding applications such as insulating and mechanical properties, the epoxy can be improved by adding more cross-linking to the system, by incorporating 'tetrafunctional' or 'multifunctional' epoxies. However, this may make the material more brittle and less flame retardant. Fibreglass cloth is therefore normally used as reinforcement to ensure toughness and at the same time retain the flame retardant property.

An SEM surface mapping analysis of Figure 39b presented in

Figure *41* showed that the epoxy resin matrix was doped with bromine and chlorine. "For several decades, brominated and chlorinated compounds have been used extensively in the manufacture of printed circuit boards (PCBs)" [150].The epoxy resin substrate owe their flame resistance due to its bromine content, a non-reactive halogen commonly used in industry for its flame retarding properties. This brings meaning the name FR4 to such substrates which implies 'Fire retardant grade 4'. Other similar grades used for PCBs include FR2, which is a type of fire retarding fiberglass resin bonded paper and G10 (commercial epoxy glass grade 10) which is not flame resistant at all. FR2 is cheaper and so has its uses in mass production of low-end electrical equipment. G10, a predecessor to FR4, has all but been taken over by the safer FR4 standard. Its only use in PCBs now are in designs that desire this flammable property.

Also, the SEM surface mapping showed silicon, calcium and oxygen as components of the fibreglass cloth (see

Figure *41*). This indicates that a silica-based fibre glass cloth was used as reinforcement. Reinforcement materials are the backbone of a laminate structure. They provide the strength and dimensional stability required to make

the laminate a viable interconnection structure. They also contribute to the insulating properties of the laminate and can influence manufacturability.

Whilst some of the low-cost laminates use multiple plies of paper, glass fabric continues to be the most widely used reinforcement in rigid laminates as it has good electrical properties, good dimensional stability, good chemical resistance, low water absorption, high tensile strength and good heat resistance.
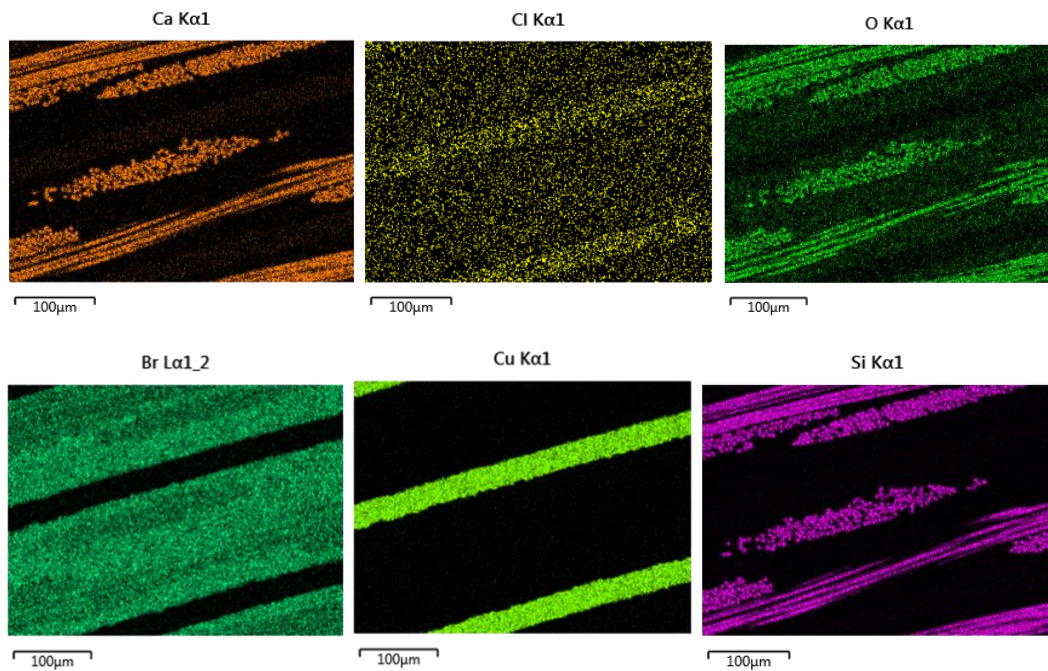
Figure 41: *Mapping of surface elements from* ***Figure 39****b obtained by EDS analysis.*

A line scan measurement (see Figure 42) across the surface metal plate showed a three-layered structure of different metals. Copper, measuring an average thickness of 56.05 microns, forms the base metal which is directly in contact with the epoxy resin substrate. A very thin layer of nickel is plated on the copper with average thickness of 2.03 microns. Finally, to finish up laminate is a 1.17 microns thin gold film. In connector applications where reliability is critical, the separable contact interface must be protected from environmental deterioration. Gold is recognized as the best material to use for this purpose. When applied to the interface of a separable connector, gold

has all of the qualities needed to maintain a stable and low contact resistance over the operating life of most applications.
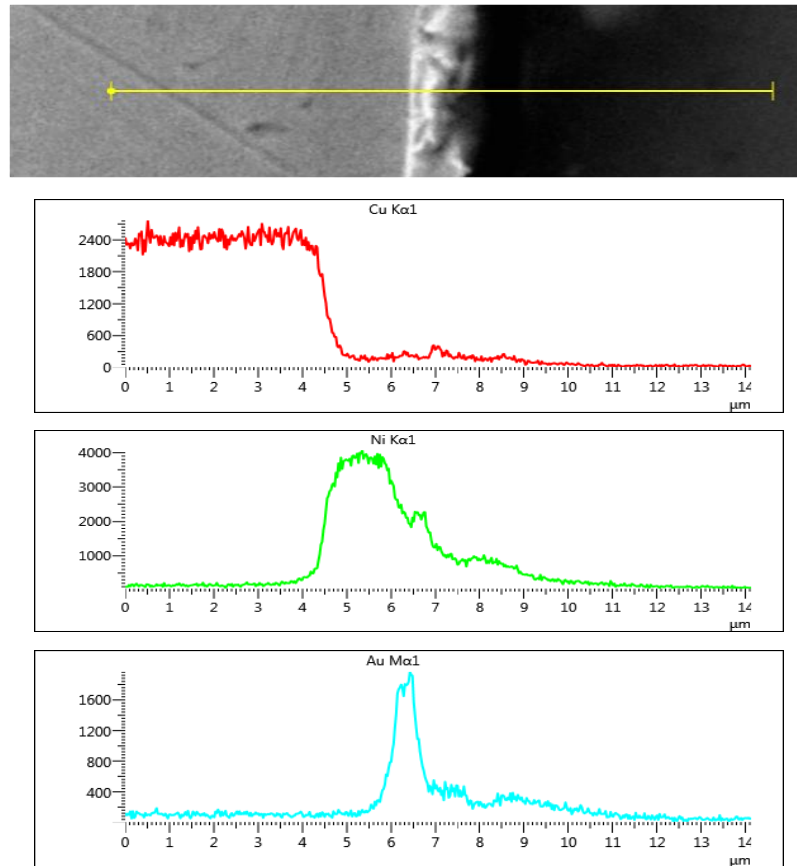
Figure 42: *Line scan across a surface metal plate of the PCB finger showing three plated layers of metal; Copper, Nickel and Gold.*

Because gold is a noble metal, it does not chemically interact with any constituents normally found in a connector environment to form an electrically insulating film. Gold is also a good thermal conductor.

Environments which contain high humidity and/or corrosive pollutants, such as sulphur or chlorine containing gases, can attack metals like copper or nickel to form corrosion products which disrupt electrical contact. However, gold does not degrade under the environmental conditions that are likely to be encountered by electronic components. The protection offered by gold can be compromised if there are pores or cracks in the coating. These act as openings through which atmospheric pollutants can attack the substrate metal to form insulating corrosion products. Because gold is a noble metal and

because thin gold plating tends to be porous, gold coatings are susceptible to the creep of base metal corrosion products across the surface of the gold after formation at pore sites and edge boundaries. Corrosion creep can be inhibited by applying an overall nickel coating prior to application of the gold. The nickel under-layer serves as a diffusion barrier to most base metal constituents, and nickel corrosion products are self-limiting, passive and not susceptible to corrosion creep.

Gold coating endures high durability. Coating a contact with pure gold generally results in a connector with low durability and high insertion forces (i.e., high coefficient of friction), especially when the thickness is greater than 0.13 microns.

Nickel is plated between the copper and gold to prevent copper diffusion and weak bond strength between the copper and gold plates. It also prevents the diffusion of copper into the gold layer at high temperatures especially during heat treatment. A relatively hard nickel under-plate also serves as a mechanical support for the gold coating, and increase its durability.

A model structure shown in

Figure 43 attempts to conceptualize the structure of a typical multi-layered finger as used in this research work. An average thickness for each metal plate determined from several line scan measurement (one is shown in Figure 42 above) is displayed in Table 14 below.
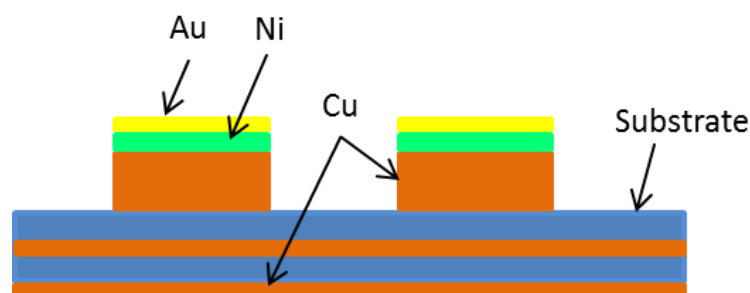
Figure 43*: A schematic one-sided model structure of the PCB finger showing the epoxy resin substrate; multi-layered surface metal plates of Cu, Ni and Au; and internal plates of Cu embedded in the epoxy resin substrate.*

Table 14: Average thickness of metal layers that form the multi-layered surface plate of a PCB finger sample.

Metal	Thickness (µm)
Au	1.17
Ni	2.03
Cu (surface plate)	56.05
Cu (embedded stripes)	23.62

4.2.2 Mass fraction analysis

In this section, the mass fraction of each element is calculated based on information from SEM-EDS analysis, literature and measurements taken directly from the lab. The thickness for each plate was attained from SEM-EDS analysis. The length and breadth of the metal plates were measured using a micrometre screw gauge in the lab and their density obtained from literature. The volume for each metal was therefore calculated as the product of their average dimensions (length x breath x height). An average volume over 10 samples were taken to represent the volume for each component. The mass of each component was also found as the product of their density and deduced volume. The mass fractions derived for each component is represented in a pie-chart shown in Figure 44. Mass fraction analysis shown on a pie chart in Figure 44-*top* indicates that a tonne of PCB fingers contains 3.1 kg gold (0.31 %), 2.4 kg Nickel (0.24 %), 298.4 kg copper (29.84 %) and 696.1 kg fibre glass reinforced TEPR (69.61 %). This makes a composite of approximately 30 % metal and 70 % fibre glass reinforced polymer. The copper metal which is the most abundant metal found in the PCB fingers is found both laminated to the surface plate and also embedded in the TEPR substrate. Considering only the multi-layered surface plates, copper alone makes up almost 93% (Figure 44-bottom). Gold and nickel make approximately 4 % and 3 %, respectively. Thus, considering the surface plates alone, the ratio of nickel to copper was thus 1:31 whiles the ratio of nickel to gold was found to be 3:4.
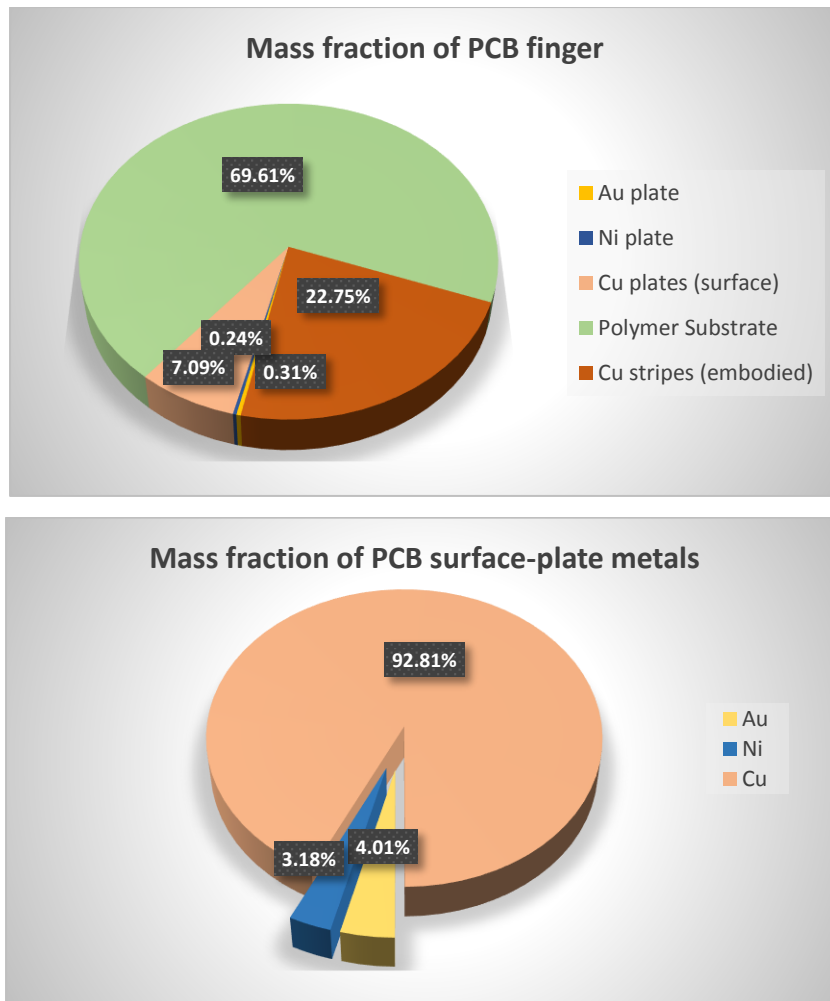
Figure 44: *Top: mass fraction of computer card edge connector (PCB finger);*
Bottom: Mass fraction of the surface metal plates on a PCB finger.

4.2.3 Value share analysis

As emphasised in Chapter one, the scrap e-waste contains many kinds of
metals, which is a rich mine of wealth. Gold, nickel and copper all have
economic values that are of interest to both the metal recycling and the mining
industry. In this section, the values of each component of the PCB finger is
calculated relative to its mass fraction against current market prices as at 1st
march, 2018. Calculations were based on these findings: £30,800.00/kg for
gold, £10.00/kg for nickel and £5.03/kg for copper [151-153].

Table 15: Value share of PCB finger components. Au: Gold, Ni: Nickel, Cu: Copper, TEPR: Epoxy resin relative to the date: 1st March 2018.

	Mass per tonne (kg)	Price per tonne (£)	Value share (%)
Au	3.30	101640.00	98.52
Ni	2.40	24.00	0.02
Cu	298.40	1500.95	1.45
TEPR	696.10	0.00	0.00

A tonne of PCB fingers had a value of £103,164.00. Out of this amount, gold which is only 0.33 wt%, had a value £101,640.00 (a whopping 98.52% value share). The 29.8 wt% of copper was worth £1500.00 whereas Nickel was priced at £24.00 due to its very low weight percent of 0.24.

The polymeric part, the fibre glass reinforced TEPR, was found to be valueless on the material market. The low economic value of TEPR may explain its general treatment practice; either controlled incineration or uncontrolled incineration (open burning). They are sometimes used as landfills. Some researchers have reported the use of these non-metals as fillers for epoxy resin products such as paints, glues, agents of decoration and building materials [154-158].

Phenolic resins are one of the oldest and most common thermoset resins. Phenolic moulding composites (PMC) are produced with phenolic resin, acting as a binding agent, various fillers, gelling and dyes under high temperature and a certain pressure. Due to its relative low price, ease of fabrication, high mechanical strength, heat resistance and high dielectric strength, PMC is widely used and is being used in radios, kitchen appliances, and electronic switches. The growth in production of PMC in recent years greatly increased the need for wood flour, which is used as organic filler in moulding compounds. With the depletion of timber resources and the increasing price of wood flour, it is a task for PMC producers to protect timber resources and reduce the cost of raw materials by finding alternative materials to wood flour. Some researchers have used non-metals, especially TEPR, recovered from PCBs to replace wood flour for the production of PMC [7, 159].

4.3 Chapter summary

The physical properties including molar weight, density and viscosity of the selected ionic liquids were taken from literature and compared. Their electrical conductivity were however measured using the home-made conductivity cell. A comparison of the conductivity values to values from literature indicates that the conductivity setup showed accurate values since there measured values did not change much from values obtained from literature. For example bmim[HSO$_4$] had a measured conductivity of 1.34 mS/cm, whiles a value of 1.4 mS/cm was obtained from literature [140]. Emim[SCN] measured 22 mS/cm compared a literature value of 21 [142].

An inverse relationship between the viscosity and the conductivity of the liquids was observed which was explained using the Stoke-Einstein viscosity model and the Nernst-Einstein law [143]. Both models when combined provides an apparent inverse relationship between conductivity and viscosity of the conducting medium irrespective of its composition and particular properties of the constituent ions. Amongst the four ILs investigated, the Bmim$^+$[HSO$_4$]$^-$ IL has the highest viscosity of 164 cP at 80°C, and consequently the lowest electrical conductivity of 1.34 mS/cm at room temperature. On the other end, the IL emim[SCN] exhibits high electrical conductivity of 22 mS/cm and low viscosity of 21 cP at 25 $^\circ$C

The ILs were analysed using FTIR for their molecular composition. A summary of some characteristic peaks have been presented in Table 16 below:

Table 16: Some characteristic peaks for all ILs measured using Fourier transform Infrared spectroscopy (FTIR).

ILs	Characteristics	
	Cation	Anion
bmim[HSO4] mpim[N(CF$_3$SO$_2$)$_2$] emim[SCN] emim[HSO4]	3158 and 3118 (C-H stretching from imidazole ring), 2965 and 2872 C-H,CH$_2$ and CH$_3$ stretching peak	1344, 1334 (S=O stretching), 1164, 1176 (asymmetric SO$_2$ stretching)

	on lateral chain of imidazole ring, 1569 and 1459 (skeletal vibration peaks of imidazole ring) 1170 (in-plane bending vibration peak of C-H from imidazole ring)	1164 (SOH bending modes)

In terms of microwave heating with the ILs, it is understood that microwaves interact with dielectric materials either through conduction process or by polarization. Conduction losses occur when the moving ions collide with other species in the liquid whereas polarization losses occur when frictional forces resist induced motions by the microwaves. Both conduction and polarization loss mechanisms dissipates heat into the system which results in volumetric heating.

It was observed that the dielectric losses decrease with frequency which may be attributed to the various polarization mechanisms which occur as a function of microwave frequency namely electronic, ionic, dipolar and interfacial. The masses of the entities to be displaced in these mechanisms are different, with mass getting larger from electronic to ionic to dipolar polarization. This has a direct relation with the frequency of the applied field as expressed in Figure 36. As a results, at higher frequencies, interfacial and dipole polarization cease to contribute.

Temperature was seen to have an influence on the dielectric losses of the ILs as an increase in the dielectric constant and loss factor values was observed with increasing temperature. This behaviour was explained using the Debye model which directly relates the relaxation time of polarization and/or temperature with the viscosity of the medium. It is apparent in this model that the viscosity must decrease was temperature is increased which would consequently increase the random motion and kinetic energy of the liquid molecules and number of collisions and resulting in more conduction and dipolar losses.

Moreover, chapter 4 provides results of elemental analysis performed on the PCB fingers and gives an idea of molecular composition of the four selected

ionic liquids using SEM-EDS and FTIR spectroscopy, respectively. SEM-EDS analysis reveals that the structure of a typical PCB finger is made up of fibreglass reinforced TEPR substrate with copper plates embedding within the substrate. About 6 parallel copper plates were counted for all samples analysed. On the surface of the TEPR substrate are mounted several parallel multi-layered plates made up of copper, nickel and gold. Gold is used as the finishing metal on the multi-layered surface plate whiles nickel is sandwiched between gold and copper. Copper forms the bottom metal that connects the surface plate to the TEPR substrate. A schematic conceptual structure was established to make it easy to visualize the elemental structure of a typical PCB finger.

Mass fraction analysis (MFA) revealed that TEPR makes up ~70 wt% of the PCB finger, ~23 wt% of the finger is made of internal copper plates and ~7 wt% forms the surface plates. Of the surface plates, MFA showed ~93 wt% copper, ~3 wt% nickel and ~4 wt% gold. This indicates that a typical PCB finger would contain 0.31 wt% gold. The masses were valued using prices obtained from 1st March, 2018 in a value share analysis which revealed that gold though constitutes only 0.31 wt% of the PCB finger sample was worth 98.52%. From the MFA and value share analysis, a tonne of PCB fingers was found to contain 3.3 kg of gold worth £ 101,640.00.

Chapter 5

PCB finger separation technique

5.1 Process flow

The process used in this study to separate PCB finger waste is outlined and discussed in this chapter. This separation technique employs the use of bmimHSO$_4$ ionic liquid to completely delaminate the PCB fingers under microwave irradiation. Delamination is simply a separation of the PCB finger composite that occurs when the TEPR substrate is dissolved by the ionic liquid. Since the TEPR acts as the substrate, once it is moved into solution, the surface plates, embedded plates and fibreglass reinforcements are freed as a results. Further techniques such as acid leaching and electrowinning are utilized to further recover individual components of the delaminated products. A regeneration process is utilized to purify the ionic liquid leachate to enable reuse. Figure 45 shows a flow chart of the entire separation and recovery route adapted for the treatment of PCB finger wastes in this study. Each step is carefully analysed under sub-sections and discussed
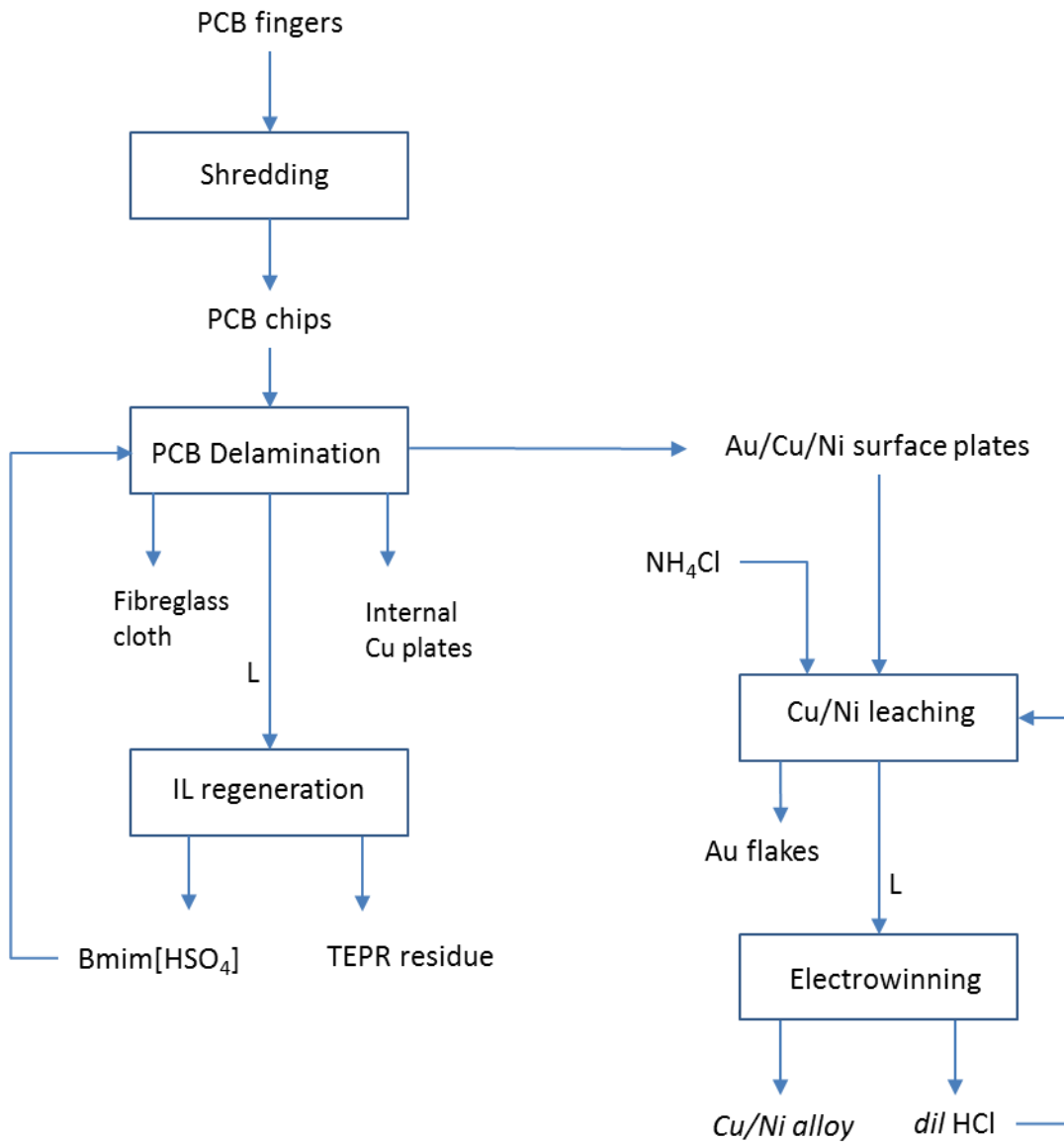
Figure 45: *A process flow diagram employed in this study used in the treatment of PCB fingers. It outlines the major separation and recovery steps. Product materials include fibre glass cloth, gold metal flakes, TEPR residue, Cu/Ni alloy.*

5.2 PCB delamination process

5.2.1 Visual observation

The PCB chips were leached in bmim[HSO$_4$] ionic liquids under 200W, 2.45GHz microwave irradiation. A total delamination of the PCB chips was achieved after two hour. The polymeric component, the thermosetting epoxy resin (TEPR), was leached by the ionic liquid which resulted in a total separation or delamination of the PCB chips. During the delamination process, the ionic liquid changed colours from colourless to dark brown eventually. These colour changes are displayed in **Figure 46** below.
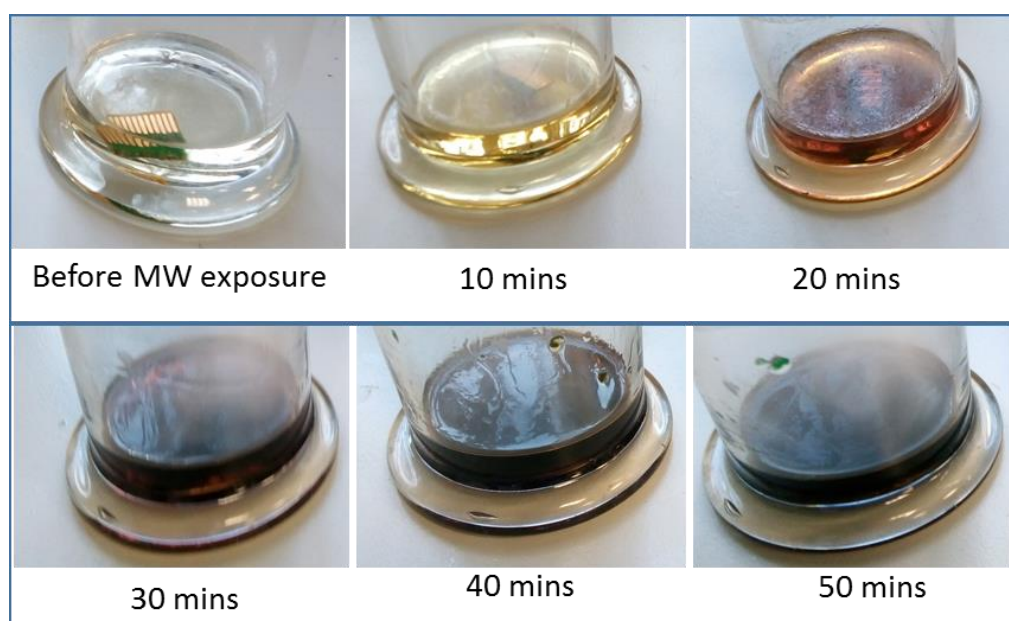
Figure 46: *Bmim[HSO$_4$] liquid changes colour as it dissolves TEPR substrate over time in a 200W, 2.45GHz microwave environment.*

The first colour change was observed after 10 mins, where the colourless liquid adopted a bright yellow shade. No visible changes to the PCB finger such as swelling or size reduction were however observed. After 20 mins, the colour of the ionic liquid had changed from bright yellow to brown which may indicate a significant stage of epoxy dissolution reaction. No physical changes to the PCB chips could be observed at this stage. After 30mins of microwave exposure, the ionic liquid adopted a dark brown shade. Some green particles

obviously from the TEPR were seen in the IL solvent. The PCBs were swollen, moreover, some surface plates were disoriented as if they had been partly detached. Figure 47a shows the floating particles of TEPR after 30 mins of microwave-assisted delamination process. After 40mins, the metal plates had begun to fall off into the substrate. Even though the TEPR substrate was still seen as intact, many more green particles were seen in the IL solvent. Pieces of Fibre glass cloth were seen in the leaching solvent after 50 mins as evident in Figure 47c. The colour remained dark brown for about two hours where a complete delaminated of the PCB finger was achieved. The metal plates at this stage had totally been detached from the TEPR substrate as shown in Figure 48b.
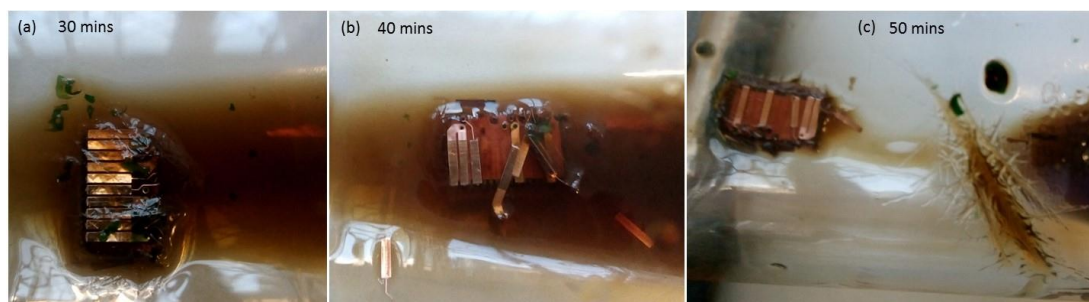
Figure 47: *Dissolution of FR4 epoxy resin and detachment of surface metal plates of PCB fingers in bmim[HSO$_4$] liquid after (a) 30 minutes; (b) 40 minutes; (c) 50 minutes.*
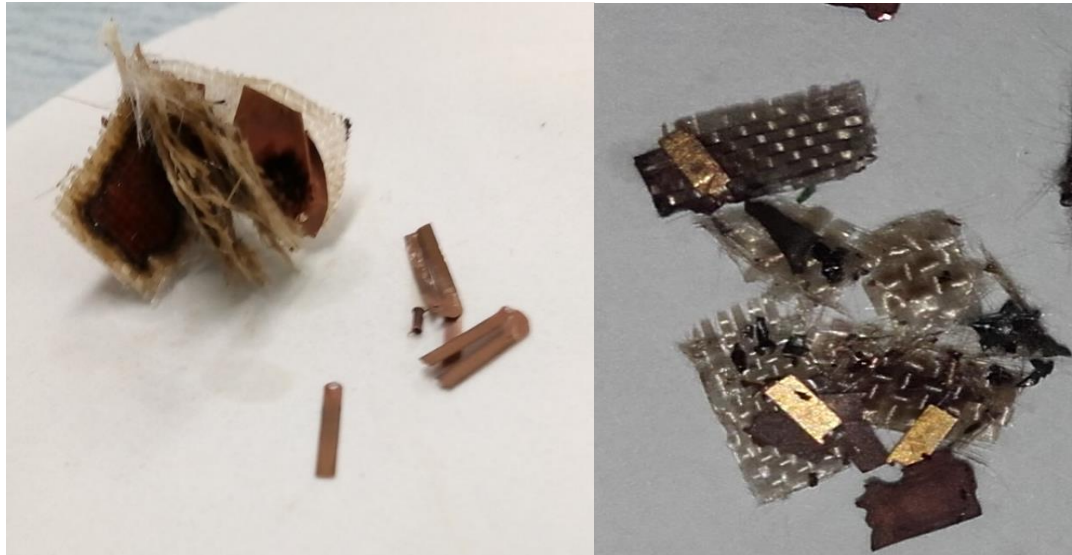
Figure 48: *A delaminated PCB chips: (left) After 1 hour of microwave-assisted leaching in bmim[HSO$_4$]; (right) After 2 hours of microwave-assisted leaching in bmim[HSO$_4$] liquid.*

5.2.2 Rate of reaction

Rate of reaction is described as the speed at which a chemical reaction proceeds. It is often expressed in terms of either the concentration of a product that is formed in a unit of time or the concentration of a reactant that is consumed in a unit of time. Alternatively, it may be defined in terms of the amounts of the reactants consumed or products formed in a unit of time. In this section, the rate of reaction is expressed as the amount of products formed over a given time. Two set of tests were conducted to determine the rate of reactions and consequently an activation energy for this delamination process was determined.

The set of first tests, the leaching of TEPR by bmim[HSO$_4$] was performed in a microwave oven at 200 W power and 2.45 GHz frequency. The measured temperature of ionic liquid during MW-assisted reaction was found to be 250 ^{o}C. PCB samples were put in the ionic liquid and then exposed to microwave irradiation. A total delamination of the PCB chips were achieved after 2 hours. The second set of tests were conducted without microwave assistance. Instead, a hot plate was utilized to reach isothermals of 80 ^{o}C, 100 ^{o}C, 120 ^{o}C and 150 ^{o}C. No chemical reaction occurred for delamination tests conducted

at room temperature, 80 °C nor 100 °C even though the reaction was left to run for ~48 hours. This can be understood by the activation energy model. All molecules possess a certain minimum amount of energy. The energy can be in the form of kinetic energy or potential energy. When molecules collide, the kinetic energy of the molecules can be used to stretch, bend, and ultimately break bonds, leading to chemical reactions. The activation energy is the minimum energy required by the molecules to initiate a chemical reaction. It is apparent that the molecules had not reached the activation energy at 100 °C, hence no reaction occur at or below this temperature.

At 120 °C, a clear sign of delamination reaction was seen after 3 hours which was marked by changed colour of the leaching solvent from clear to bright yellow. The colour changes followed a similar pattern as was observed in the microwave-assisted delamination reaction described in section 5.2.1. A complete delamination was observed after 9 hours.

At 150 °C, a colour change to bright yellow was observed after 1 hour. A quicker reaction rate was witnessed at this temperature as complete delamination of the PCB samples was observed after 5 hours.

5.3 Regeneration process of bmim[HSO$_4$]

A regeneration method was adopted to purify and restore the ionic liquids after delamination process where the bmim[HSO$_4$] IL becomes filled with TEPR residue and metal plates of both internal copper plates and multi-layered surface plates of copper, nickel and gold. A dark brown and very viscous liquid with no fluidity was achieved after delamination reaction. This thick bmim[HSO$_4$] leachate was diluted with distilled water to allow fluidity and enable separation of the solids; internal copper plates, the multi-layered surface plates and the fibreglass cloth by utilizing a 0.5 mm mesh sieve. The filtrate liquid was allowed to sit for about an hour to allow decantation.
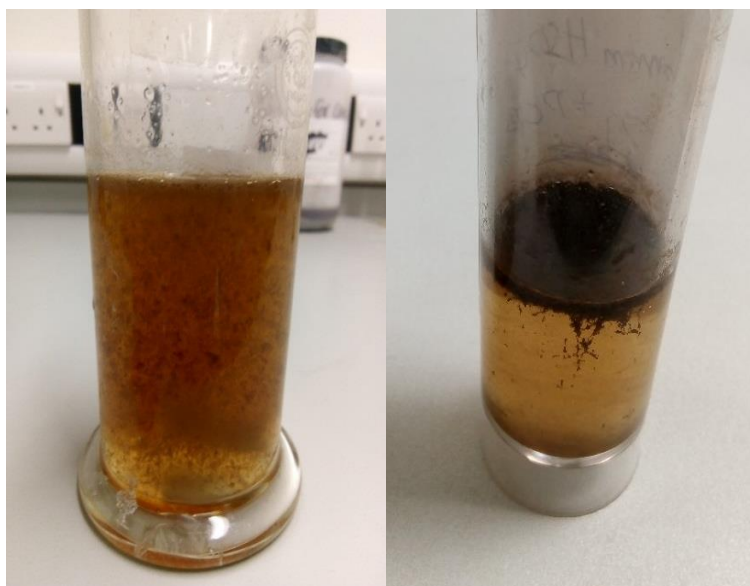
Figure 49: H_2O diluted Bmim[HSO_4] leachate after delamination process: (left) leachate after sieving out the surface plates, internal plates and fibreglass cloth reinforcement; (right) decanted leachate after sitting for 1 hour.

From Figure 49 the TEPR residue settles on the surface of the liquid after 1 hour. Filtration is performed after decantation using a filter paper to separate the TEPR residue from the diluted ionic liquid.

Figure 50: (left) TEPR residue obtained after filtration; (b) H_2O diluted bmim[HSO_4] after filtration.
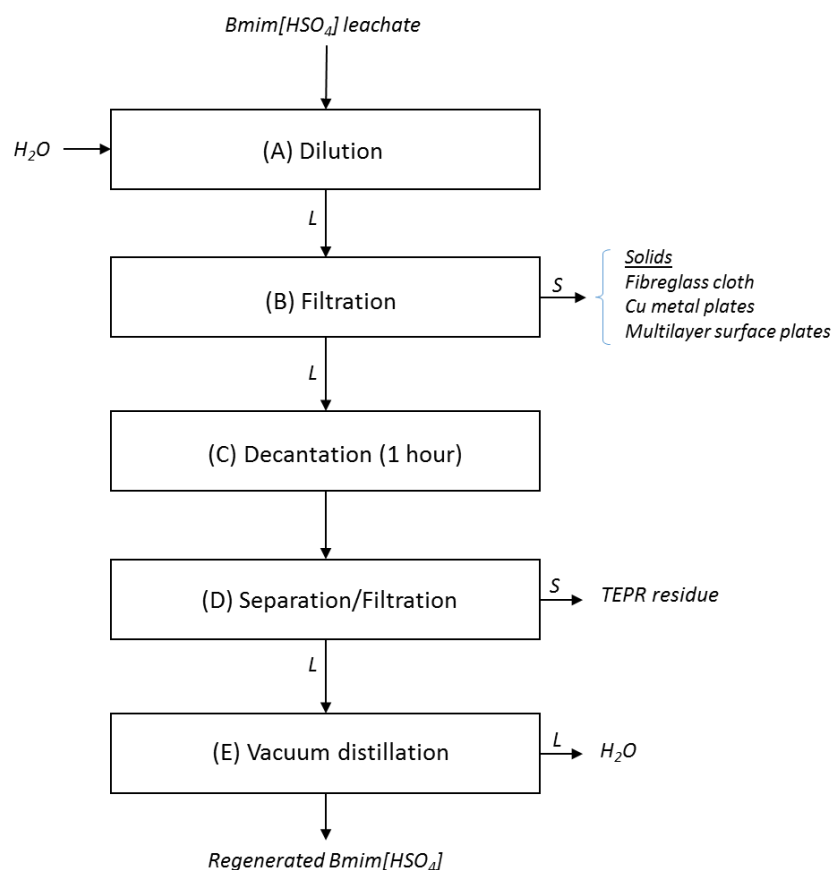
Figure 51: *A flow chart of bmim[HSO$_4$] regeneration process showing the various steps of the process namely; dilution, filtration, decantation, separation/filtration and vacuum distillation.*

The filtrate obtained after step D of Figure 51 or from *Figure 50*b was taken through vacuum distillation in a setup explained at the experimental section to remove the water from the ionic liquid. The regenerated ionic liquid had a bright yellow colour which is similar to the colour it attains after 10 mins during the delamination process shown in Figure 46. This suggests that a small amount of the TEPR residue still remained in the ionic liquid after the regeneration process. It may be similar the amount of TEPR that moves into the liquid after 10min leaching process in microwave environment due to their same colour. An FTIR spectral analysis shown in Figure 52 compares a pure bmimHSO$_4$ liquid to a regenerated liquid after delamination process.
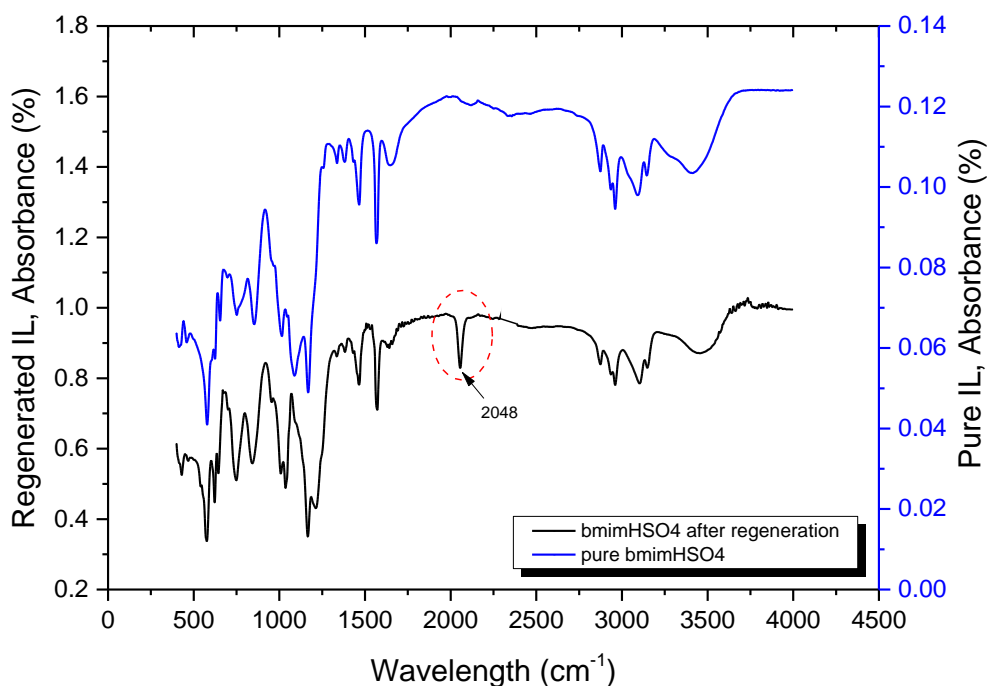
Figure 52: *An FTIR spectra comparing pure bmim[HSO$_4$] to a regenerated bmim[HSO$_4$] liquid after delamination process. A new peak at 2048 cm^{-1} present in the regenerated IL spectrum shows the presence of CN bond characteristic of the diamine hardener found in the TEPR substrate.*

The lone peak at 2048 cm-1 which indicates the presence of a CN bond stretching was observed in the regenerated IL spectrum [145]. This may be attributed to the diamine hardener used in the production of the TEPR substrate. The ionic liquid may have broken the hardening chains of the TEPR substrate to succeed in moving it into solution.

The most common and important class of TEPR used in PCB applications is formed from reacting epichlorohydrin with bisphenol A to form diglycidyl ethers of bisphenol A, commonly abbreviated as DGEBA. DGEBA resins are transparent colourless to pale-yellow liquids at room temperature. In order to convert epoxy resins into a hard, infusible, and rigid material, it is necessary to cure the resin with hardener. Amines are the most commonly used curing agents for epoxy cure. The curing process is a chemical reaction in which the epoxide groups in epoxy resin reacts with a curing agent (hardener) to form a

highly crosslinked, three-dimensional network. A schematic for such reaction is shown in Figure 53 where an epoxy group reacts with one amine-hydrogen, i.e. one hydrogen attached directly to a Nitrogen atom.
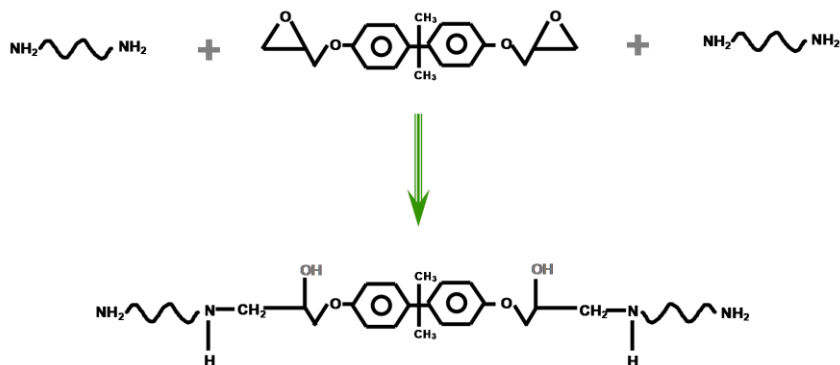
Figure 53: *An initial reaction between epoxy resin and amine hardener where hydrogen from the two amine groups are linked to the epoxy rings at both ends of the epoxy resin. A linear molecule is achieved.*

As can be seen in Figure 53 every time that an epoxy group is opened, one hydroxyl group is generated. Initial chemical reaction builds linear molecular weight, the molecules get longer and longer giving thereby increasing its viscosity.
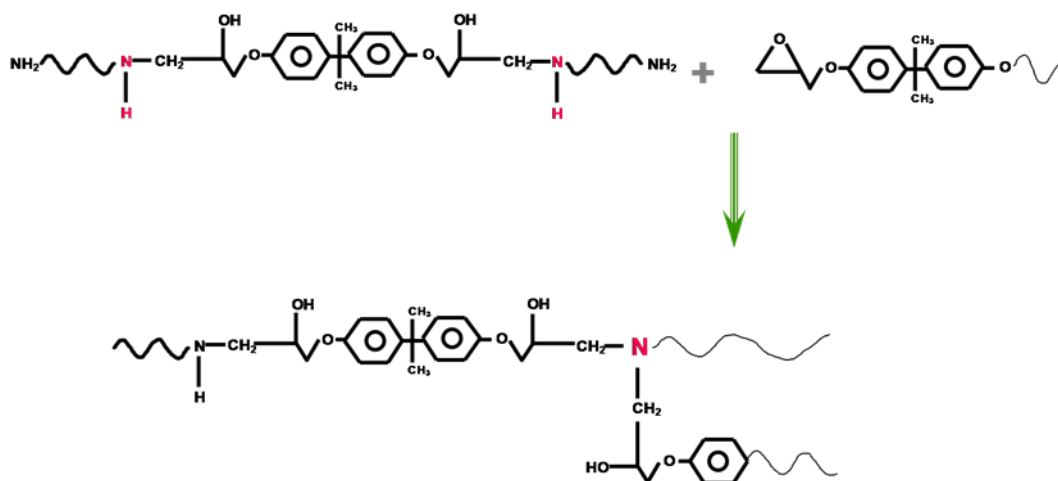
Figure 54: *A crosslinking process where the linear molecules generated from Figure 53 are linked to one another in a 3D manner to all active amine hydrogens sites. CN bonds are formed as a result.*

The next step in the curing process is the linking of the chains with each other called crosslinking. In order for this to occur it is necessary that each amine molecule will have more than two active amine hydrogen's. The inter-linking of larger molecules causes a rapid increase of the liquid's viscosity which eventually results in the curing of the epoxy resin.

The lone peak at 2048 cm^{-1} may very well represent the breaking of the CN bonds from the TEPR substrate which forms the main crosslinking elbows as shown in Figure 54. The breaking of CN bonds by the ionic liquid would explain the easy movement of the TEPR into IL solvent and the possible physical separation technique employed in removing TEPR residue from the IL solvent after delamination process. The breaking of the CN bonds may be the only chemical reaction that occurred in the delamination step. To probe this theory further, an FTIR analysis was conducted to investigate the lone peak at 2048 cm^{-1}. In this analysis, delamination processes were conducted over different times to enable a comparison of the intensity of the lone peak. Samples obtained from delamination steps outlined in Figure 46 and Figure 47 were taken through the regeneration process (shown in Figure 51) and their regenerated samples were analysed using FTIR. The intensity of the CN stretching peak increased with resident time of reaction as shown in *Figure 55* which proves that the leaching reaction is related to the breaking of the CN bonds in the TEPR
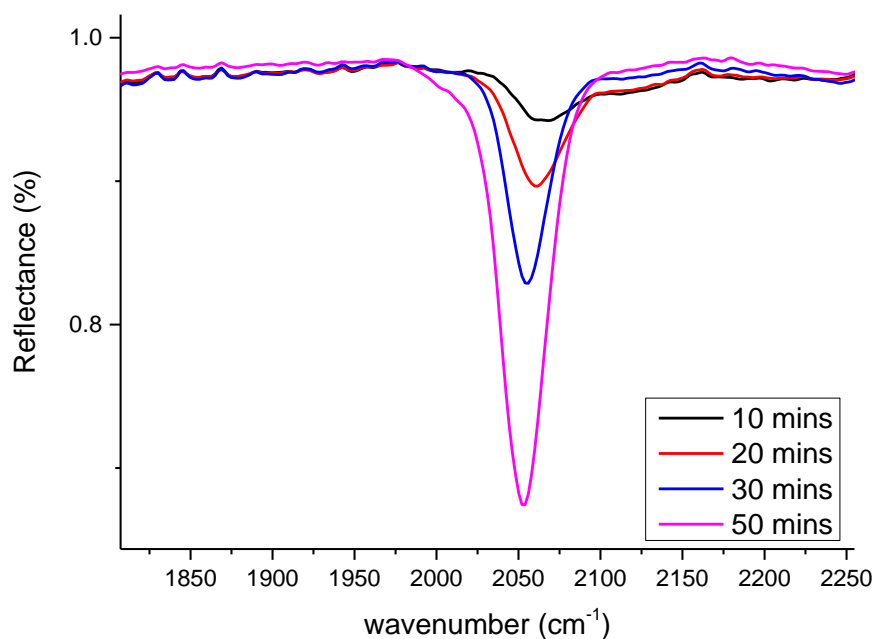
Figure 55: *Lone peak at 2048, characteristic of CN bond, increases in intensity as resident time of delamination reaction is increased.*

The regenerated bmim[HSO$_4$] was reused successfully in MW-assisted delamination processes for up to four times without any decrease in the reaction time. The colour changed to bark brown at the end of each reaction but returned to bright yellow after regeneration process.

5.4 Cu/Ni Acid leaching process

Two kinds of metal plates were obtained from the delamination step, the internal copper plates and the multi-layered surface plates. These were separated by hand since the internal plates are very wide (size of the PCB finger approximately 30 mm x 5 mm as compared to the surface plates (approximately 2mm x 5 mm). Figure 56 shows pictures of the different kind of plates obtained from the delamination step. The target sample, the multi-layered surface plate, were populated for the leaching experiment aimed to free the gold layer.
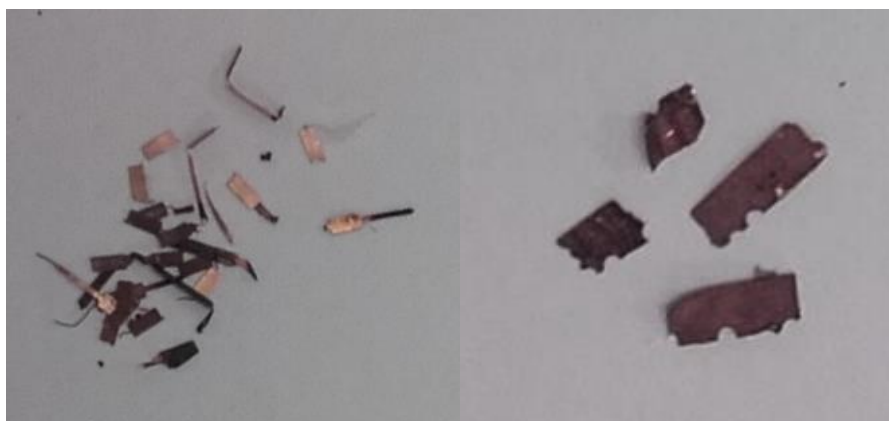
Figure 56: (*left) multi –layered surface plates (Au, Ni, Cu) found on the surface of the TEPR substrate, right) internal copper plates embedded in the TEPR substrate.*

Three sets of tests were conducted on the multi-layered surface plates in order to leach both copper and nickel plates. The first set of tests were conducted at room temperature. 1 g of PCB fingers was put in 10 mL of 1 M HCl acid. 1g NH_4Cl was added as oxidant to aid in the dissolution of copper and nickel metal. A full dissolution reaction was achieved after 7 days.

The second set of trails performed in in a microwave environment at 100 W power and 2.45 GHz frequency. Same solution concentration, solute and oxidant was used in same ratio as the first set of test. A total reaction was achieved after 3 hours in this microwave-assisted set of tests.

In the third set of trails, the dissolution reaction of copper and nickel was performed at 120 $^\circ$C by using a hot plate. Here, the reaction time taken to complete the reaction was 6 hours.

5.4.1 Visual observation

The visual observations reported *Figure 57* is based on microwave-assisted leaching even though same observations are made for all sets of Cu/Ni leaching tests. The leaching solution of HCl acid and NH_4Cl was colourless.
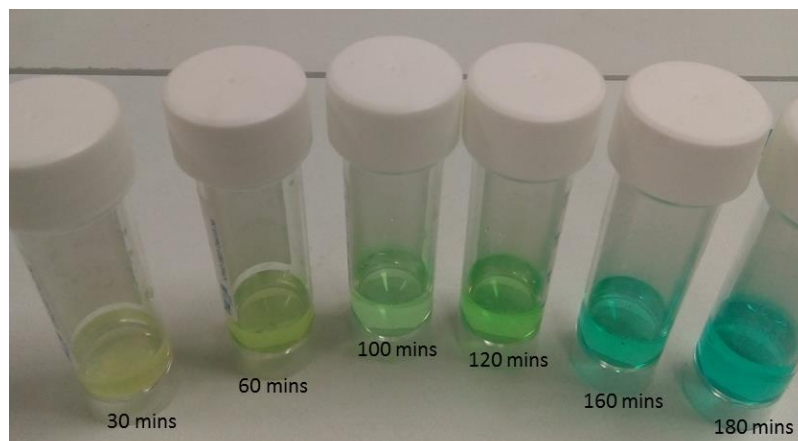
Figure 57: Change of colour of 1.0 M HCl / NH₄Cl leachate solvent during microwave-assisted leaching of copper and nickel. Aqua green colour was achieved at the end of reaction after 3 hours.

Figure 58: A comparison between a rigid multi-layered surface plate before leaching and a gold flake after leaching reaction: (a) a top view of the surface plate compared to a gold flake; (b) a bottom view of the surface plate compared to a gold flake after leaching away copper and nickel layers.

After adding PCBs and exposing them to microwave irradiation, the colour of the liquid began to change from yellow to various shades of green during the leaching process but ended with aqua green. *Figure 57* displays the colour shades observed during the leaching reaction of copper and nickel with microwave-assistance. Also observed was the multi-layered plates before and after leaching reaction. A curvy and flaky shaped gold plate was left after the

leaching reaction of copper and nickel. An initial rigid plate with a gold plate on one side and a dark copper plate on the other was drastically changed into an all gold metal as displayed in *Figure 58* evident of successful leaching of the copper and nickel underlayers.

5.4.2 Rate of reaction

The rate of Cu-Ni leaching reaction by 1M HCl and NH₄Cl solution was found for all three different cases; at room temperature, at elevated temperature of 120 °C and in microwave environment at 100W, 2.45 GHz which is equivalent to ~200 °C. From

Figure *61*, an ultraviolet-visible spectra of various leachate solutions obtained at different conditions are shown. Notable are the copper peak at 800 nm [160] and the nickel peak at 970 nm [161]. It is observed that both absorption peaks increase with residence time of leaching reaction which indicates a progressive leaching reaction over time as indicated in the reaction equation 25 and 26 below and their corresponding Eh-pH diagrams produced by FactSage software shown in Figure 59 and Figure 60.

$$Cu_{(s)} + HCl_{(aq)} + NH_4Cl_{(s)} \rightarrow CuCl_{2(aq)} + NH_{3(g)} + H_{2(g)} \qquad (25)$$

$$Ni_{(s)} + HCl_{(aq)} \rightarrow NiCl_{2(aq)} + H_{2(g)} \qquad (26)$$
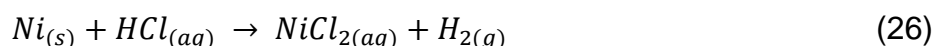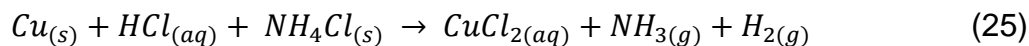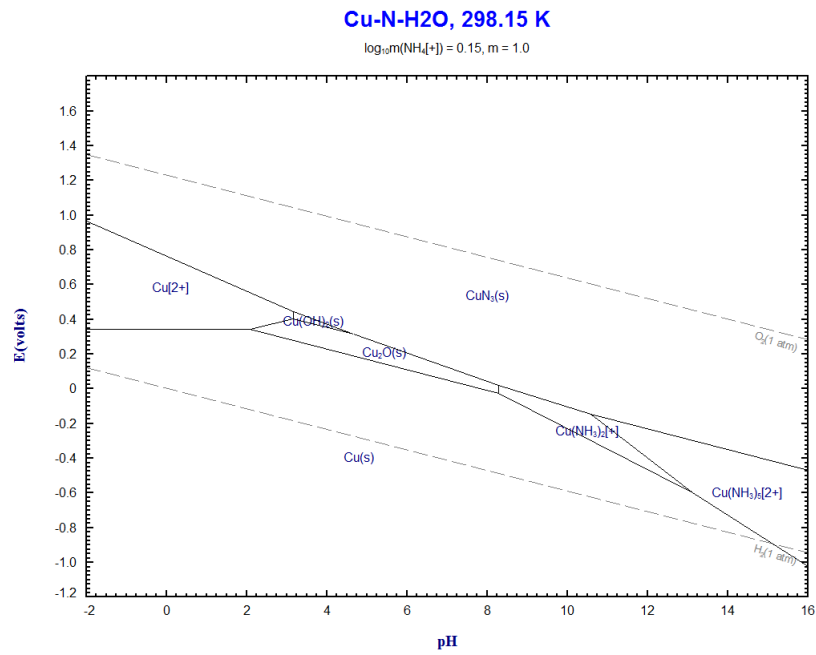
Figure 59: *Eh-pH diagrams of Cu-N-H₂O system corresponding to eqn. 25.*
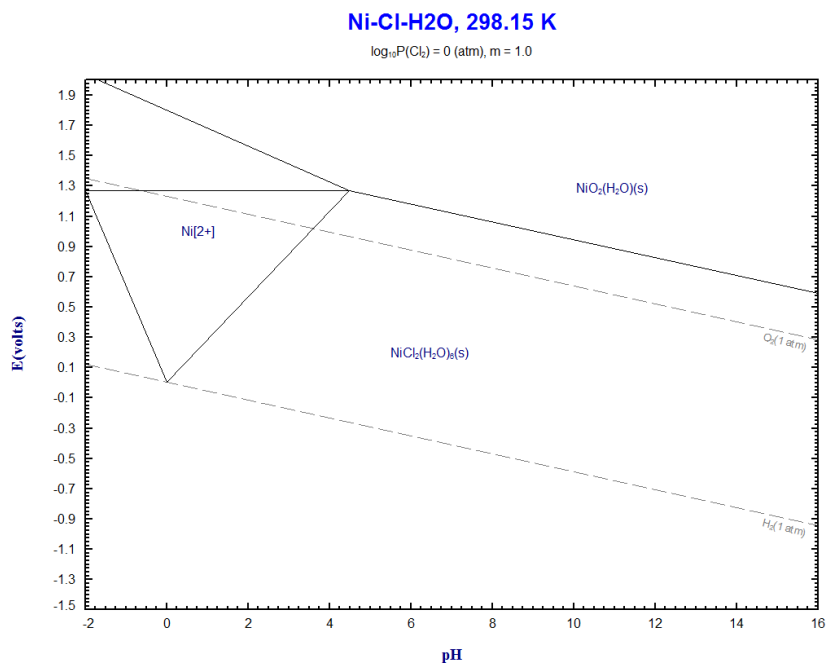
Figure 60: *Eh-pH diagrams of Ni-Cl-H₂O system corresponding to eqn. 26.*
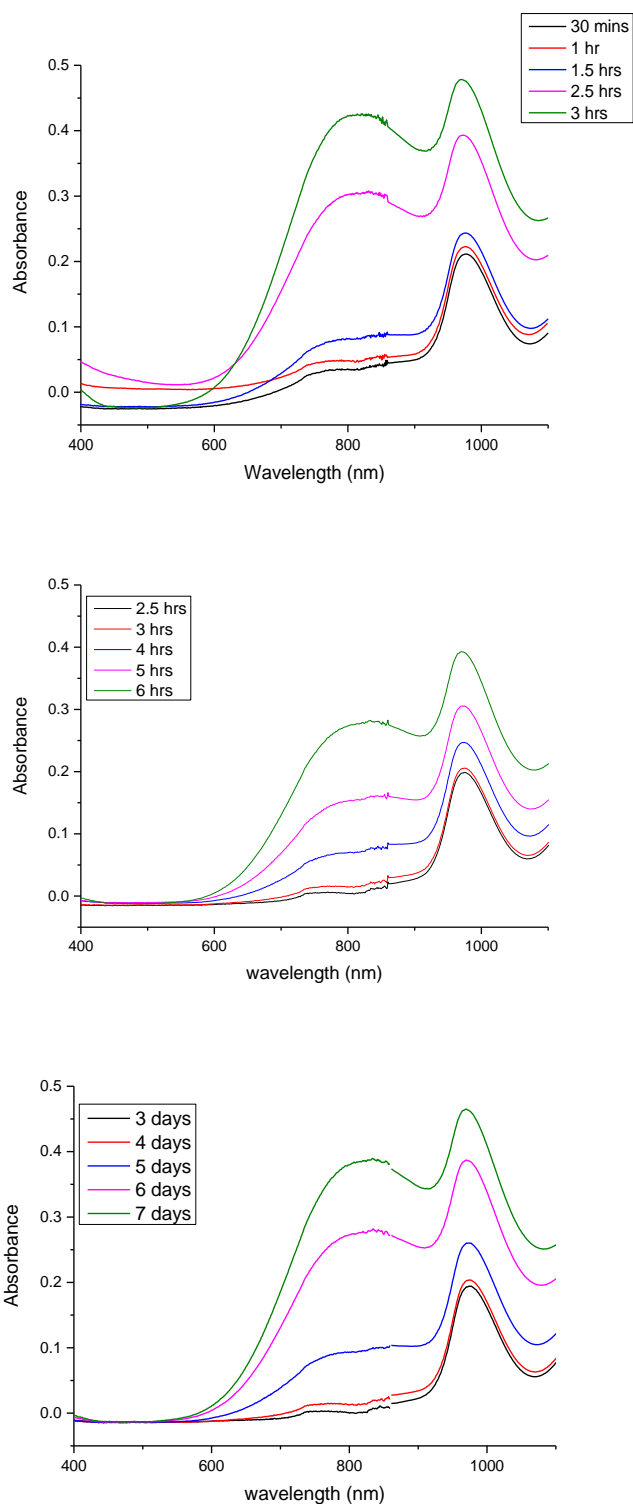
Figure 61: UV-Visible spectra of HCl acid leachate after Cu/Ni dissolution reaction: (a) microwave-assisted leaching; (b) leaching at 120°C; (c) leaching at Room Temperature.

The energies of the orbitals involved in electronic transitions have fixed values, and as energy is quantised, it would be expected that absorption peaks in

ultraviolet/ visible spectroscopy should be sharp peaks. However this is rarely actually observed. Instead, broad absorption peaks are seen. This is because a number of vibrational energy levels are available at each electronic energy level, and transitions can occur to and from the different vibrational levels. This results in peak broadening. The situation is further complicated by the fact that different rotational energy levels are also available to absorbing materials. This explains the broadening of the copper peak at 800 nm.

According to Beer's law, absorption is proportional to the concentrations of the attenuating species in the material sample. The Beer- Lambert law thus presents a way to deduce the concentration of the dissolved copper species given their absorbance. A few $CuCl_2$ solutions of known concentration were prepared and measured by UV-visible spectroscopy. Their measured absorbance were correlated to their concentrations to develop a calibration line based of Beer's law. A same procedure was followed to develop a calibration plot for Nickel in a $NiCl_2$ solution. As a result, calibration plots for both copper and nickel were developed as displayed in Figure 62 to aid in the deduction of the concentration of copper and nickel found in the leachate solution.
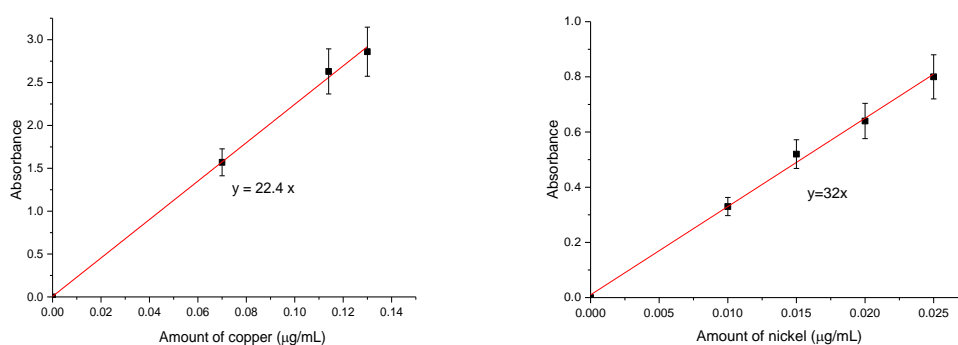
Figure 62: Calibration plots based on Beer-Lambert Law that relates the Absorbance from UV-Visible spectra to the Amount of substance or concentration dissolved (µg/mL).
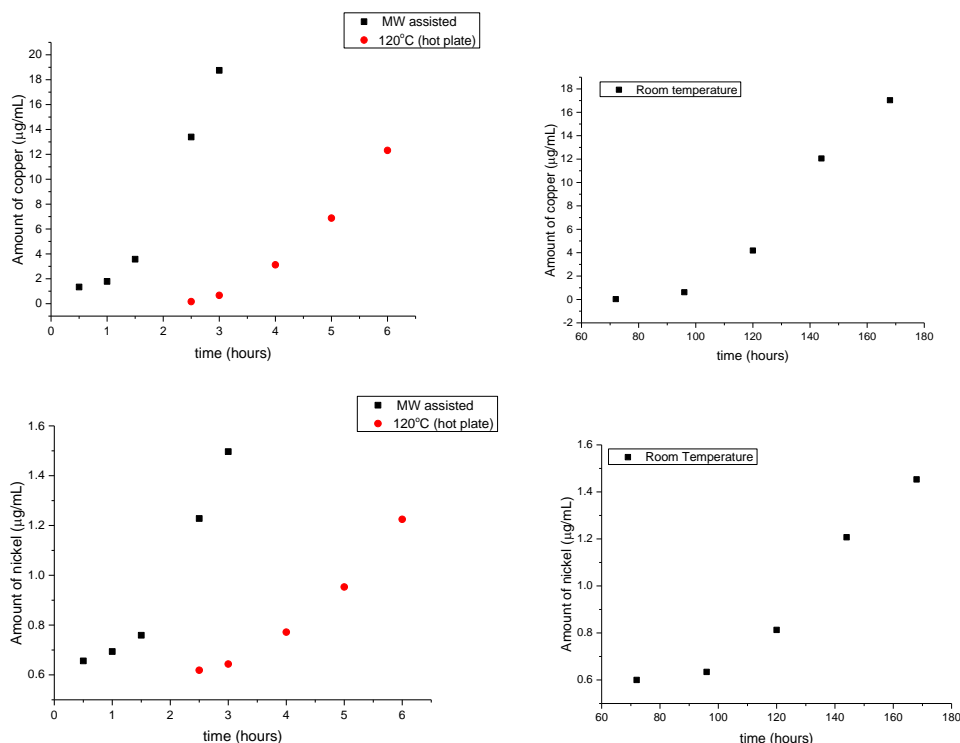
Figure 63: The rates of reaction for leaching of copper and nickel at different conditions: MW environment; heating plates at 120ºC and at Room temperature (25ºC).

At standard condition (25ºC, 1 atm.), it took seven days for all the copper and nickel to be leached into solution. However when the measurement was performed in a 100W, 2,45 GHz MW environment, a time of just 3 hours was taken to completely leach away all of the copper and nickel layers. An enormous amount of time and energy is saved in a MW-assisted leaching compared to leaching at standard condition. Reaction performed on hot plate at 120ºC also took 6 hours to complete. Again half the amount of time is saved when MW-assisted leaching is compared to hot plate heating at 120ºC.

An aqua green colour of leachate solution was observed at the end of the leaching reaction, and the firm multi-layered surface plates had become very light and easily suspended when the solution was stirred or agitated. A typical gold flake obtained after copper and nickel had been leached away has been compared to a rigid surface plate before leaching process in *Figure 58*.

It is evident from *Figure 63* that the reaction rate is affected by temperature. Increasing the temperature of a system increases the average kinetic energy of its constituent particles. As the average kinetic energy increases, the particles move faster and collide more at favourable orientations. This effect

increases the reaction rate, hence the reaction rate of leaching of copper and nickel plates increases with increasing temperature. MW-assistance provided the quickest reaction speed due to its rapid heating at 100W, 2.45Hz which was equivalent to ~200°C when measured.

5.4.3 Activation Energy
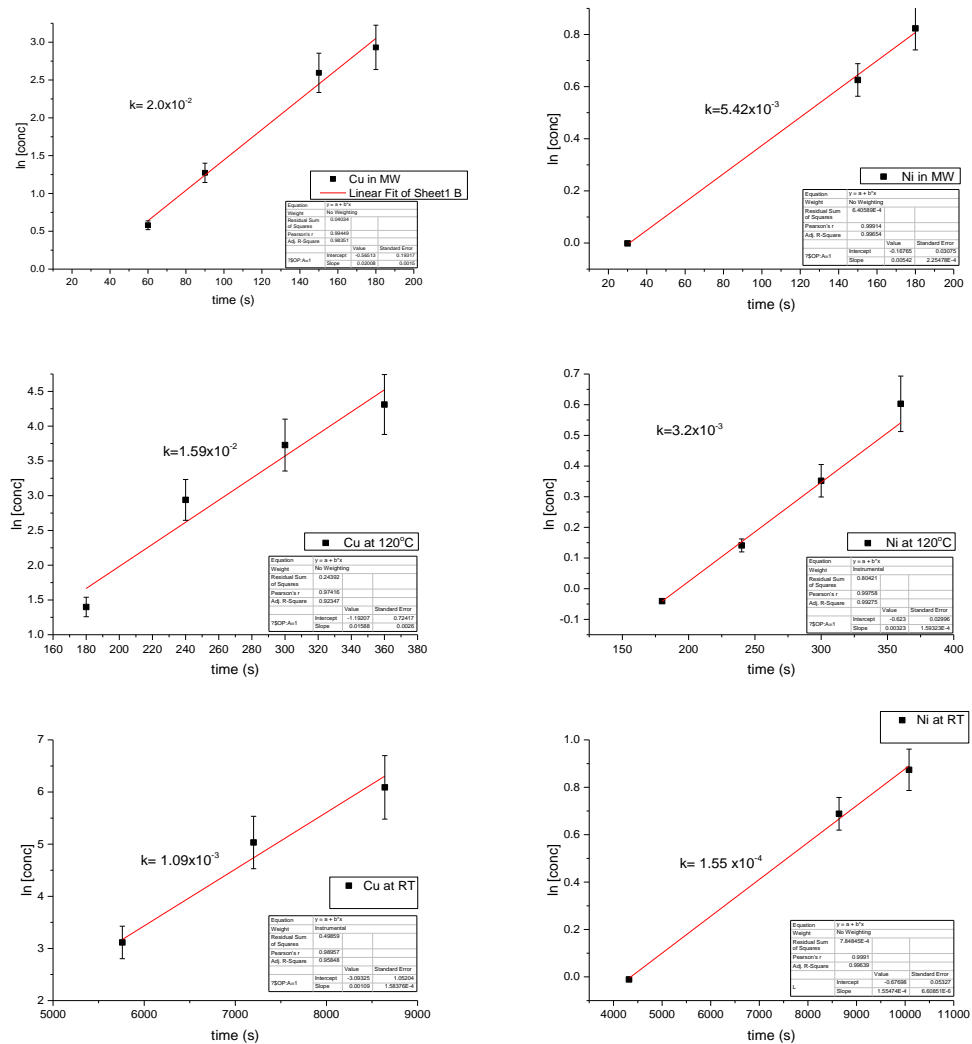
Figure 64: A plot of ln[product concentration] against time, used in the determination of the order or reaction and the reaction rate constant for copper and nickel leaching in 1M HCl acid using NH₄Cl as oxidant.

The rate constant, (k, s^{-1}) which quantifies the speed of leaching reaction was determined for all cases by using graphical method according to integrated rate laws.

Just like the delamination reaction of the PCB chips as described above, by graphical analysis, the overall reaction order for the leaching of copper and nickel from the PCB multi-layered surface plates was determined to be a first order since a straight line was achieved after plotting the ln [product concentration] against time, as evident in *Figure 64*.

Using Arrhenius equation, the activation energy was determined by plotting the ln k against 1/T.

Equation	y = a + b*x		
Weight	No Weighting		
Residual Sum of Squares	3.89558E-6	1.0083E-7	
Pearson's r	-0.99011	-0.99639	
Adj. R-Squar	0.96063	0.98557	
		Value	Standard Erro
Cu	Intercept	0.05407	0.00602
	Slope	-0.01562	0.00221
Ni	Intercept	0.01409	9.68968E-4
	Slope	-0.00418	3.56159E-4

Ea (Cu) = 129.8 J/mol

Ea (Ni) = 34.8 J/mol
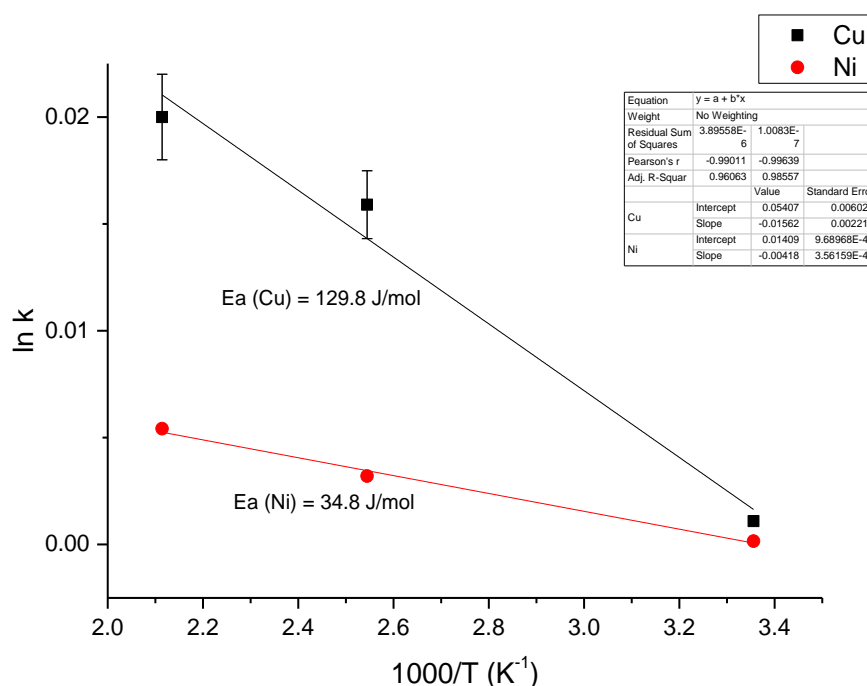
Figure 65: Arrhenius plot used to determine the activation energy for copper and nickel leaching in 1M HCl acid where NH_4Cl is used as oxidant.

The gold flakes obtained from the leaching process were melted with borax in a furnace to densify it. An SEM-EDS analysis revealed 100% gold purity with no trace of foreign element.
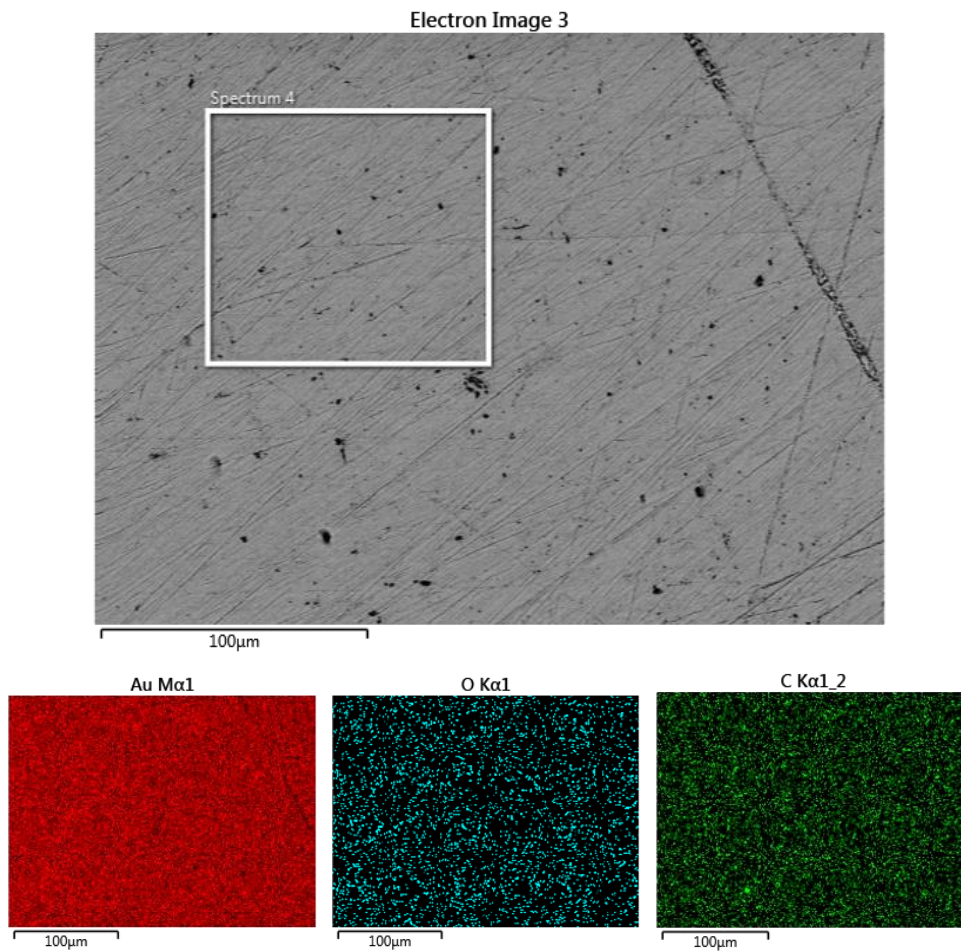
Figure 66: *A SEM-EDS elemental mapping of the recovered gold metal from waste computer PCB fingers.*
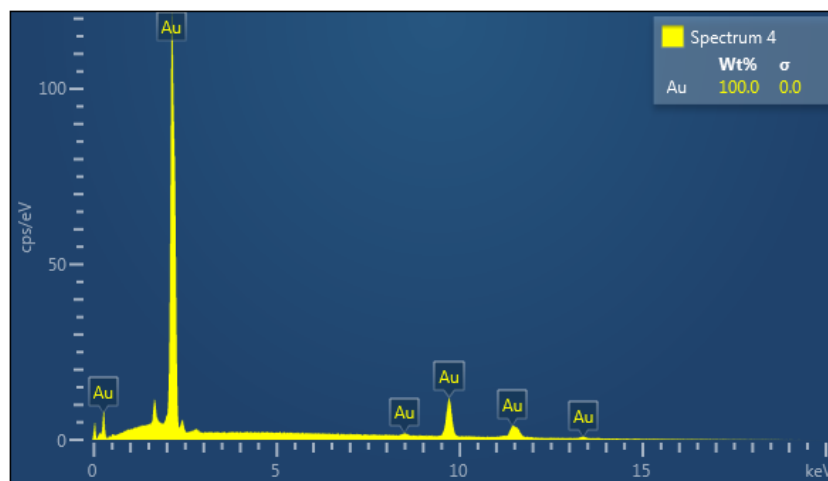
Figure 67: *SEM-EDS elemental analysis over an area specified by spectrum 4. Pure gold of 100 wt% purity was recovered from the waste PCB fingers using the proposed technique in this research.*

5.3 Electrodeposition of Cu-Ni alloy

Electrowinning employs direct current which passes from anodes to cathodes in a suitably arranged cell containing an electrolyte as described in the experimental chapter. For the winning of cooper-nickel alloy, cations go to the cathode which acts as the working electrode, where reduction occurs and anions go to the anode where oxidation occurs as shown in eqns. 27, 28 and 29 below:

$$Cu^{2+}_{(aq)} + 2e^- \rightarrow Cu_{(s)} \qquad (27)$$
$$Ni^{2+}_{(aq)} + 2e^- \rightarrow Ni_{(s)} \qquad (28)$$
$$NH_4Cl_{(aq)} \rightarrow NH_{3(g)} + HCl_{(aq)} \qquad (29)$$
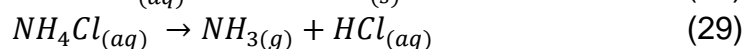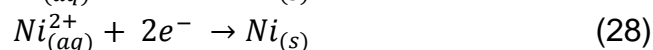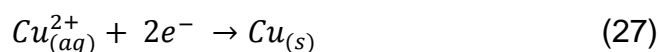
From mass fraction analysis of the PCB samples, treated in chapter 4, the mass ratio of nickel to copper in the multi-layered surface plates in terms of mass was found to be 1:31 (3 wt% Nickel and 93 wt% copper). This ratio implied that electrodeposited alloy would be a copper based alloy with ~97 wt% copper purity as Nickel will only constitute ~3 wt%.

Figure 68: (a) Leachate from Cu-Ni leaching used as electrolyte; (b) Cu-Ni alloy deposited on a graphite electrode after electrodeposition step at 3V for 3mins; (c) Cu-Ni alloy deposits being washed in distilled water.

Figure 68 presents visuals during the electrowinning process. The leachate obtained from Cu-Ni dissolution reaction was used as the electrolyte. Using graphite rods as electrodes, copper alloy was deposited as indicated in *Figure 68*b on the graphite cathode which was subsequently washed in distilled water, filtered out using a filter paper, dried in air and stored in its powdered form. Each electrowinning step lasted 3 minutes and was performed at 3 V after which the copper alloy deposited on the graphite cathode was collected. UV-

Vis analysis of the leachate was conducted after 4, 8 and 16 steps of electrowinning. The results shown in *Figure 69* shows that the copper recovery increased by every step. After 4 steps of electrowinning, more than 50 % of the copper alloy was recovered from the electrolyte. The recovery followed an asymptotic behaviour as the amount of alloy to be recovered never reached zero even after several electrowinning steps as revealed in Figure 71. The resulting electrolyte recorded a pH of 1.26 which was recycled into the Cu-Ni leaching processes.
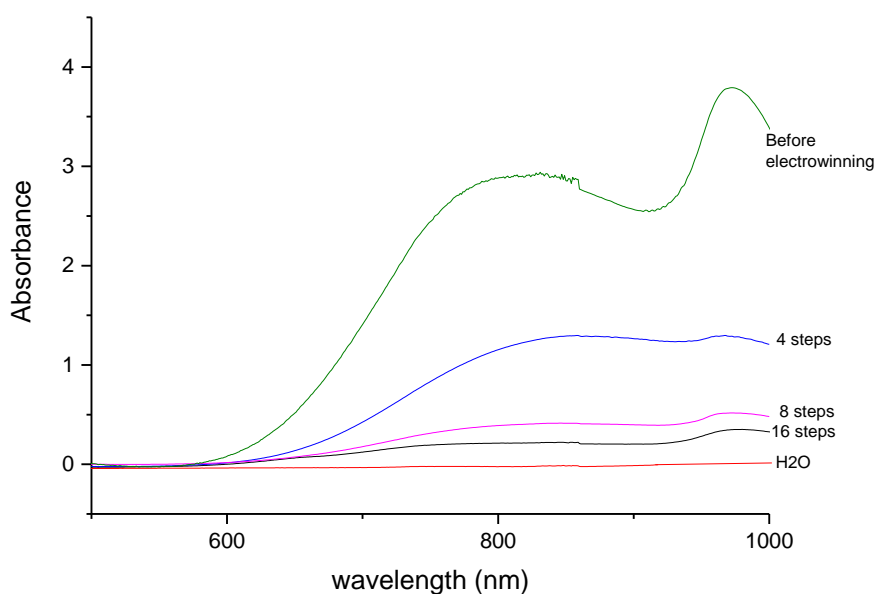
Figure 69: *UV-Visible spectra of Cu-Ni alloy taken after various steps of electrowinning process. Each electrowinning step lasted 3 minutes at 3V.*
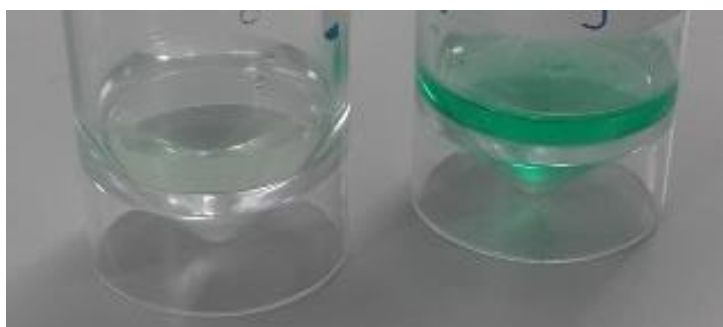
Figure 70: A comparison of electrolytes before and after electrodeposition steps. (left) pale green liquid after 16 electrodeposition steps, each step conducted at 3 V for 3 mins; (right) aqua green liquid before electrodeposition.
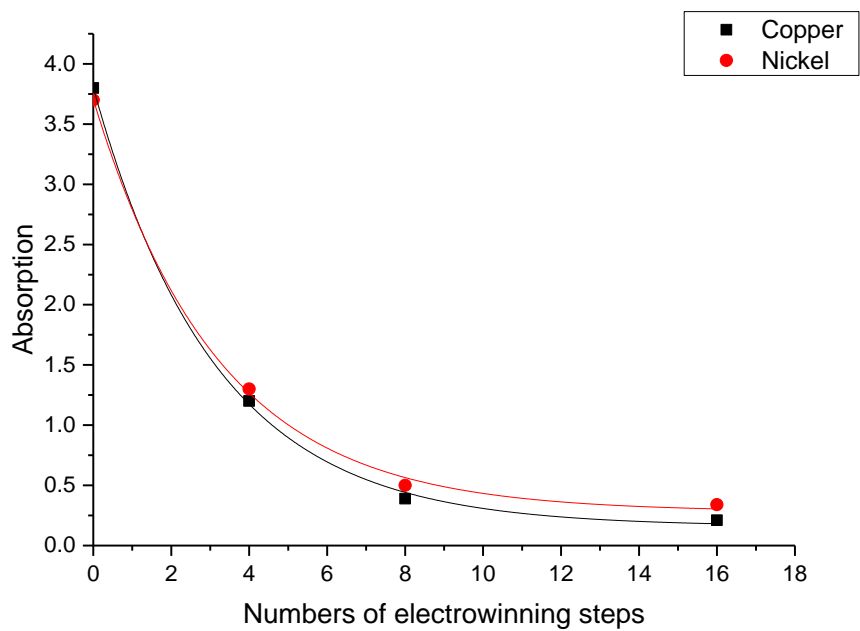
Figure 71: *A decreasing concentration of copper and nickel after electrowinning steps.*
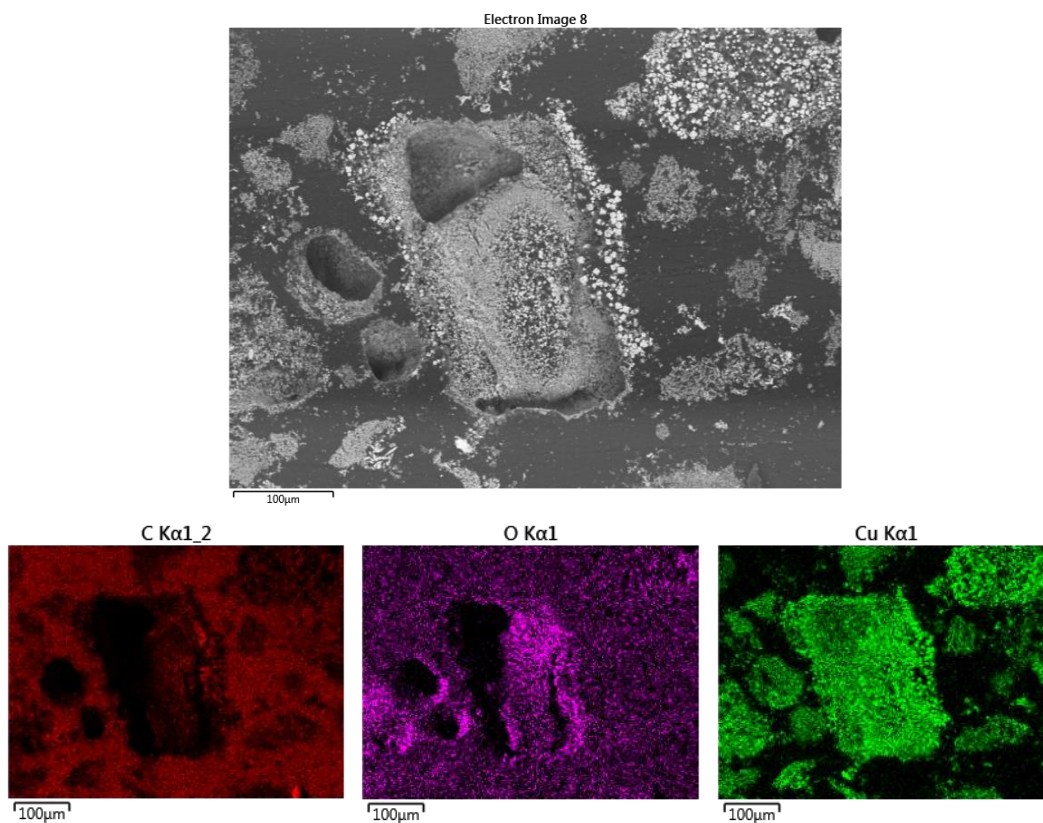
Figure 72: *SEM-EDS elemental mapping of copper powder obtained after electrowinning technique*
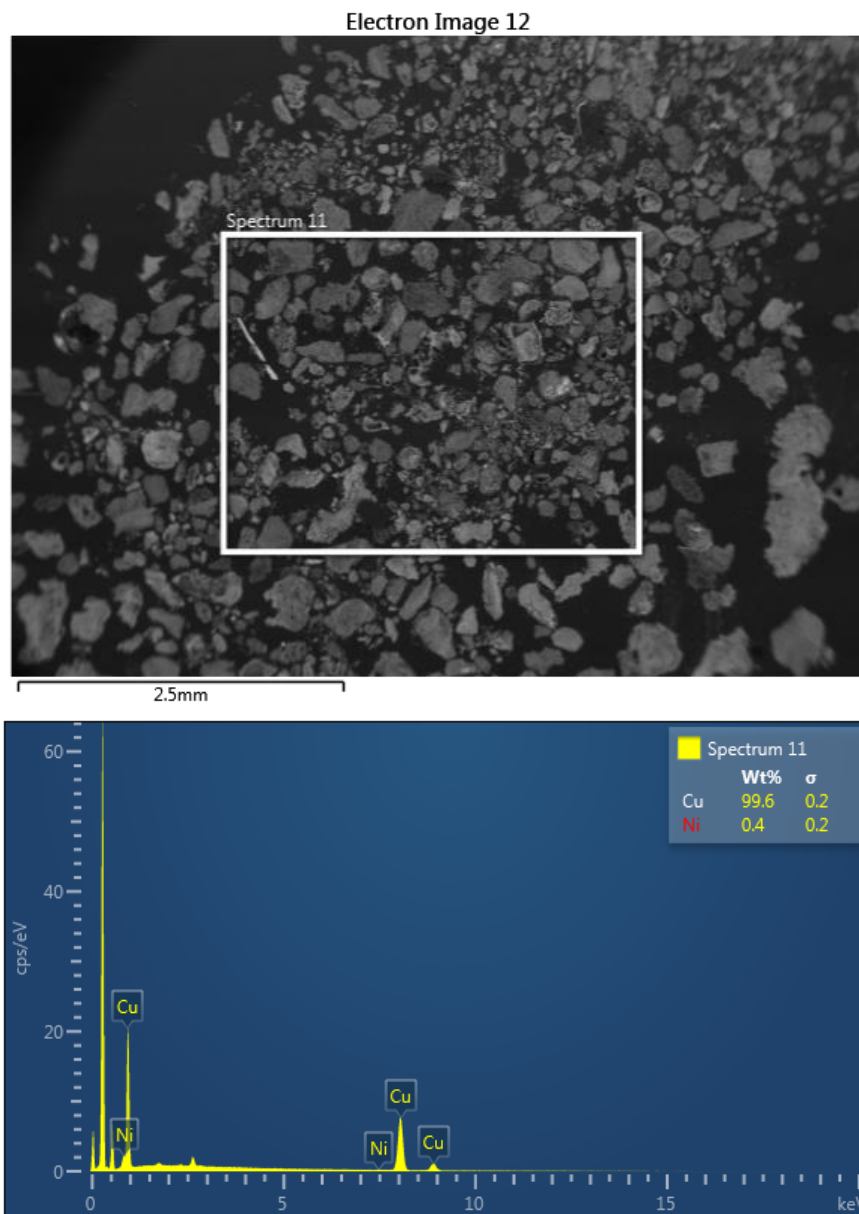
Figure 73: *SEM-EDS elemental analysis of copper-nickel powder obtained from electrowinning technique. An alloy of 99 wt% Cu and 0.4 wt% Ni was discovered.*

5.4 Scale-up experiment

In the scale up experiment, ~75 g of PCB fingers was sampled from 10 broken down desktop computers. The delamination process was performed in 200 W. 2.45 HZ microwave oven for exactly 2 hours. A 1000 mL Teflon container was used on this occasion as the reactor vessel, covered with its lid and sealed in place using scotch tape. A solid to liquid (S:L) ratio of 1:10 was used as

adapted in the research; therefore 20 g of PCB chips were mixed with 200 mL of bmim[HSO$_4$] IL in the Teflon container. The ionic liquid was regenerated and reused four times in this scale up experiment. In four batches of delamination processes and subsequent copper and nickel leaching and electrowinning processes, the 75 g PCB fingers were separated and their metal values recovered. Exactly 0.247 g of 99.99% pure gold was obtained which contributes 0.329% of the PCB finger wastes sampled.

Figure 74: (a) The copper mesh used as cathode, copper-nickel alloy powder dropping off copper mesh into distilled water; (b) some gold flakes collected after Cu-Ni leaching process.

During the electrowinning process, a circular-cathode copper mesh setup was used as described in the experimental section [Chapter 3.3.3]. This provided a larger surface area for the electrodeposition process and thus resulted in 12 steps of voltage pulse after which the electrolyte was recycled. After each step, the deposited copper was collected off the cathode. A total amount of 5.138 g copper-nickel alloy powder was collected which represents 6.85% of the PCB fingers sampled. All these amounts of metals recovered are close to amounts obtained from mass fraction analysis study in Chapter 4.2.2.

5.4 Chapter summary

Bmim[HSO$_4$] was successfully used to delaminate the PCB chip samples after 2 hours in 200 W, 2.45 GHz microwave environment. The colour of the liquid

changed from time to time during the delamination process which informed the use of UV-Visible spectroscopy to determine product concentration as a function of time to enable kinetic study. The delamination process was also successfully conducted on a hot plate at 120 ^oC and 150 ^oC. The rate constants of delamination reaction at 120 ^oC, 150 ^oC and in MW oven were found to be 0.539 s^{-1}, 0.802 s^{-1} and 2.604 s^{-1}, respectively. An activation energy of 17.6 kJ/mol for the delamination reaction was found using Arrhenius principle.

A regeneration process for the bmim[HSO_4] leachate after delamination process was developed. Firstly the thick leachate solution was diluted with distilled water to increase its fluidity. The metal plates and fibreglass cloth were separated or filtered using a sieve. The filtrate was then allowed to settle to enable effective filtration of the TEPR residue using filter paper. Subsequently, vacuum distillation was performed to separate the water from the ionic liquid. A yellow liquid was obtained after the regeneration process with indicated the presence of an impurity. FTIR spectroscopy analysis revealed the appearance of a peak at 2048 cm^{-1} in the regenerated bmimHSO4 liquid which was attributed to a CN bond stretching and vibration ripped from the crosslinking elbows of the TEPR substrate. Irrespective of the yellowish colour or the presence of the CN bond in the regenerated ionic liquid, it was successfully reused four times in various delamination processes without any decrease in its activity or reaction time.

In the coper-nickel leaching process, a UV-visible spectroscopy analysis was used to determine the product concentration of leachate at various times at different conditions. Using beer's principle, a calibration graph was developed to aid kinetic study. An activation energy for the leaching of copper and nickel were found to be 129.8 J/mol and 34.8 J/mol, respectively. The gold flakes obtained after copper-nickel leaching was put in a crucible, borax added, and melted to produce 100 wt% pure gold as ascertained by SEM-EDS analysis.

Chapter 6 Conclusions

6.1 General Conclusions

Recycling and recovery of metals from WEEE is an obvious choice to meet the global demand for technology metals. 80% less resource consumption could be achieved when desktop computers are recycled and the metals are recovered [162]. From a recycling point of view, WEEE is a mixture of polymetallic substances consisting metals, found mostly in their elemental form (dissimilar to the primary ores) along with plastics, silicates, mixed in a complex matrix. Particularly printed circuit boards (PCB) are an important source of copper (Cu) and gold (Au). The concentration of these metals in discarded PCB are many times higher than those of primary ores [163]. This requires a novel approach to selectively and sustainably recover metals from this metal-rich secondary resource. The complexity of the PCB recycling, the concentration of the metals found in the waste material and their chemical properties distinguishes this material from primary ores. Technology selection for metal recovery from waste PCBs streams must be done taking into account all pillars of sustainable development, including environmental, and social factors. The decision for technology selection should incorporate factors involving the characterization of the waste, available technologies and their recovery efficiencies, as well as their social implications and environmental impacts.

The main aim of this project was to develop an energy efficient and environmentally friendly recycling technique for the recovery of gold, copper and nickel from PCB finger wastes, to be adopted by e-waste workers especially in the developing countries where process resources such as power, chemicals, machinery and advanced technology are limited. Ionic liquids were employed due to their low vapour pressure, thermal stability and reusability. Microwaves were used to assist leaching processes to help increase the reaction rate. Firstly, analytical studies were conducted both on the PCB fingers and the ILs to understand their composition and structure.

Secondly, microwave-absorption study of four selected ionic liquids was conducted to investigate the microwave dielectric and thermal behaviour of the ILs under microwave irradiation. Finally, a technique was developed to totally separate the PCB finger composite and to enable the recovery of gold and coper-nickel alloy. The main points of conclusions drawn from each investigation addressing the objectives are listed below.

Research plays a major role in the systematic testing of techniques, understanding of the mechanisms, and evaluation of the performance of the technology in terms of effectiveness, and environmental profile. This research mainly focused on the recovery rate and efficiency and environmental profile, and techno-economic assessment of the technology. The performance was evaluated on the basis of the technical system. Evaluation of this technique can assist to identify the bottlenecks, flows and other gaps, and future research needs. This allows for further improvement of the technology in terms of effectiveness and environmental profile and brings it closer to the market.

In urban mining of waste streams, PCBs are an important and strategic secondary source of valuable metals. The main economic motivation to recycle discarded PCB is the recovery of Cu and Au. These two metals make up to 99.97% of the total value (Chapter 4). PCB is a predominantly Cu-rich material (up to 30% by weight), which makes the recovery of this metal a priority in metal recovery operations. These findings are in agreement line with those of Wang and Gaustad [164] who used statistical tools for the prioritization of metals. The selective recovery of Cu, the main material found in PCB, is a priority to serve a twofold purpose: to facilitate the recovery of other more valuable metals from PCB and to decrease a potential competition in the subsequent recovery step. Other metals are found in low quantities relative to Cu, in case of Au, which though constitutes 0.31 wt% is worth 98.52% of the PCB waste finger samples.

6.2 The Technique

The separation technique employed the use of bmimHSO4 ionic liquid as leaching solvent for the delamination of PCB fingers by dissolving TEPR

mainly to prevent fuming. BmimHSO$_4$ has very high viscosity of ~1572 cP at room temperature, as a result it showed the lowest response to microwave heating amongst the four ILs. At 120 °C dielectric loss factor of 3.5 was recorded at 2.45 GHz for bmimHSO$_4$ whereas loss factor values of ~80, ~50, ~32 were recorded for emim[HSO$_4$], emim[SCN] and mpim[N(CF$_3$SO$_2$)$_2$], respectively at same condition. A 160mL reactor vessel was used in all microwave-assisted and high temperature leaching processes to ensure that all gases were contained in the reactor. A maximum volume of 20 mL leaching solvent was filled into the vessel to allow 140 mL space above the solution to contain any fumes that would result from leaching process. Not very much fuming was observed inside the reactor vessel during MW-assisted delamination process (TEPR leaching) at 200 W, 2.45 GHz. However, a thick white cloud was observed in the reactor vessel during copper-nickel leaching but was successfully contained in the vessel throughout the reaction period. There was neither any smell during or after reaction that hinted the release of gas into the environment. After each experiment, the vessel was allowed to cool down to room temperature before further processes were conducted which ensured no release of gases into the environment. In the scale-up experiment where 20 g of PCB samples and 200 mL bmimHSO4 was used, a well-sealed 1000 L Teflon vessel was used which resulted in no release of gases into the atmosphere.

To meet economic benefit, the speed of reaction was aided by microwaves instead of using hot plate. Moreover the leachates were reused. In the delamination process, the reaction wasn't possible until the temperature was increased to 120 °C. This suggested that under 120 °C, the activation barrier for TEPR leaching reaction had not been reached. The delamination reaction commenced after 3 hours at 120 °C where the IL changed colour from clear to bright yellow. A complete delamination was observed after 9 hours. Also at 150 °C, the delaminated began after 1 hour and ended after 5 hours. Both high temperature reaction was aided by hot plate that operates at 698W. In comparison to a 200 W microwave-assistance, the reaction commenced after 10 minutes and completed after 2 hours. Also in the copper-nickel leaching reaction, a complete dissolution of both metals was achieved at RT after 7

days. At 120 °C using a hot plate, reaction was completed after 6 hours but under 100W microwave radiation, the reaction was completed after 3 hours.

A tremendous amount of energy and time is saved during MW-assisted leaching reactions as compared to conventional hot plate heating which can be attributed to the microwave-metal interaction discussed in section 2.3.3.1.

Microwave irradiation induces eddy current on the metal surface which results in joule heating of the metal. Also since the interaction occurs on the surface of the metal, charges of the surface of the metal are energised and eventually discharged in the form of arcing which generates and transfers enormous amount of energy to the surrounding medium. An enhanced leaching reaction rate was therefore released for all MW-assisted reactions. Table 17 shows a contrast of energy consumed for MW-assisted and conventional heating reactions at 120 for both copper-nickel and TEPR leaching conducted in this study. An amount of 5.68 kW.hr representing ~90% of energy was saved by using microwaves compared to conventional hot plate heating for TEPR leaching. Similarly, percentage of ~93% was saved when microwaves was used to assist Cu-Ni leaching as compared to hot plate assistance.

Table 17: *Energy consumption calculated for leaching reactions. MW-assisted leaching reaction saved a remarkable amount of energy over the reaction period compared to hot-plate assisted leaching reaction at 120°C for both TEPR leaching and Cu-Ni leaching processes.*

	Power utilized (kW.hr)		Power saved	
	MW leaching	hot-plate leaching	Power (kW.hr)	Percentage (%)
TEPR leaching	0.60	6.28	5.68	90.45
Cu-Ni leaching	0.30	4.19	3.89	92.84

The ionic liquid leachates from TEPR leaching (PCB finger delamination) as well as the electrolyte from Cu-Ni electrowinning were reused. With respect to bmim[HSO_4] ionic liquid, a regeneration process was developed to separate

the TEPR residue from the ionic liquid. FTIR analysis showed the presence of a CN bond in the regenerated IL, which didn't have any influence on the liquids activity during reuse since the reaction time was averagely constant. The regenerated bmim[HSO$_4$] ionic liquid was reused four times in this research. Considering the product electrolyte after Cu-Ni recovery, the acidic liquid obtained was recycled as leaching solvent in the Cu-Ni leaching process. No product liquid was therefore discarded or thrown away in this recycling and recovery route but were reused either straight away or after a systematic regenerative process.

Ionic liquids have been branded "green," environmentally friendly, and non-flammable due to their negligible vapour pressures. However, ionic liquids may pose thermal stability hazards when used in large-scale processes at elevated temperatures. Bmim[HSO$_4$] however experiences an onset of degradation from 342°C [144]. A ceiling temperature of 250°C was reached in this study during delamination reaction where BmimHSO$_4$ was used as the leaching solvent. No harmful side of this very useful ionic liquid was therefore realised. Moreover a safely sealed Pyrex vessel is used to contain any gas released during the experiment. Considering the use of HCl, a very dilute solution of 1M is utilized in all leaching processes, which are reused after Cu-Ni recovery. The entire technique requires the use of basic PPE such as safety overall, hand gloves, boots and goggles which are available even in third world countries where resources are limited.

Gold of 100% purity was obtained at the end of this technique which presents a very valuable and attractive venture. From the scale up experiments, 0.33% of pure gold can be obtained from PCBs by this technique. This means that a mass of 3.3 kg of gold can be recovered from 1 tonne of PCB fingers which is very worthwhile. Current price of gold is £ 29,371.00 per kilo as at 16th September, 2018.

6.3 Shortcomings of the technique

Most studies in ionic liquids have used analogous handling procedures to hydrometallurgy. One of the main differences between these media and aqueous solutions is the viscosity and hence the mass transport. The intimate contact of a solid particle and a viscous liquid phase generates difficulties associated with the slow extraction kinetics and material loss resulting from entrapment or physical loss, particularly in the processes of filtering [165]. Since evaporation of the solvent is not an option, excess ionic liquid has to be extracted with a molecular solvent of on the tailings of the digestion process. If these are released into the environment, the residual ionic liquid will have to have negligible environmental toxicity and be of low cost since mechanical loss could be in excess of 10 wt%. Filtration is the most common separation technique used and so one technical issue is that will have to be addressed is how to filter viscous solutions containing suspensions of fine particles. "In the only scale up study to date, the particulate were <1 microns dust particles suspended in an ionic liquid with a viscosity of 20cP. A double bag filter was used but visible amounts of particles were still left in the ionic liquid which became entrapped during the electrowinning stage of upstream processing. The physical losses of ionic liquid on the filtrate were in the order of 10 wt%" [165].

6.4 Recommendations for follow-up work

Working on this thesis has uncovered some areas that require further investigation. Some of the suggested are highlighted herein.

a) Bmim[HSO$_4$] ionic liquid was used to successfully delaminate the PCB fingers by dissolving the TEPR substrate which undoubtedly is the major impurity. A physical separation method of filtration and vacuum distillation was employed to separate the TEPR impurities. However, after these steps, a bright yellow IL was achieved instead of a colourless liquid colour. FTIR revealed a new peak at 2048 cm-1 particular that represents a CN bond present after regeneration steps

were taken. The presence on this peak nor the yellowish colour of the IL however did not have any effect on the reactivity of the IL when it was reused. Nevertheless, further investigation is definitely required to clearly determine the nature of CN bonds and how to totally remove this TEPR impurity from the IL during regeneration process.

b) It would be useful to conduct a 'blank' experiment where ionic liquids are heated under microwaves without the PCB finger samples to determine the cause of IL colour change observed in this study after delamination and regeneration processes since it could be as a result of some level of degradation of the ionic liquid. In a study by Kosmulski et al., where the thermal stability of low temperature ionic liquids were studied, it was obvious that working with ionic liquids at higher temperatures saves time, but there is also a risk that the ionic liquid decomposes. Some changes in colour of the ionic liquids at elevated temperatures were attributed to some level of decomposition of the liquid at those temperatures [166].

c) Further kinetic study of the dissolution of copper and nickel is recommended. A broader UV-Vis spectrum from 200 to 1200nm should be conducted to determine copper peaks at lower wavelengths ~ 200-400nm.

d) Delamination reaction could be optimised if the solute to solvent (S:L) ratio relating to TEPR leaching process is investigated further. A 1:10 ratio was adopted in this study however, in the last batch of the scale up experiment, a 1:13 was used, but delamination was completed at same reaction time of 2 hours. A study into lower S:L ratios would be worthwhile to determine the optimum use of IL used as leaching solvents.

e) A dilute HCl concentration of 1 M was used in the leaching process of copper and nickel metals. This concentration was unchanged

throughout the research work. An investigation into the effect of HCl acid concentration within 0.1 – 1 M would be imperative to ensure that the least effective concentration of the acid is used in the leaching process of copper and nickel.

References

1.   Azuka, A.I., *Influx of Used Electronics into Africa: A Perilous Trend, The.* Law Env't & Dev. J., 2009. **5**: p. 90.
2.   Sthiannopkao, S. and M.H. Wong, *Handling e-waste in developed and developing countries: Initiatives, practices, and consequences.* Science of the Total Environment, 2013. **463**: p. 1147-1153.
3.   Drechsel, C., *Mechanical Processes for Recycling Waste Electric and Electronic Equipment with the Rotorshredder and Rotor Impact Mill.* Aufbereitungs Technik-Mineral Processing, 2006. **47**(3): p. 4-14.
4.   Petranikova, M., *Treatment of end of life computers.* Diploma Work, Technical University of Kosice, Kosice, Slovakia, 2008.
5.   Oguchi, M., H. Sakanakura, and A. Terazono, *Toxic metals in WEEE: Characterization and substance flow analysis in waste treatment processes.* Science of the total environment, 2013. **463**: p. 1124-1132.
6.   Xiu, F.R., Y. Qi, and F.S. Zhang, *Leaching of Au, Ag, and Pd from waste printed circuit boards of mobile phone by iodide lixiviant after supercritical water pre-treatment.* Waste Manag, 2015. **41**: p. 134-41.
7.   Guo, J., Q. Rao, and Z. Xu, *Application of glass-nonmetals of waste printed circuit boards to produce phenolic moulding compound.* Journal of Hazardous Materials, 2008. **153**(1-2): p. 728-734.
8.   Tuncuk, A., et al., *Aqueous metal recovery techniques from e-scrap: hydrometallurgy in recycling.* Minerals Engineering, 2012. **25**(1): p. 28-37.
9.   Zhou, Y. and K. Qiu, *A new technology for recycling materials from waste printed circuit boards.* Journal of Hazardous Materials, 2010. **175**(1): p. 823-828.
10. De Marco, I., et al., *Pyrolysis of electrical and electronic wastes.* Journal of Analytical and Applied Pyrolysis, 2008. **82**(2): p. 179-183.
11. Quan, C., A. Li, and N. Gao, *Thermogravimetric analysis and kinetic study on large particles of printed circuit board wastes.* Waste management, 2009. **29**(8): p. 2353-2360.
12. Zhang, J., et al., *Preparation of anion exchange resin by recycling of waste printed circuit boards.* RSC Advances, 2015. **5**(129): p. 106680-106687.
13. Kasper, A.C., et al., *Printed wiring boards for mobile phones: Characterization and recycling of copper.* Waste management, 2011. **31**(12): p. 2536-2545.
14. Davis, G. and S. Herat, *Electronic waste: The local government perspective in Queensland, Australia.* Resources, Conservation and Recycling, 2008. **52**(8-9): p. 1031-1039.
15. Moltó, J., et al., *Thermal decomposition of electronic wastes: mobile phone case and other parts.* Waste management, 2011. **31**(12): p. 2546-2552.
16. Khanna, R., et al., *Novel carbon micro fibers and foams from waste printed circuit boards.* Fuel Processing Technology, 2015. **134**: p. 473-479.

17. Li, J., et al., *Recycle technology for recovering resources and products from waste printed circuit boards.* Environmental science & technology, 2007. **41**(6): p. 1995-2000.

18. Menad, N., B. Björkman, and E.G. Allain, *Combustion of plastics contained in electric and electronic scrap.* Resources, conservation and recycling, 1998. **24**(1): p. 65-85.

19. Berbardes, A., et al. *Recycling of printed circuit boards by melting with oxidising/reducing top blowing process.* in *EPD Congress 1997.* 1997.

20. Gungor, A. and S.M. Gupta, *Disassembly sequence planning for products with defective parts in product recovery.* Computers & Industrial Engineering, 1998. **35**(1-2): p. 161-164.

21. Schmelzer, G., S. Wolf, and H. Hoberg, *New wet treatment for components of incineration slag.* Aufbereitungs Technik, 1996. **37**(4): p. 149-157.

22. Cui, J. and E. Forssberg, *Mechanical recycling of waste electric and electronic equipment: a review.* Journal of hazardous materials, 2003. **99**(3): p. 243-263.

23. Iuga, A., et al., *Corona-electrostatic separators for recovery of waste non-ferrous metals.* Journal of Electrostatics, 1989. **23**: p. 235-243.

24. Iuga, A., et al., *Optimal high-voltage energization of corona-electrostatic separators.* IEEE Transactions on Industry Applications, 1998. **34**(2): p. 286-293.

25. Dascalescu, L., et al., *Charging of particulates in the corona field of roll-type electroseparators.* Journal of Physics D: Applied Physics, 1994. **27**(6): p. 1242.

26. Iuga, A., et al. *High-voltage supplies for corona-electrostatic separators.* in *Industry Applications Conference, 1995. Thirtieth IAS Annual Meeting, IAS'95., Conference Record of the 1995 IEEE.* 1995. IEEE.

27. Zhan, L. and Z. Xu, *State-of-the-art of recycling e-wastes by vacuum metallurgy separation.* Environmental science & technology, 2014. **48**(24): p. 14092-14102.

28. Siva, P. *Toxic waste 'major global threat'.* 2013 [cited 2013 20 Nov]; Available from: http://www.bbc.co.uk/news/science-environment-24994209.

29. Oteng-Ababio, M., *E-waste: an emerging challenge to solid waste management in Ghana.* International Development Planning Review, 2010. **32**(2): p. 191.

30. Chun, S., S.V. Dzyuba, and R.A. Bartsch, *Influence of structural variation in room-temperature ionic liquids on the selectivity and efficiency of competitive alkali metal salt extraction by a crown ether.* Analytical Chemistry, 2001. **73**(15): p. 3737-3741.

31. Branco, L.C., et al., *Preparation and characterization of new room temperature ionic liquids.* Chemistry-A European Journal, 2002. **8**(16): p. 3671-3677.

32. Whitehead, J., et al., *Application of 1-alkyl-3-methyl-imidazolium ionic liquids in the oxidative leaching of sulphidic copper, gold and silver ores.* Hydrometallurgy, 2007. **88**(1): p. 109-120.

33. Galiński, M., A. Lewandowski, and I. Stępniak, *Ionic liquids as electrolytes.* Electrochimica Acta, 2006. **51**(26): p. 5567-5580.

34. Allen, D.T. and D.R. Shonnard, *Green engineering: environmentally conscious design of chemical processes.* 2001: Pearson Education.

35. Freemantle, M., *Designer solvents: ionic liquids may boost clean technology development.* Chemical & engineering news, 1998. **76**(13): p. 32-37.

36. Docherty, K.M. and C.F. Kulpa Jr, *Toxicity and antimicrobial activity of imidazolium and pyridinium ionic liquids.* Green Chemistry, 2005. **7**(4): p. 185-189.

37. Han, X. and D.W. Armstrong, *Ionic liquids in separations.* Accounts of Chemical Research, 2007. **40**(11): p. 1079-1086.

38. Dzyuba, S.V. and R.A. Bartsch, *Influence of structural variations in 1-alkyl (aralkyl)-3-methylimidazolium hexafluorophosphates and bis (trifluoromethylsulfonyl) imides on physical properties of the ionic liquids.* ChemPhysChem, 2002. **3**(2): p. 161-166.

39. Poole, C.F., *Chromatographic and spectroscopic methods for the determination of solvent properties of room temperature ionic liquids.* Journal of chromatography A, 2004. **1037**(1): p. 49-82.

40. Baker, G.A., et al., *An analytical view of ionic liquids.* Analyst, 2005. **130**(6): p. 800-808.

41. Whitehead, J.A., G.A. Lawrance, and A. McCluskey, *'Green'leaching: recyclable and selective leaching of gold-bearing ore in an ionic liquid.* Green Chemistry, 2004. **6**(7): p. 313-315.

42. Kingston, H.M. and L.B. Jassie, *Introduction to microwave sample preparation: theory and practice.* 1988: American Chemical Society.

43. Tatár, E., I. Varga, and G. Záray, *Microwave assisted dissolution of aluminium oxide samples.* Microchimica Acta, 1993. **111**(1-3): p. 45-54.

44. Kratochvil, B. and S. Mamba, *Microwave acid dissolution of soil samples for elemental analysis.* Canadian journal of chemistry, 1990. **68**(2): p. 360-362.

45. Sah, R.N. and R.O. Miller, *Spontaneous reaction for acid dissolution of biological tissues in closed vessels.* Analytical Chemistry, 1992. **64**(2): p. 230-233.

46. Suzuki, T. and M. Sensui, *Application of the microwave acid digestion method to the decomposition of rock samples.* Analytica chimica acta, 1991. **245**: p. 43-48.

47. Chang, T.-Y., F.-J. Hsieh, and C. Lee, *Comparing microwave dissolution with hot-plate dissolution for the analysis of tool steels.* MRL Bulletin of Research and Development, 1990. **4**(2): p. 45-51.

48. Joret, L., G. Cote, and D. Bauer, *Effect of microwaves on the rate of dissolution of metal oxides (Co 3 O 4 and CeO 2) in nitric acid.* Hydrometallurgy, 1997. **45**(1): p. 1-12.

49. Haque, K.E., *Microwave energy for mineral treatment processes—a brief review.* International Journal of Mineral Processing, 1999. **57**(1): p. 1-24.

50. Kuo, C.-Y., C.-H. Wu, and S.-L. Lo, *Leaching efficiency of copper from industrial sludge with traditional acid extraction (TAE) and microwave assisted treatment (MAT).* Journal of Environmental Science and Health, Part A, 2005. **40**(12): p. 2203-2214.

51. Khaliq, A., et al., *Metal extraction processes for electronic waste and existing industrial routes: a review and Australian perspective.* Resources, 2014. **3**(1): p. 152-179.

52. ESYS. *Introducing PCB Circuit Technology.* 2018, July 4; Available from: http://esys.ir/Page.aspx?i=25.

53. SPICE. *Single and double-sided board with PCB Designer.* 2018, July 5; Available from: http://www.youspice.com/235/2/.

54. Hagelüken, C. *Improving metal returns and eco-efficiency in electronics recycling.* in *Proceedings of the 2006 IEEE Int. Symposium on Electronics and the Environment. IEEE.* 2006.

55. Huang, K., J. Guo, and Z. Xu, *Recycling of waste printed circuit boards: A review of current technologies and treatment status in China.* Journal of hazardous materials, 2009. **164**(2): p. 399-408.

56. Guo, J., Q. Rao, and Z. Xu, *Application of glass-nonmetals of waste printed circuit boards to produce phenolic moulding compound.* Journal of Hazardous Materials, 2008. **153**(1): p. 728-734.

57. Lengyel Norbert. *Gold plating for edge connectors* 2012, November 1; Available from: https://www.eurocircuits.com/blog/gold-plating-for-edge-connectors/.

58. Kuper, J. and M. Hojsik, *Poisoning the poor: electronic waste in Ghana.* 2008, Amsterdam: Greenpeace.

59. International, G. *Where does e-waste end up?* 24 February, 2009; Available from: https://www.greenpeace.org/archive-international/en/campaigns/detox/electronics/the-e-waste-problem/where-does-e-waste-end-up/.

60. Brigden, K., et al., *Recycling of electronic wastes in China and India: workplace and environmental contamination.* Greenpeace International, 2005. **55**.

61. Tash Morgan. *Agbogbloshie: Welcome to the world's digital dumping ground (Part 1).* 2014, March 26; Available from: https://www.earthtouchnews.com/conservation/human-impact/agbogbloshie-welcome-to-the-worlds-digital-dumping-ground-part-1/.

62. guardian. *Agbogbloshie: the world's largest e-waste dump.* 2014 [cited 2014 27 Feb]; Available from: http://www.theguardian.com/environment/gallery/2014/feb/27/agbogbloshie-worlds-largest-e-waste-dump-in-pictures.

63. Atiemo, S.M., et al., *Assessing the heavy metals contamination of surface dust from waste electrical and electronic equipment (e-waste) recycling site in Accra, Ghana.* Res J Environ Earth Sci, 2012. **4**(5): p. 605-611.

64. Muller, G., *Index of geoaccumulation in sediments of the Rhine River.* 1969.

65. Taylor, S.R. and S.M. McLennan, *The continental crust: its composition and evolution.* 1985.

66. Lăcătuşu, R., et al., *Heavy metals soil pollution state in relation to potential future mining activities in the Roşia Montană area.* Carpathian Journal of Earth and Environmental Sciences, 2009. **4**(2): p. 39-50.

67. Daum, K., J. Stoler, and R.J. Grant, *Toward a more sustainable trajectory for E-Waste policy: a review of a decade of E-Waste research*

in Accra, Ghana. International journal of environmental research and public health, 2017. **14**(2): p. 135.

68. Srigboh, R.K., et al., *Multiple elemental exposures amongst workers at the Agbogbloshie electronic waste (e-waste) site in Ghana.* Chemosphere, 2016. **164**: p. 68-74.

69. Manomaivibool, P., *Extended producer responsibility in a non-OECD context: The management of waste electrical and electronic equipment in India.* Resources, Conservation and Recycling, 2009. **53**(3): p. 136-144.

70. Bizzo, W.A., R.A. Figueiredo, and V.F. de Andrade, *Characterization of printed circuit boards for metal and energy recovery after milling and mechanical separation.* Materials, 2014. **7**(6): p. 4555-4566.

71. Settimo, F., P. Bevilacqua, and P. Rem, *Eddy current separation of fine non-ferrous particles from bulk streams.* Physical Separation in Science and Engineering, 2004. **13**(1): p. 15-23.

72. Xiang, D., et al., *Printed circuit board recycling process and its environmental impact assessment.* The International Journal of Advanced Manufacturing Technology, 2007. **34**(9-10): p. 1030-1036.

73. Helsen, L. and A. Bosmans. *Waste-to-Energy through thermochemical processes: matching waste with process.* in *Proceedings of the 1st International Academic Symposium on Enhanced Landfill Mining.* 2010. Haletra.

74. Luda, M., et al., *Thermal decomposition of fire retardant brominated epoxy resins cured with different nitrogen containing hardeners.* Polymer degradation and stability, 2007. **92**(6): p. 1088-1100.

75. Seetharaman, S., *Treatise on process metallurgy, volume 3: industrial processes.* Vol. 3. 2013: Newnes.

76. Sohaili, J., S.K. Muniyandi, and S.S. Mohamad, *A review on printed circuit board recycling technology.* Journal of Emerging Trends in Engineering and Applied Sciences, 2012. **3**(1): p. 12-18.

77. Park, Y.J. and D.J. Fray, *Recovery of high purity precious metals from printed circuit boards.* J Hazard Mater, 2009. **164**(2-3): p. 1152-8.

78. Ritcey, G.M., *Solvent extraction in hydrometallurgy: present and future.* Tsinghua Science & Technology, 2006. **11**(2): p. 137-152.

79. Tavlarides, L., J. Bae, and C. Lee, *Solvent extraction, membranes, and ion exchange in hydrometallurgical dilute metals separation.* Separation Science and Technology, 1987. **22**(2-3): p. 581-617.

80. Quinet, P., J. Proost, and A. Van Lierde, *Recovery of precious metals from electronic scrap by hydrometallurgical processing routes.* Minerals and Metallurgical Processing, 2005. **22**(1): p. 17-22.

81. Liu, R., et al., *The general utilization of scrapped PC board.* Waste management, 2009. **29**(11): p. 2842-2845.

82. Sheng, P.P. and T.H. Etsell, *Recovery of gold from computer circuit board scrap using aqua regia.* Waste management & research, 2007. **25**(4): p. 380-383.

83. Chmielewski, A., T. Urbański, and W. Migdał, *Separation technologies for metals recovery from industrial wastes.* Hydrometallurgy, 1997. **45**(3): p. 333-344.

84. Zhou, P., Z. Zheng, and J. Tie, *Technological process for extracting gold, silver and palladium from electronic industry waste.* Chinese Patent, CN1603432A (C22B 11/00), 2005.

85. Kogan, V., *Process for the recovery of precious metals from electronic scrap by hydrometallurgical technique.* International Patent, WO/2006/013568 (C22B 11/00), WIP Organization, 2006.

86. Veit, H.M., et al., *Recovery of copper from printed circuit boards scraps by mechanical processing and electrometallurgy.* Journal of Hazardous Materials, 2006. **137**(3): p. 1704-1709.

87. Mecucci, A. and K. Scott, *Leaching and electrochemical recovery of copper, lead and tin from scrap printed circuit boards.* Journal of Chemical Technology and Biotechnology, 2002. **77**(4): p. 449-457.

88. Bradshaw, S., E. Van Wyk, and J. De Swardt, *Microwave heating principles and the application to the regeneration of granular activated carbon.* Journal of the South African Institute of Mining and Metallurgy(South Africa), 1998. **98**(4): p. 201-210.

89. Clark, D.E. and W.H. Sutton, *Microwave processing of materials.* Annual Review of Materials Science, 1996. **26**(1): p. 299-331.

90. Faxvog, F.R. and M.K. Krage, *Microwave acoustic spectrometer.* 1981, Google Patents.

91. Moulson, A. and J. Herbert, *Electronic ceramic materials and their applications.* Chappman and Hall, London, 1990.

92. George, C., G. Rao, and V. Thalakola. *Thermal desorption of contaminants using microwave heated rotary mixture.* in *Proceedings of the 29th Microwave Power Symposium, Chicago, IL.* 1994.

93. Sun, J., W. Wang, and Q. Yue, *Review on microwave-matter interaction fundamentals and efficient microwave-associated heating strategies.* Materials, 2016. **9**(4): p. 231.

94. Mishra, P., A. Upadhyaya, and G. Sethi, *Modeling of microwave heating of particulate metals.* Metallurgical and Materials Transactions B, 2006. **37**(5): p. 839-845.

95. Hartz, C.L., et al., *Innovative surface wave plasma reactor technique for PFC abatement.* Environmental science & technology, 1998. **32**(5): p. 682-687.

96. Oghbaei, M. and O. Mirzaee, *Microwave versus conventional sintering: A review of fundamentals, advantages and applications.* Journal of Alloys and Compounds, 2010. **494**(1-2): p. 175-189.

97. Wang, W., et al., *Experimental study on the heating effects of microwave discharge caused by metals.* AIChE Journal, 2012. **58**(12): p. 3852-3857.

98. Sun, J., et al., *Study on the coupled effect of wave absorption and metal discharge generation under microwave irradiation.* Industrial & Engineering Chemistry Research, 2014. **53**(5): p. 2042-2051.

99. Menéndez, J., et al., *Microwave heating processes involving carbon materials.* Fuel Processing Technology, 2010. **91**(1): p. 1-8.

100. Hussain, Z., K.M. Khan, and K. Hussain, *Microwave–metal interaction pyrolysis of polystyrene.* Journal of Analytical and Applied Pyrolysis, 2010. **89**(1): p. 39-43.

101. Chen, W., B. Gutmann, and C.O. Kappe, *Characterization of Microwave-Induced Electric Discharge Phenomena in Metal–Solvent Mixtures.* ChemistryOpen, 2012. **1**(1): p. 39-48.
102. Roy, R., et al., *Full sintering of powdered-metal bodies in a microwave field.* Nature, 1999. **399**(6737): p. 668-670.
103. Sueyoshi, H. and S. Kakiuchi, *Microwave heating of thin Au film.* Materials transactions, 2007. **48**(3): p. 531-537.
104. Huang, J. and N. Rowson, *Hydrometallurgical decomposition of pyrite and marcasite in a microwave field.* Hydrometallurgy, 2002. **64**(3): p. 169-179.
105. Hinds, M.W., S. Littau, and P. Moulinié, *Determination of trace metals in platinum by electrothermal atomic absorption spectrometry following a closed-vessel microwave dissolution procedure.* Analyst, 1992. **117**(9): p. 1473-1475.
106. Bonomi, C., et al. *Ionometallurgical leaching process of bauxite residue: a comparison between hydrophilic and hydrophobic ionic liquids.* in *Proceedings, Travaux 46. Presented at the 35th International ICSOBA Conference, ICSOBA, Hamburg, Germany.* 2017.
107. Dai, S., et al., *Comparative UV− Vis studies of uranyl chloride complex in two basic ambient-temperature melt systems: The observation of spectral and thermodynamic variations induced via hydrogen bonding.* Inorganic chemistry, 1997. **36**(21): p. 4900-4902.
108. Huang, H.-L., et al., *Recovery of nanosize zinc from phosphor wastes with an ionic liquid.* Environmental Chemistry, 2009. **6**(3): p. 268-272.
109. Abbott, A.P., G. Frisch, and K.S. Ryder, *Metal complexation in ionic liquids.* Annual Reports Section" A"(Inorganic Chemistry), 2008. **104**: p. 21-45.
110. Hardacre, C., *Application of EXAFS to molten salts and ionic liquid technology.* Annu. Rev. Mater. Res., 2005. **35**: p. 29-49.
111. Lee, J.-M., S. Ruckes, and J.M. Prausnitz, *Solvent polarities and Kamlet− Taft parameters for ionic liquids containing a pyridinium cation.* The Journal of Physical Chemistry B, 2008. **112**(5): p. 1473-1476.
112. Oehlke, A., K. Hofmann, and S. Spange, *New aspects on polarity of 1-alkyl-3-methylimidazolium salts as measured by solvatochromic probes.* New Journal of Chemistry, 2006. **30**(4): p. 533-536.
113. Correia, I. and T. Welton, *An old reaction in new media: kinetic study of a platinum (II) substitution reaction in ionic liquids.* Dalton Transactions, 2009(21): p. 4115-4121.
114. Wellens, S., et al., *Dissolution of metal oxides in an acid-saturated ionic liquid solution and investigation of the back-extraction behaviour to the aqueous phase.* Hydrometallurgy, 2014. **144**: p. 27-33.
115. Abbott, A.P., et al., *Preparation of novel, moisture-stable, Lewis-acidic ionic liquids containing quaternary ammonium salts with functional side chainsElectronic supplementary information (ESI) available: plot of conductivity vs. temperature for the ionic liquid formed from zinc chloride and choline chloride (2∶ 1). See http://www. rsc. org/suppdata/cc/b1/b106357j.* Chemical Communications, 2001(19): p. 2010-2011.

116. Abbott, A.P., et al., *Solubility of metal oxides in deep eutectic solvents based on choline chloride.* Journal of Chemical & Engineering Data, 2006. **51**(4): p. 1280-1282.

117. Abbott, A.P., et al., *Deep eutectic solvents formed between choline chloride and carboxylic acids: versatile alternatives to ionic liquids.* Journal of the American Chemical Society, 2004. **126**(29): p. 9142-9147.

118. Abbott, A.P., et al., *Processing of metals and metal oxides using ionic liquids.* Green Chemistry, 2011. **13**(3): p. 471-481.

119. Zhu, P., et al., *A new technology for separation and recovery of materials from waste printed circuit boards by dissolving bromine epoxy resins using ionic liquid.* Journal of hazardous materials, 2012. **239**: p. 270-278.

120. Zhu, P., et al., *Treatment of waste printed circuit board by green solvent using ionic liquid.* Waste management, 2012. **32**(10): p. 1914-1918.

121. Xu, W. and C.A. Angell, *Solvent-free electrolytes with aqueous solution-like conductivities.* Science, 2003. **302**(5644): p. 422-425.

122. Blander, M., *Molten salt chemistry.* 1964: Interscience Publishers.

123. Abbott, A.P., *Application of hole theory to the viscosity of ionic and molecular liquids.* ChemPhysChem, 2004. **5**(8): p. 1242-1246.

124. Frenkel, J., *Kinetic Theory of Liquids-Oxford Univ.* Press-1946, 1946.

125. Fürth, R. *On the theory of the liquid state: I. The statistical treatment of the thermodynamics of liquids by the theory of holes.* in *Mathematical Proceedings of the Cambridge Philosophical Society.* 1941. Cambridge University Press.

126. Bockris, J.O.M. and A.K. Reddy, *Modern electrochemistry 2B: electrodics in chemistry, engineering, biology and environmental science.* Vol. 2. 2000: Springer Science & Business Media.

127. Bresme, F. and J. Alejandre, *Cavities in ionic liquids.* The Journal of chemical physics, 2003. **118**(9): p. 4134-4139.

128. Lefler, L., *An assessment of early-stage forest restoration outcomes and the instruments used to evaluate ecosystem recovery.* 2006, University of Waterloo.

129. Clarke, A., C.N. Eberhardt, and C. Eberhardt, *Microscopy techniques for materials science.* 2002: Woodhead Publishing.

130. Goldstein, J.I., et al., *Scanning electron microscopy and X-ray microanalysis.* 2017: Springer.

131. Reimer, L., *Scanning electron microscopy: physics of image formation and microanalysis.* Vol. 45. 2013: Springer.

132. junejo, U. *Schematic of ATR-FTIR Spectrometer.* 20 August, 2017; Available from: https://commons.wikimedia.org/wiki/File:Schematic_of_ATR-FTIR_Spectrometer.png.

133. Soares, J.A., *Introduction to optical characterization of materials*, in *Practical Materials Characterization.* 2014, Springer. p. 43-92.

134. Sabarwiki. *Schematic of UV- visible spectrophotometer.* 2 September, 2013; Available from: https://commons.wikimedia.org/wiki/File:Schematic_of_UV-_visible_spectrophotometer.png.

135. Ballo, D., *Network analyzers simplify mixer test.* Microwave & RF, 2002. **10**: p. 98-106.

136. Element, C., *Method 3051A microwave assisted acid digestion of sediments, sludges, soils, and oils.* Z. Für Anal. Chem., 2007. **111**: p. 362-366.

137. Papovic, S., M. Vraneš, and S. Gadzuric, *A comprehensive study of {c-butyrolactone propylimidazolium bis (trifluoromethylsulfonyl) imide} binary mixtures.* 2015.

138. Gómez, E., et al., *Effect of the temperature on the physical properties of pure 1-propyl 3-methylimidazolium bis (trifluoromethylsulfonyl) imide and characterization of its binary mixtures with alcohols.* The Journal of Chemical Thermodynamics, 2012. **45**(1): p. 9-15.

139. Kong, W., et al., *Ionic liquid based vibrational energy harvester by periodically squeezing the liquid bridge.* RSC Advances, 2014. **4**(37): p. 19356-19361.

140. Grishina, E., et al., *Water effect on physicochemical properties of 1-butyl-3-methylimidazolium based ionic liquids with inorganic anions.* Journal of Molecular Liquids, 2013. **177**: p. 267-272.

141. Costa, A.J., et al., *Densities and viscosities of 1-ethyl-3-methylimidazolium n-alkyl sulfates.* Journal of Chemical & Engineering Data, 2011. **56**(8): p. 3433-3441.

142. Sun, G.-h., K.-x. Li, and C.-g. Sun, *Application of 1-ethyl-3-methylimidazolium thiocyanate to the electrolyte of electrochemical double layer capacitors.* Journal of power sources, 2006. **162**(2): p. 1444-1450.

143. Voronel, A., et al., *Fractional Stokes-Einstein law for ionic transport in liquids.* Physical review letters, 1998. **80**(12): p. 2630.

144. Jaganathan, J., M. Sivapragasam, and C. Wilfred, *Thermal Characteristics of 1-Butyl-3-Methylimimidazolium Based Oxidant Ionic Liquids.* J Chem Eng Process Technol, 2016. **7**: p. 309.

145. Socrates, G., *Infrared and Raman characteristic group frequencies: tables and charts.* 2001: John Wiley & Sons.

146. Daguenet, C., et al., *Dielectric response of imidazolium-based room-temperature ionic liquids.* The Journal of Physical Chemistry B, 2006. **110**(25): p. 12682-12688.

147. Michael P áMingos, D., *Tilden Lecture. Applications of microwave dielectric heating effects to synthetic problems in chemistry.* Chemical Society Reviews, 1991. **20**(1): p. 1-47.

148. Fröhlich, H., *Theory of dielectrics: dielectric constant and dielectric loss.* 1958: Clarendon Press.

149. Hoffmann, J., et al., *Ionic liquids and their heating behaviour during microwave irradiation–a state of the art report and challenge to assessment.* Green Chemistry, 2003. **5**(3): p. 296-299.

150. Nimpuno, N., A. McPherson, and T. Sadique, *Greening Consumer Electronics: Moving Away from Bromine and Chlorine.* 2009: CPA (North America).

151. *Gold Price per Kilo.* 2018 01/03/2018]; Available from: https://www.gold.co.uk/gold-price/gold-price-per-kilo/.

152. *Gold Spot Price UK in GBP per Kilogram.* [website] 2018 01/03/2018; Available from: https://www.bullionbypost.co.uk/gold-price/gold-spot-price/.

153. LME. *London metal Exchange official prices.* 2018 01/03/2018]; Available from: https://www.lme.com/Metals.

154. Yokoyama, S. and M. Iji. *Recycling of thermosetting plastic waste from electronic component production processes.* in *Electronics and the Environment, 1995. ISEE., Proceedings of the 1995 IEEE International Symposium on.* 1995. IEEE.

155. Yokoyama, S. and M. Iji. *Recycling of printed wiring boards with mounted electronic parts.* in *Electronics and the Environment, 1997. ISEE-1997., Proceedings of the 1997 IEEE International Symposium on.* 1997. IEEE.

156. Marques, A.C., J.-M.C. Marrero, and C. de Fraga Malfatti, *A review of the recycling of non-metallic fractions of printed circuit boards.* SpringerPlus, 2013. **2**(1): p. 521.

157. Mou, P., D. Xiang, and G. Duan, *Products made from nonmetallic materials reclaimed from waste printed circuit boards.* Tsinghua Science & Technology, 2007. **12**(3): p. 276-283.

158. Zheng, Y., et al., *The reuse of nonmetals recycled from waste printed circuit boards as reinforcing fillers in the polypropylene composites.* Journal of Hazardous Materials, 2009. **163**(2-3): p. 600-606.

159. Guo, J., J. Guo, and Z. Xu, *Recycling of non-metallic fractions from waste printed circuit boards: A review.* Journal of Hazardous Materials, 2009. **168**(2-3): p. 567-590.

160. Hong, Y., et al., *High sensitive detection of copper II ions using D-penicillamine-coated gold nanorods based on localized surface plasmon resonance.* Nanotechnology, 2018. **29**(21): p. 215501.

161. Han, J., et al., *Construction of flexible and stable near-infrared absorbing polymer films containing nickel-bis (dithiolene) moieties via ligand-exchange post-polymerization modification.* Polymer Chemistry, 2017. **8**(27): p. 3977-3991.

162. Van Eygen, E., et al., *Resource savings by urban mining: The case of desktop and laptop computers in Belgium.* Resources, conservation and recycling, 2016. **107**: p. 53-64.

163. Akcil, A., et al., *Precious metal recovery from waste printed circuit boards using cyanide and non-cyanide lixiviants–a review.* Waste Management, 2015. **45**: p. 258-271.

164. Wang, X. and G. Gaustad, *Prioritizing material recovery for end-of-life printed circuit boards.* Waste management, 2012. **32**(10): p. 1903-1913.

165. Abbott, A.P. and G. Frisch, *Ionometallurgy: Processing of Metals using Ionic Liquids.* Element Recovery and Sustainability, 2013(22): p. 59.

166. Kosmulski, M., J. Gustafsson, and J.B. Rosenholm, *Thermal stability of low temperature ionic liquids revisited.* Thermochimica Acta, 2004. **412**(1-2): p. 47-53.

Appendix

The temperature-dependent microwave frequency sweep measurement conducted using PNA has been presented in this section:
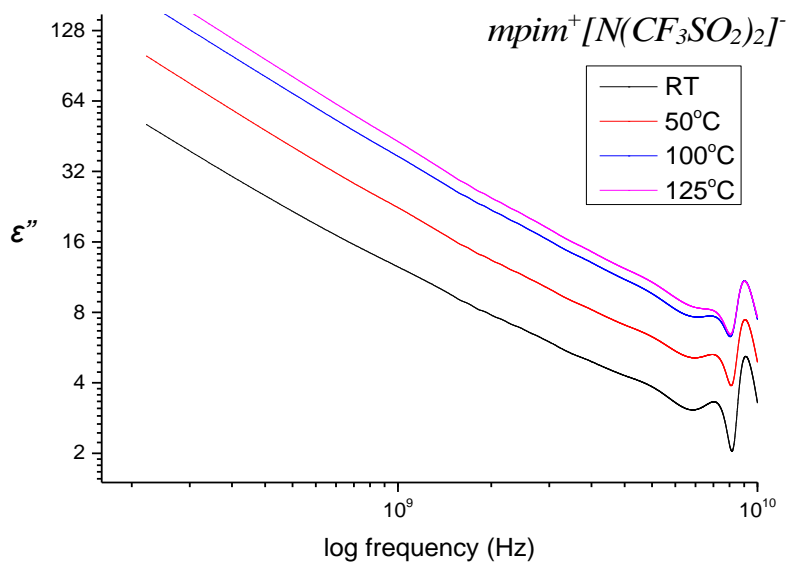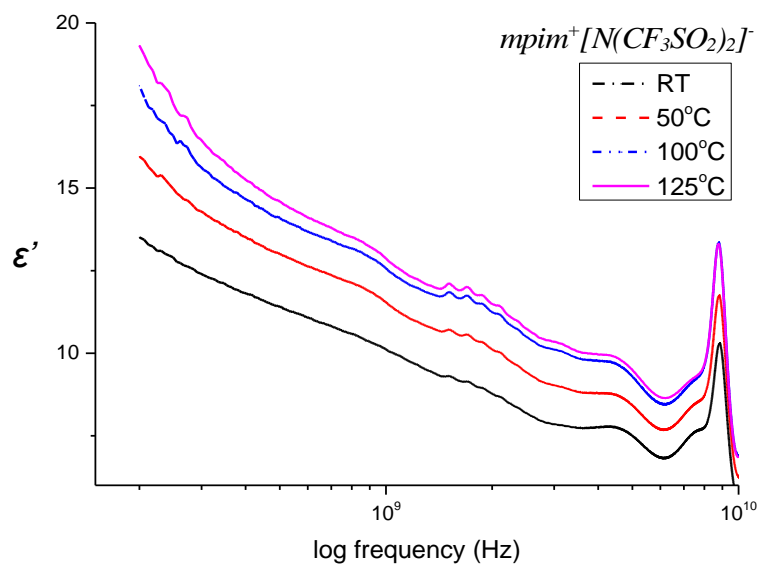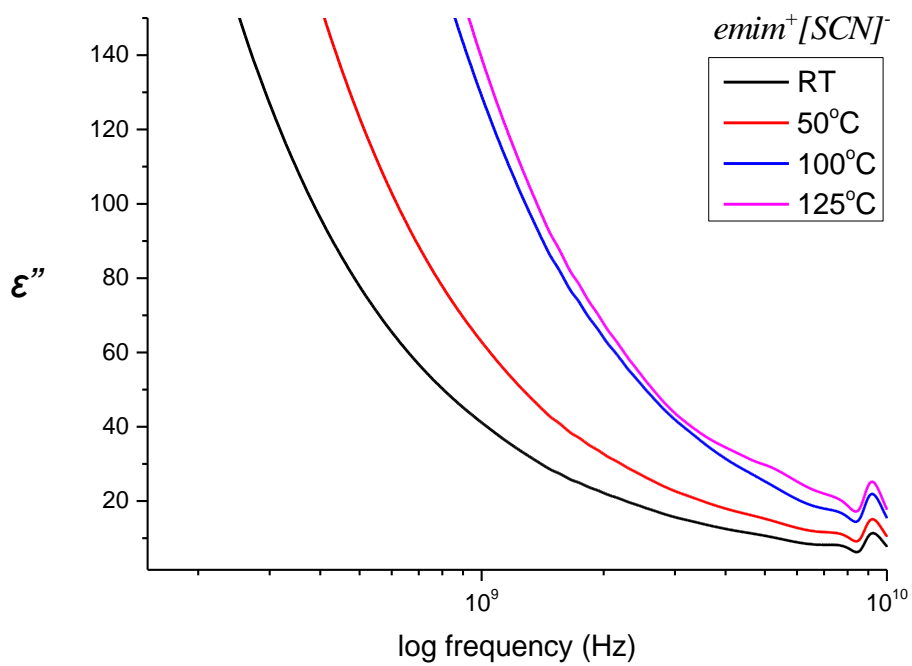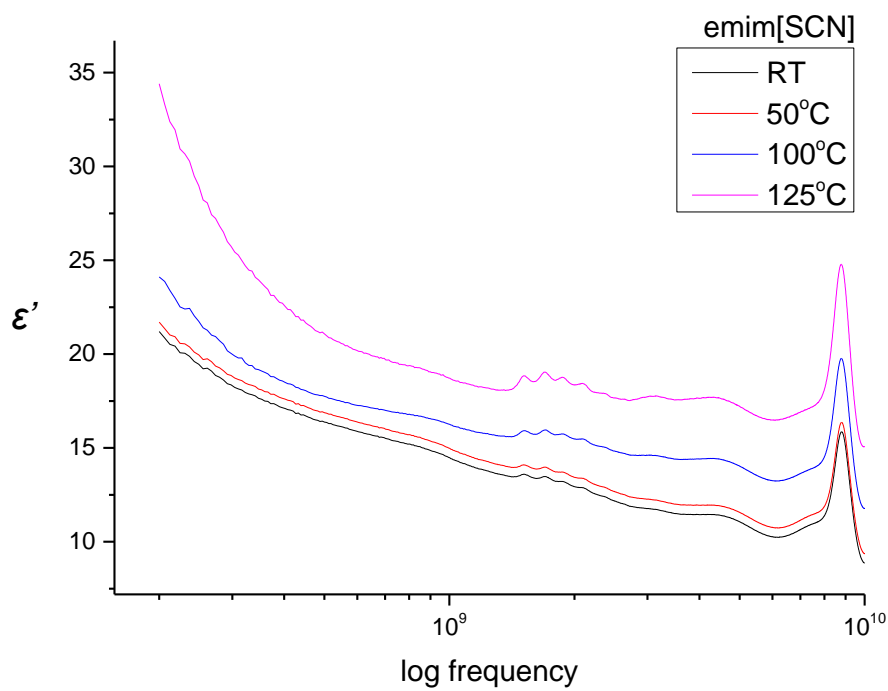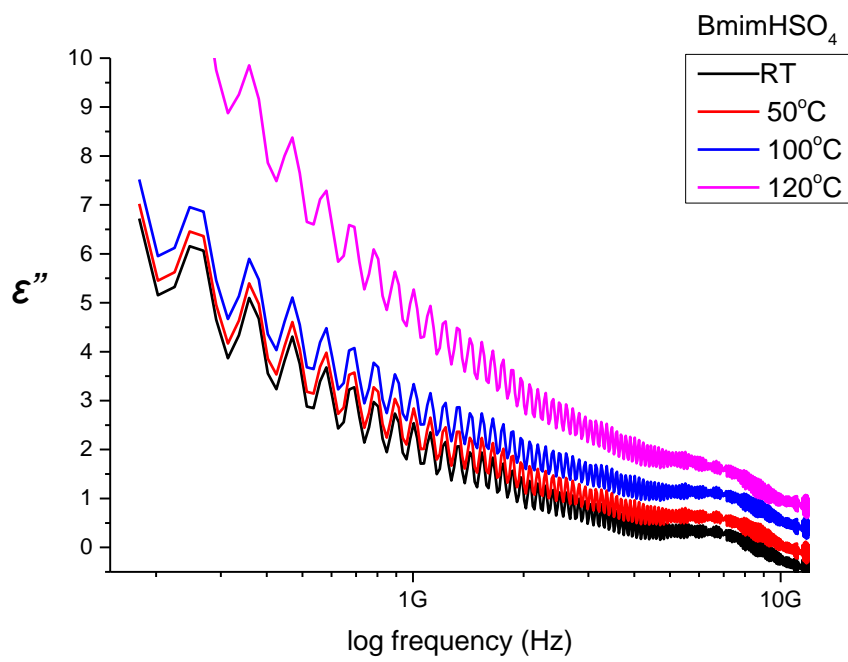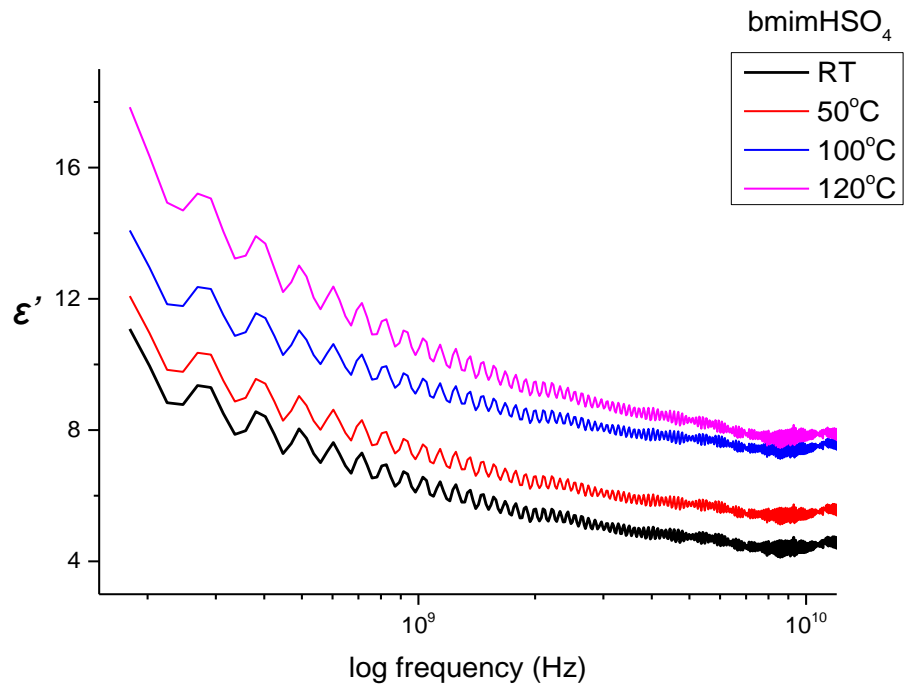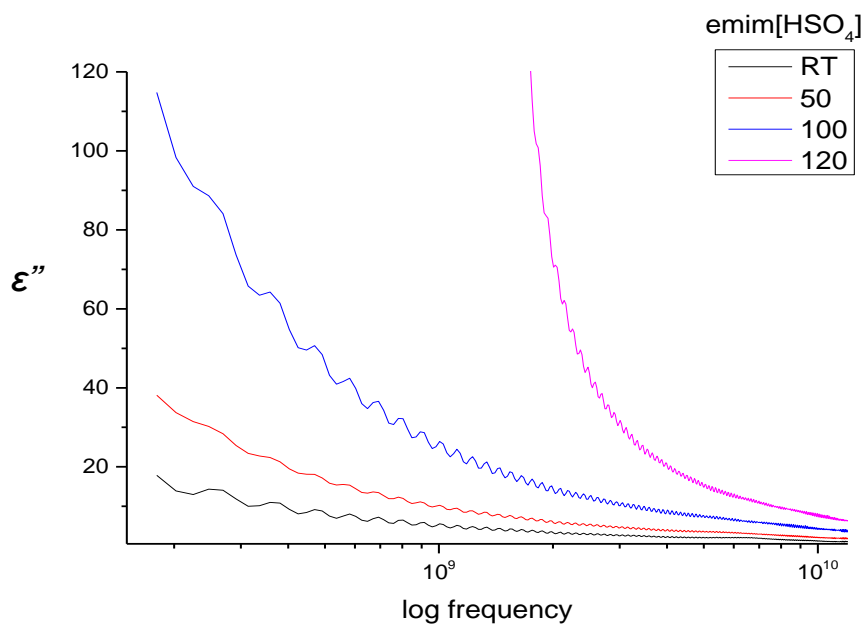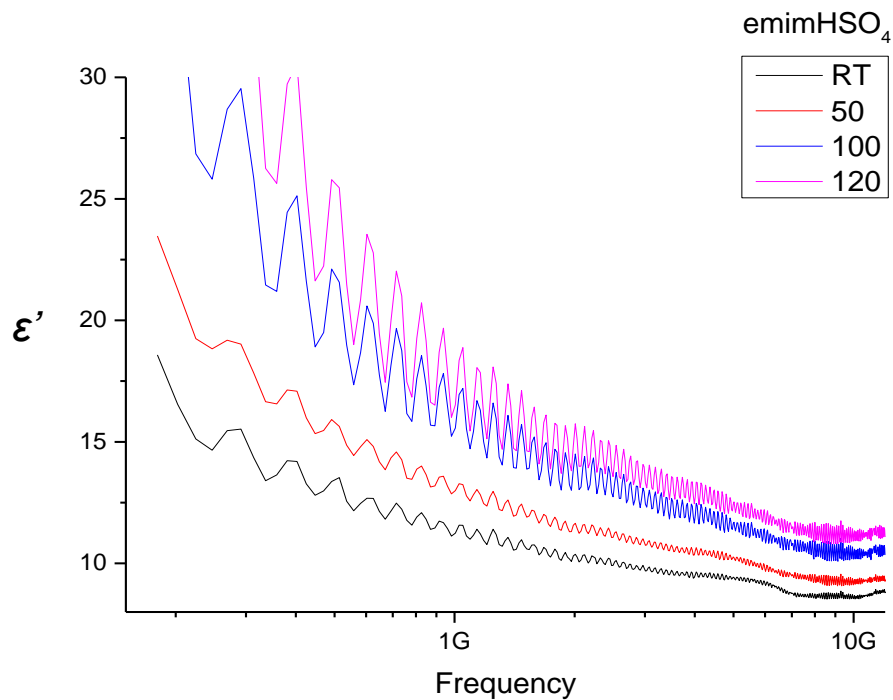
Figure 75 *A temperature-dependant frequency sweep reading of microwave properties at an isotherm, maintained at (25, 50, 100 and 125ºC) by using a hot plate. Both the microwave dielectric constant and loss factor increase as temperature is increased*